Wind tunnel testing of shelterbelt effects on dust emissions from swine production facilities

by

David Joseph Laird

A thesis submitted to the graduate faculty

in partial fulfillment of the requirements for the degree of

MASTER OF SCIENCE

Major: Aerospace Engineering

Major Professor: Dr. Bruce Munson

Iowa State University

Ames, Iowa

1997

Graduate College

Iowa State University

This is to certify that the Master's thesis of

David Joseph Laird

has met the thesis requirements of Iowa State University

TABLE OF CONTENTS

LIST OF SYMBOLS

a	Speed of sound
A_1	Dimensionless threshold friction speed
b	Spire width
B	Friction Reynold's number
C_D	Drag Coefficient
C_f	Friction coefficient
d	Particle diameter
D	Roughness block spacing, Particle diameter
e	Coefficient of restitution
F	Pressure drop factor
g	Gravitational acceleration
h	Reference height, Boundary layer thickness
H	Spire height
H_o	Test section height
k	Roughness block height
l	General horizontal length
L	Reference length
M	Mass

R	Reynold's number
t	Time
u	Mean velocity
u_*	Friction speed
u_f	Terminal speed
u_t	Threshold speed
u_{*_t}	Threshold friction speed
u_∞	Freestream Velocity
U	Wind speed at reference height
v_f	Fall velocity
w	Width
z	Distance above floor
z_o	Roughness height
α	Boundary layer shape coefficient
δ	Boundary-layer thickness
η	General height
ν	Kinematic viscosity
ρ	Fluid density

Subscripts:

m	Model
p	Particle
ref	Condition at reference location

ABSTRACT

Dust emissions from swine containment facilities are a constant nuisance in the areas near by. The strong odors produced offend neighbors and can lower property values. Ways to minimize the problem of dust emissions through the use of wind breaks can be explored through wind tunnel testing. The wind tunnel can be used to conduct quick, inexpensive, and repeatable experiments that would be difficult to accomplish on a full scale. Modeling wind transport effects on a small scale involves proper matching of many properties such as geometric, kinematic, and dynamic similarities. It is also important to distinguish what similitude requirements are most important, since they cannot all be matched. Proper modeling allows small scale testing to predict full scale results. Experiments to determine the effects of wind breaks involve varying the wind speed and direction, and also changing the height, thickness, and number of model bushes. Methods of data acquisition include collecting the particle deposit on the wind tunnel floor and recording the mass, and using digital photography to analyze the dust deposits. It has been determined that wind speed has the biggest effect on the amount of dust that is carried far downstream. The number and height of bushes are also influential. In the best case scenarios, the

amount of dust carried far from the model decreased by between 35% to 56%. A technique of using digital photographs to determine the amount of deposit by relating it to image intensity is also introduced, but so far errors have rendered the method ineffective.

CHAPTER I: INTRODUCTION

Hog production is one of Iowa's strongest economic forces, bringing in $12 billion in 1995. However the expansion of this industry is meeting resistance by local communities because of its offensive odor. Larger hog facilities are being built in the state, some of them holding thousands of hogs at a time. There are already tough regulations imposed on large hog operations, but odor remains the biggest problem. Senator Berl Priebe, D-Algona, chair of the Senate Agriculture Committee has commented that if odor problems can be corrected, many of the problems now facing the Iowa pork industry will be resolved.

The motivation behind the following text is to explore and understand the movement of dust from swine production facilities into the surrounding areas. The purpose is to investigate how dust from these facilities is transported downwind, and how this transport can be reduced by appropriate barriers.

The cause of odor from these facilities can be broken down into two categories: dust emission and gaseous emission. The subject of this study will concentrate solely on dust emission, gases being reserved for future examination. The dust is formed by dried manure, feed stuff, and dandruff being agitated by the trampling of hogs, and it is swept away by

the wind. Even though the hogs are inside, the buildings have large open windows that allow the breeze to cool the hogs. The transport of this dust depends on many factors, the most important of which is wind speed.

Particle motion by the atmosphere is a well researched subject. Scientists have used wind tunnel testing to study the effects of erosion, snow drifts, desert growth, pollution, and most importantly, how to prevent these effects. Our goal is to extend this field of research to the modeling of a hog production facility, examining the dust entrainment process and determining shelterbelt effects on the volume of, and/or distance traveled by particles.

For this research, the Environmental Wind Tunnel at Iowa State University is used. Wind tunnels are used to perform this kind of research because it is less expensive, quicker, and easier to test atmospheric wind phenomenon with a small scale model, whether the test is of the air flow around a model building, or the means of controlling particle transport. Control of the experiment (wind direction, velocity, duration, etc.) is a primary advantage with small scale models. Experiments are also relatively cheap to perform and many more experiments can be conducted in a given period of time. The important question for model experiments concerns the validity of full scale prediction from model results. It is sometimes difficult to properly

simulate at small scale the wind, temperature, and turbulence profiles which occur naturally in the atmosphere (1).

CHAPTER II: EQUIPMENT AND PROCEDURE

Equipment

The equipment used in this experiment is as follows:

1. Low speed wind tunnel
2. Model of swine production facility
3. Spires and roughness blocks
4. Pitot-static tube, pressure transducer, amplifier
5. Ricoh RDC-1 remote control digital camera
6. Hewlett Packard PC
7. Vertical collector device
8. Remote digital thermometer
9. Transversing pitot-static tube system
10. Vacuum cleaner
11. Mass balance
12. Crushed walnut shell

An atmospheric wind tunnel is designed to simulate testing in the natural boundary layer. Two types of atmospheric wind tunnels are commonly used, both having long test sections. The first is called a meteorological wind tunnel, and may have a test section up to 15 test

section heights long, and has the capability to both cool and heat the air and test section floor. This is especially important when it is necessary to simulate an atmospheric temperature gradient, as when testing with some types of tests of pollution. When it is not required to cool or heat the air and test section floor, as in our case of particulate saltation, the effect of temperature gradients can be ignored. For these kinds of tests, simulating the boundary layer structure and turbulence will be adequate, which can be done using the second type of atmospheric wind tunnel, the environmental wind tunnel. This type of tunnel normally has test sections about 10 test section heights long. This research was performed using the Environmental Wind Tunnel at Iowa State University. A drawing of the wind tunnel floor depicting important items of the experiment is shown in Figure 1, and a photograph of the facility is shown in Figure 2.

For general tests involving particle entrainment, there are some advantages to having a straight through, open circuit tunnel (or even a closed circuit tunnel which may be converted to open circuit) because many types of these tests could damage a closed circuit type. These tests may involve smoke, "snow material", erosion with sand, model failure, water troughs, or rain simulations which could hurt plywood construction or rust balance components. In our particular case, any recirculation of

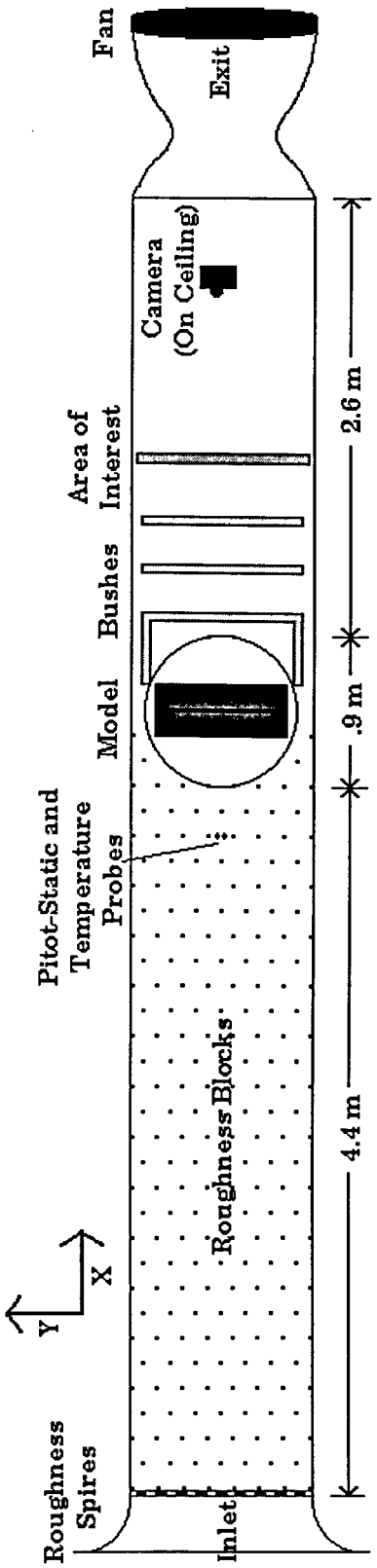

Figure 1: Floor plan of the wind tunnel

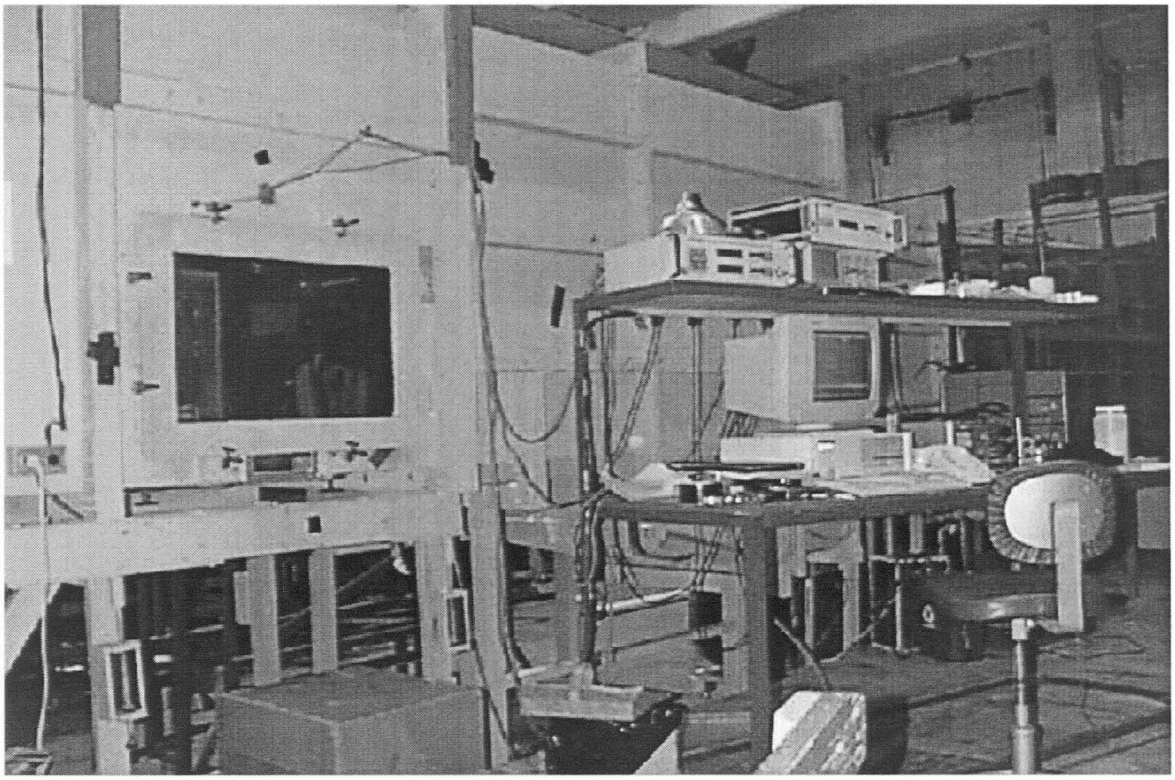

Figure 2: The Environmental Wind Tunnel at Iowa State University

the walnut shell particles could possibly influence the experimental data. Also necessary for such tests is an adequately long test section to fully develop the modeled boundary layer, which tends to favor an open circuit type. However, if a closed circuit wind tunnel has the sufficient length to model the boundary layer, there is no reason that it could not be used (2).

A wind tunnel is often required to operate at very low velocities during airborne dispersion tests. A direct-current drive motor plus a variable pitch propeller is the best arrangement. An alternating current

motor with a variable pitch propeller tends to be cheaper and is usually adequate, and is the type of system employed in our wind tunnel. Adjusting tunnel speed by rpm is not necessary with thick boundary layer flow because the flow pattern can be adjusted by spires and roughness elements in the test section. The tunnel drive system should be capable of maintaining flow speeds within 1-2% (2).

Flow velocity was determined by using Bernoulli's incompressible equation, which requires pressure and temperature inputs. Pressure measurements are difficult to obtain in turbulent flow. Normal procedure is to use a pressure transducer that has a flat frequency response to around 150 Hz, and then to average samples taken at rates of 50-150/s for 20 seconds or so. The most commonly used pressure transducers are diaphragm types. These generally measure a differential pressure, where a preselected reference pressure is applied to the reference side. Absolute pressure types are also available. Pressure transducers come in a wide range of differential pressure values, though 2.5 psid and 5.0 psid are the most widely used. Because accuracy at low speed is important in this experiment, a 2 inH_20 (~ .07 psid) transducer was used. Transducers require a bridge power supply similar to strain gages, and the output voltage varies with pressure. A calibration is performed to translate the output voltage into pressure. This is done by applying a series of known

pressures to the transducer. Transducers are calibrated using a primary standard in a dead weight tester or a calibrated secondary standard. These units most often apply pressure to the reference side of the transducer, but this is not mandatory. In our case, a crank manometer was connected to the reference port, and the output was recorded at varied inputs of mmH_2O. This data can be fed into a curve-fitting routine to determine the calibration curve. Transducers tend to be linear, but often a third degree curve fit is used. The calibration curve for this system is shown in Figure 3. Transducers may sometimes need to be recalibrated. For our experiments, the only recalibration consisted of zeroing the transducer prior to each test by measuring the voltage output during a zero wind condition, and shifting the calibration curve to intersect that point (2,3).

The most common device used with a pressure transducer is the pitot-static tube, an instrument that provides both the total head and the static pressure. This experiment uses two pitot-static tubes. The primary tube is at a fixed position in the test section 31 cm upstream of the model, and 6 cm above the floor, as shown in Figure 2. The second pitot-static device is placed on a transversing rack above the test section, which is only employed while determining velocity profiles. The orifice at the tip of

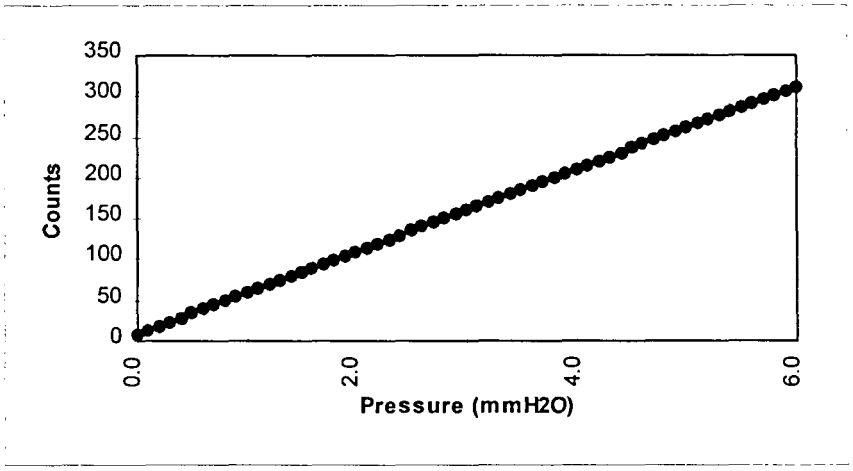

Figure 3: Calibration curve for pressure transducer and amplifier

a pitot-static tube reads total pressure, $p + \frac{1}{2}\rho V^2$, and the orifices on the sides read the static pressure, p. If the pressures from the two orifices are connected across a differential type pressure transducer, the result will be the dynamic pressure $q = \frac{1}{2}\rho V^2$, from which the velocity may be calculated, provided air density is known. This is found using the state equation, $p = \rho RT$, and the temperature.

The static temperature is essentially constant through a boundary layer in incompressible flow. Thus, the easiest method of measuring static temperature is through the use of a flush, wall mounted temperature probe. It is beneficial if the probe is remote indicating, enabling the temperature to be read in a convenient location. The probe

should be located in an area of the test section where the chance of damage is minimal. The temperature probe should have an output in millivolts so that it can be recorded by a digital data acquisition system if one is used. The temperature probe in this experiment is located approximately 6 cm above the floor, next to the pitot-static tube, as shown in Figure 2.

Finally, a one fiftieth scale model of a typical containment facility was constructed out of plywood using an architectural drawing provided by the Iowa State University Agricultural and Biosystems Engineering Department. The ceiling, outside walls, and roof are modeled, but window frames and interior pen rails are not. Also, only a single structure is present, whereas in real life the buildings are often grouped in rows, columns, or both, and include large feed bins at the end of each structure. It is also important to realize that not all facilities are the same. They may have different lengths, roof styles, or other geometric properties that may impact the aerodynamics and consequently the pattern of dust transport. Further investigations my be required to determine the effect of different facility styles. The roof of the model is removable, to allow the floor inside to be filled with walnut shell, simulating the dust particles. Figure 4 shows the model.

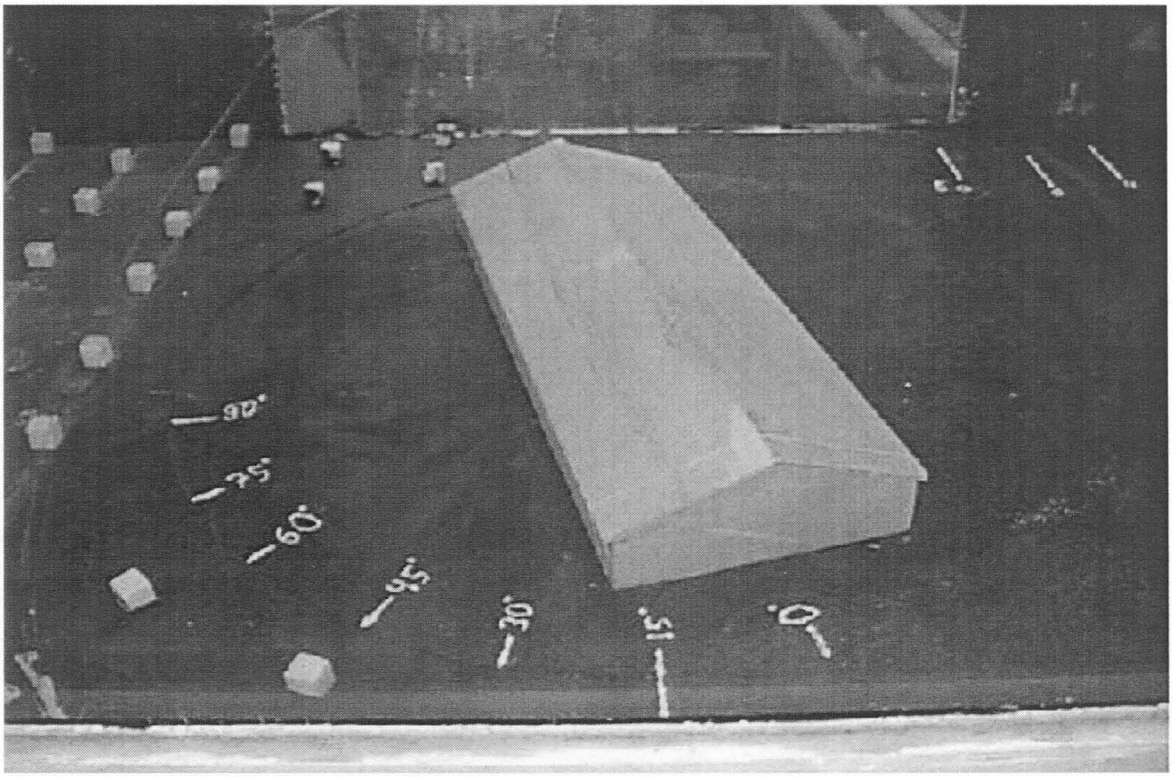

Figure 4: The wind tunnel model

Wind Modeling

Model testing is based on the laws of similarity. For the model to be representative of the full size structure, there must be geometric, kinematic, and dynamic similarity.

For geometric similarity, all the relevant linear dimensions of the model must have the same direct proportionality to the corresponding full size dimensions. For kinematic similarity, there must be a constant ratio between the two sets of corresponding velocities. Finally, there must be a

constant ratio between the corresponding sets of forces to achieve dynamic similarity (4).

In most situations, the exact similitude requirements for modeling dust emission problems cannot be met, or are impractical to satisfy on a small scale, because of the large number of modeling parameters that cannot be solved simultaneously. Because of this problem, it is better to ignore factors which have only minor influence on the situation, and concentrate on those with a predominant influence. However, the complexity of the similitude problem is emphasized by the lack of agreement as to the most important or appropriate sets of parameters on which to base a similitude (1,4).

The following variables describe the boundary layer problem:

g	gravitational acceleration
h	reference height
L	reference length
l	other horizontal lengths
z_0	roughness height
U	wind speed at reference height
η	other heights
ν	kinematic viscosity

Important nondimensionalized testing parameters identified in references 1, 2, 4, 5, 6, and 7 describe the following modeling conditions of a meteorological wind tunnel in order to provide useful information:

- Reynold's number, $\frac{\rho}{\mu}UL = \frac{UL}{\nu}$
- Mach number, $\frac{U}{a}$
- Rossby number, $\frac{U}{L\Omega}$
- Scaling of buildings and topographic features, $\frac{h}{L}, \frac{l}{L}, \frac{\eta}{h}$
- Kinematic simulation of air flow, boundary layer velocity distribution, turbulence, and roughness criterion, $\frac{z_0}{L}$
- Matching the zero pressure gradient found in the atmosphere

The predominant forces in air flow are those caused by inertia and viscosity. The Reynold's number is a measure of the ratio of the inertia forces to the viscous forces. Therefore, similarity of flow between a scaled model and the full size structure can be obtained if the Reynold's number for both systems is the same. However, the reduced linear scale of wind tunnel models usually means that the Reynold's number of experimental models are orders of magnitude less than those found for full scale.

Fortunately, the effects of not achieving a proper match are usually small because of the turbulence produced by the sharp edges of most objects under study. Check runs should be made at various speeds to make sure this assumption is true. If problems were to occur, they could most likely be resolved through the use of trip strips (2, 4).

The Mach number is the ratio of velocity to the speed of sound, and provides another measure of inertial properties. If a model test has the same Reynold's and Mach numbers as the full scale subject, then the flow around the model and the full scale subject will be dynamically similar (4).

The Rossby number is a function of the Coriolis effect on the earth's winds. It may account for up to a 5 degree shift of wind at 600 ft. This is of little significance and would be hard to simulate if it were necessary (2).

Generally, physical structures are modeled such that the scale in all three dimensions is the same. However, since the variables used in modeling listed previously contain both a reference height and a reference length, there is the possibility of having a geometrically distorted model. Not only is it necessary to simulate the structure being tested, but also the surrounding area within 1000 to 2000 ft full scale of the building site. These surroundings may change not only the wind loads, but may add to pollution problems. The building to be tested and its surroundings should

be placed on a turntable, so when rotated the test area can experience winds from any direction. There is a small amount error because the boundary layer and turbulence in the atmosphere may be different depending on the wind direction. Sometimes, especially when a building is on a lake shore, or near a hilly area, a different wind structure should be employed (2).

The velocity distribution in the natural boundary layer should be simulated as completely as possible. In our case, at a scale of 1:50 a 5 m tall barn will be 10 cm high. The boundary layer must be duplicated to at least 15 cm high, and preferably extend to the test section ceiling. If the actual boundary layer is known at the location of a proposed site, then an effort should be made to model it. However if the boundary layer is unknown, the following guide can be used. The maximum speed at 30 ft altitude can be estimated and the boundary layer is structured according to:

$$\frac{u}{u_{ref}} = \left(\frac{z}{z_{ref}}\right)^{\alpha}$$

where u = mean velocity at height z, u_{ref} = mean velocity at reference height. The boundary layer shape coefficient α varies according to the terrain, and may be chosen using Table 1 as a guide. Wind speed increases with height, while turbulence is greatest near the ground (2).

Table 1: Choices for the boundary layer shape coefficient

	Boundary layer thickness h (ft)	α
Open country	280	0.15
Low rise buildings	1200	0.28
Urban	1700	0.40

The boundary layer velocity distribution and turbulence can be duplicated by installation of spires in the wind tunnel followed by a roughness run of 10 - 15 test section heights often made with small cubes on the floor. Using the method of reference 8, plywood spires and Styrofoam roughness blocks were constructed to produce a boundary layer thickness of 20 cm, and $\frac{u_*}{u_\infty}$ of .06 at the test section. The design of these elements can be found in Appendix D. Their layout is shown in Figure 1, and can be seen in Figure 5.

In addition, it has been shown that for simulation of the atmospheric boundary layer the roughness parameter in the model should be the same as that in the atmosphere, i.e.,

$$\frac{z_{0_m}}{z_0} = \frac{L_m}{L}$$

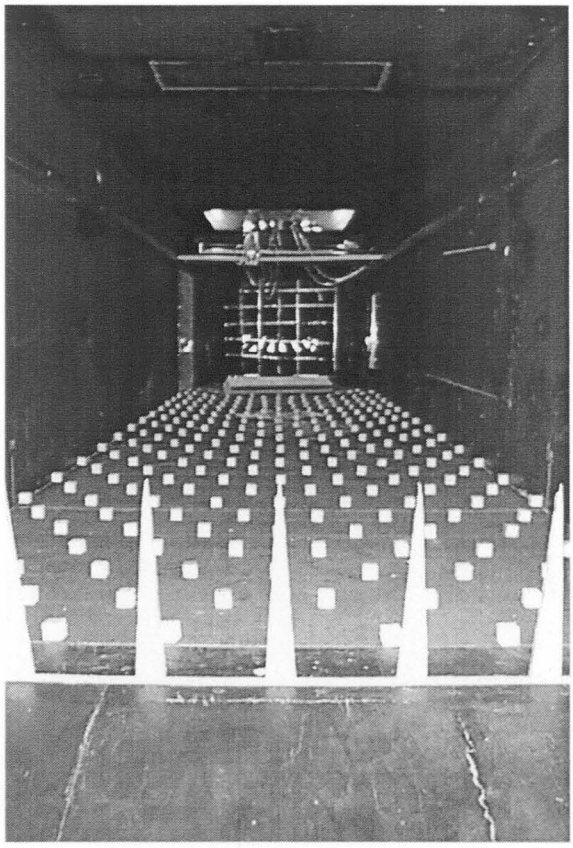

Figure 5: Spires and roughness blocks as seen through the wind tunnel inlet

Finally, the longitudinal pressure gradient normally found in a wind tunnel, and compounded by the very thick boundary layer, needs to be eliminated to match the zero pressure gradient found in the atmosphere. This is done by providing an adjustable test-section roof that may be adjusted to provide the extra cross-sectional area needed (2).

Particle Modeling

The movement of loose surface particles by wind is a complex phenomenon. Loose particles can move in one of three ways: creep, saltation, or suspension. Creep is the motion in which large particles roll along the surface but do not become airborne. Saltation is caused by medium-size and smaller particles becoming airborne due to aerodynamic lift, or a combination of lift and impact of returning particles. In saltation, particles rise from the surface nearly vertically and then gradually return by a shallow angle trajectory. This process is responsible for most of the motion and end deposits that form snowdrifts or soil erosion. The velocity below which saltation will not occur is called the threshold velocity. When the wind velocity exceeds about 5 times the threshold velocity, the particles bump hard enough to bounce into the air stream, and are then said to be in suspension. Saltation and suspension can occur at much lower speeds in the presence of falling particles. Very small particles, after becoming airborne, may go into suspension and perhaps rise to great heights before gradually settling out of the atmosphere.

The ratio of terminal speed to threshold friction speed is:

$$\frac{U_f}{u_{*_t}} = \frac{2}{A}(3C_D)^{-\frac{1}{2}}$$

where the drag coefficient C_D is a function of Reynold's number:

$$C_D = C_D\left(R = \frac{U_f B}{u_{*_t}}\right)$$

$$C_D = \frac{24}{R}, (R \leq .1), \; C_D > \frac{24}{R}, (R > .1)$$

The dimensionless threshold friction speed, A_1, is given by

$$A_1 = \frac{u_{*_t}}{\left(\frac{\rho_p g D_p}{\rho}\right)^{\frac{1}{2}}}$$

Most researchers assume A_1 is a unique function of particle friction Reynolds number B:

$$A_1 = A_1(B), \quad B = \frac{u_{*_t} D_p}{v}$$

In addition, however, the threshold parameter A_1 must be a function of cohesive forces for small particles.

The mean vertical turbulent eddy velocity in the boundary layer has the same order of magnitude as the friction speed u_*. Thus, particles go into suspension because their terminal speed , U_f, is smaller than u_* (or u_{*_t}). An approximate division between dust (material in suspension) and sand (saltating particles) is therefore found by setting the ratio

$\frac{U_f}{u_{*_t}} = 1$. For particle diameters large enough so that $\frac{U_f}{u_{*_t}}$ is greater than 1, particles will not become suspended until that ratio $\frac{u_*}{u_{*_t}}$ is reached when $\frac{U_f}{u_*}$ becomes approximately unity. Unless under the influence of very strong winds, nearly all blowing particles move in the saltation mode (2). The dust from hog facilities is an exception however, because of the small particle size. This dust mostly moves in suspension.

The introduction of moving particles to the problem requires the following additional variables:

D_p particle diameter

t time

ρ fluid density

ρ_p particle density

These variables must be considered along with the wind modeling, and result in these additional scaling requirements:

- Scale factor, $\frac{d}{L}$ where d = diameter of model particle (in) and L = length of a full-scale reference dimension (in).
- Coefficient of restitution, e. This concerns the rebound distance/drop distance.

- Particle velocity, $\frac{V_p}{V}$, where V_p = velocity of model particle (fps) and V = velocity of a full scale particle (fps).
- Fall velocity, $\frac{V_f}{V}$, where V_f = free fall velocity of model particle (fps)
- Froude number, $\frac{V^2}{gd}$ where g = acceleration of gravity, ft/s^2.
- Density ratio, $\frac{\rho}{\rho_p}$

The Froude number is important to achieve similarity in situations with blowing particles. The particle diameter to length ratio is rarely satisfied in a small scale model because the small particle size results in too small of a value of $\frac{U_f}{u_{*_t}}$. This causes motion to be due to suspension rather than saltation. The Froude number cannot be satisfied in the wind tunnel because a portion of the model must have speeds above the threshold velocity for particle motion. Thus there is a lower limit on the wind speed, in addition to the usual Reynolds number limitation (1).

The result is that small scale particle transport models are distorted, and if quantitative data is to be obtained from a model test, it is necessary to determine the effect of model distortion (1).

The material originally selected for its particle modeling properties was lycopodium spores. However, it is very expensive. Because of the cost involved, and the materials available, the material actually used in testing was ground walnut shell.

Other Scaling Effects

It must be remembered that the modeling of geometric, kinematic, and dynamic properties of air flow and particle transport will result in the

scaling of other, sometimes unexpected, properties as well. For example, the small scale properties of this experiment has resulted in the following time scaling:

Flow rate is determined by $Q = \frac{dM}{dt} \sim \frac{\rho u^2 (u - u_t)}{g}$

For full scale $\Delta t = \frac{\Delta M g}{\rho u^2 (u - u_t)}$, and for the model $\Delta t_m = \frac{\Delta M g}{\rho u^2 (u - u_t)_m}$

To satisfy the Froude number, $\left.\frac{u^2}{gH}\right|_m = \frac{u^2}{gH}$, which leads to $\frac{u}{u_m} = \sqrt{\frac{H}{H_m}} = \sqrt{50}$

$$u = \sqrt{50}\ u_m$$

Again, because the model is distorted, this is not completely true, but it is close. It is a good model for particle deposition, and is proper for

geometry. It really depends on the threshold velocity. Now using the flow rate equation,

$$\frac{\Delta t}{\Delta t_m} = \frac{\Delta M}{\Delta M_m} \frac{(u_m - u_t)}{(u - u_t)} \frac{u_m^2}{u^2}$$

and substituting for u,

$$\frac{\Delta t}{\Delta t_m} = 50^3 \frac{(u_m - u_t)}{(\sqrt{50}u_m - u_t)} \frac{u_m^2}{50u_m^2} \approx \frac{50^3}{\sqrt{50}50} = 353.55$$

So after a test run of 15 minutes, we get the results of a full scale test after more than 3 1/2 days.

Experimental Procedure

First the threshold velocity must be determined, which is the minimum airspeed required to begin the entrainment process. The model is filled with the crushed walnut shell, and is placed inside the test section. Then the wind tunnel is turned on to its lowest setting, and the airspeed is slowly increased until there is visual confirmation of airborne particles. The velocity is recorded, and the wind tunnel is turned down again. This process is repeated several times to establish an average threshold velocity. This threshold velocity is used to establish the minimum speed to be used during the experimental testing.

Next, the model is refilled, the floor is cleaned, and the tunnel is restarted. Several experimental runs are conducted near the threshold velocity, photographs are taken, and the data is analyzed. Then, additional runs are completed at higher speeds, and with the model facing different angles. The angle between the longitudinal axis of the model and the wind direction will be referred to as the angle of attack. After gathering data for the particulate deposit behind the model, the next phase is to add obstacles in order to simulate bushes, with the goal to understand the effects of these wind barriers. Bushes are made out of a coarse, fibrous packing material, and are shaped as shown in Figure 6.

The list of variables to be tested and the values used include:

Wind velocity: 4, 5, and 6 m/s

Model angle of attack: 0, 15, and 30 degrees

Hedge thickness: 3 and 4.5 cm

Hedge Height: 10, 7.5, and 5 cm

Number of hedges: 0, 1, 2, and 3Since the total combinations of all the variables are well beyond the scope of the project, help was obtained from the field of statistic analysis. Particular combinations of experimental variables are chosen to reveal the most amount of information with the least amount of testing. Table 2 lists the experiment schedule for testing without hedges, and Table 3 lists

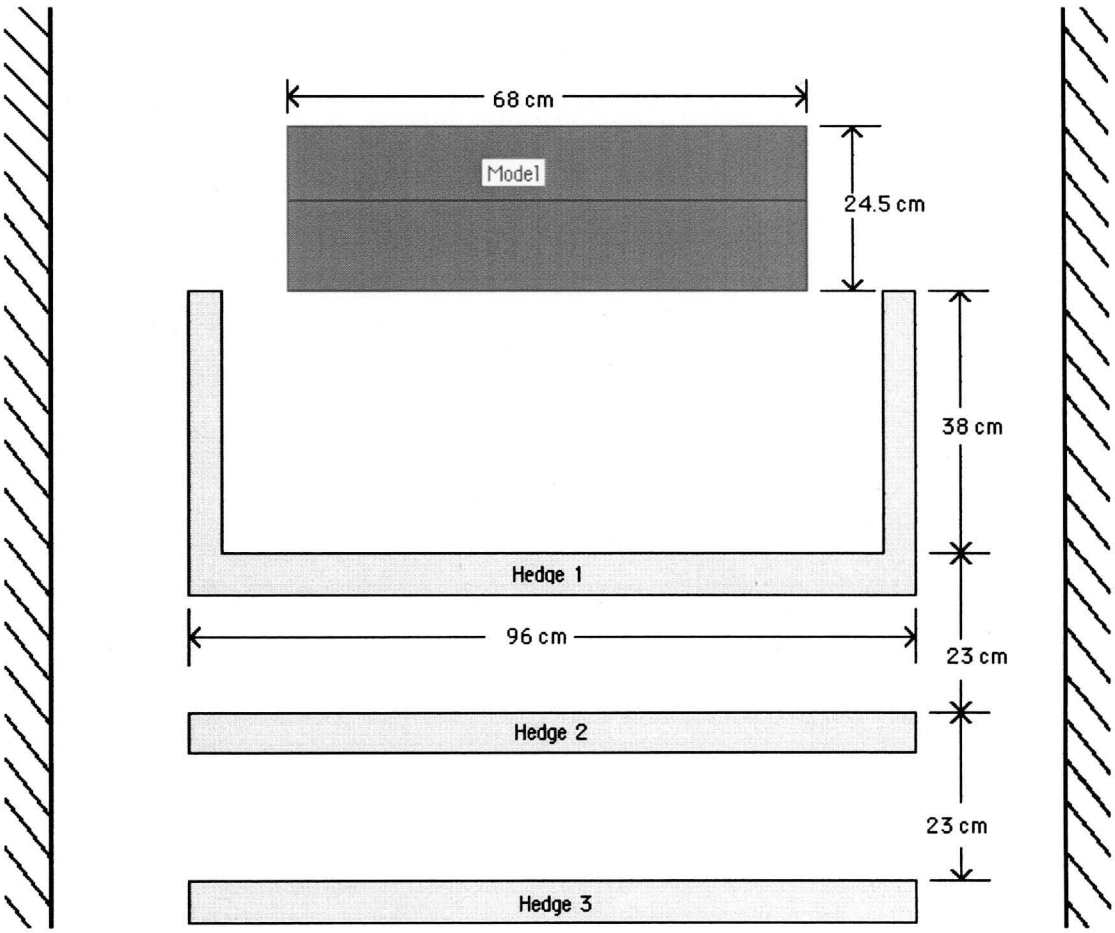

Figure 6: Model and bush arrangement

the test schedule with bushes. It is important to point out here that when the actual experiments were carried out, Run 7 on the schedule was not followed properly. This has a slight impact on the statistical analysis, and it should be noted that the Run 7 configuration listed here will not agree with the rest of this report.

Table 2: Experiment schedule without hedges

Run	Wind Speed (m/s)	Angle of Attack (o)
1	4	0
2	4	30
3	5	15
4	6	0
5	6	30
6	5	15

Table 3: Proposed experiment schedule with hedges

Run	Wind Speed (m/s)	Angle of Attack (°)	Number of Rows	Bush Height (cm)	Thickness (cm)
7**	4	0	1**	10	3
8	4	30	1	10	4.5
9	6	0	3	10	3
10	4	0	3	10	4.5
11	6	0	1	10	4.5
12	4	30	3	10	3
13	6	30	3	10	4.5
14	6	30	1	10	3
15	5	15	2	7.5	4.5
16	5	15	2	7.5	3
17	5	15	2	7.5	4.5
18	5	15	2	7.5	3
19	4	0	3	5	3
20	4	0	1	5	4.5
21	4	30	1	5	3
22	6	0	3	5	4.5
23	6	30	3	5	3
24	4	30	3	5	4.5
25	6	0	1	5	3
26	6	30	1	5	4.5

**In actual tests, 3 rows were used instead

Inputs and analysis regarding the statistical aspects of this research were provided by Jave Pascual of the Department of Statistics at Iowa State University, and Philip W. Iversen, Ph.D., senior statistician of the Eli Lilly and Company. The goals of the statistical design of the experiments are to determine which variables have the most influence on deposition, which two way interactions are important, and to select the most important variables to study further. For the experiments with the hedges, we have four variables with three values (low, middle, and high), and one variable with two values. The sixteen combinations of high and low values cover one half of all the vertices of a 5-dimensional hypercube. They are selected in a way that the effect of each variable on particle deposition can be estimated independently of each other. In addition, all ten of the two-way interactions between these five variables can be estimated independently of each other, and also independently of the main effect of each variable. It is also the case that any four dimensional sub-hypercube will have all sixteen of its vertices covered by this design.

This series of experiments also assumes that there will be some follow on studies. This sort of statistical design will determine what the linear effect of each variable is. It will also indicate if any of the variables interact with each other. For example, the effect of hedge height on odor control is different depending on the wind speed or the number of barriers.

The center runs are used to indicate if there is nonlinearity somewhere in the system. However, this design will not show which of the variables are nonlinear. It will be necessary to conduct some additional runs to determine this. If the nonlinearity is small, then these additional may not be needed.

Several of the runs are repeated. That is, Run 6 is a repeat of Run 3, Run 17 is a repeat of Run 15, and Run 18 is a repeat of Run 16. These runs are the "center" runs, meaning that they use the middle values for each variable. These repeat runs allow any experimental noise in the system to be measured. In this case, experimental noise is indicated by any irregularity in the results when the experiment is run from start to finish more than once, and under the same conditions. Further information about statistical experiment design can be found in references 9, 10, and 11.

Data Collection

There are two methods used to collect data in this experiment. One is simply to let the particle deposits build on the floor down wind of the model, and use a digital camera to photograph the deposit at different times throughout the test run. The camera is mounted on the wind tunnel ceiling, downwind of the model. Photography is a common form of

qualitative data collection for particle transport studies, however a unique method of analyzing the photographs will be presented in the following chapter.

The second method used is a mass study of the particles. After the model is filled with the walnut shell particles, the mass of the model and its contents are measured using a digital scale. Then the model is placed in the tunnel and tested. For this reason, it is important that the model be easily removable. After each test, the model is removed, and the mass of it and its remaining contents are recorded. This information provides the total mass that left the model during the experiment. Next, the mass of an empty vacuum cleaner bag is recorded before being placed in a vacuum cleaner. Then all particle deposits on the wind tunnel floor to a reference point about 1.3 m down stream of the model are carefully picked up with a vacuum cleaner. The bag is then removed and its mass recorded. Now there is enough information to determine the total mass of deposit on the floor, and also the total mass that is carried out of the wind tunnel. Again, the goal of the research would be to minimize the mass that is carried out of the tunnel because this demonstrates the amount of material that would reach surrounding neighborhoods in full scale.

An alternate method of data collection was to use a vertical particle collector, a rack made of thin strips of wood and covered with a thin coat

of grease. This was placed down wind of the model and was intended to show the vertical distribution of the airborne particles. The vertical collector was also photographed using the digital camera. Figure 7 shows how the vertical collector was used.

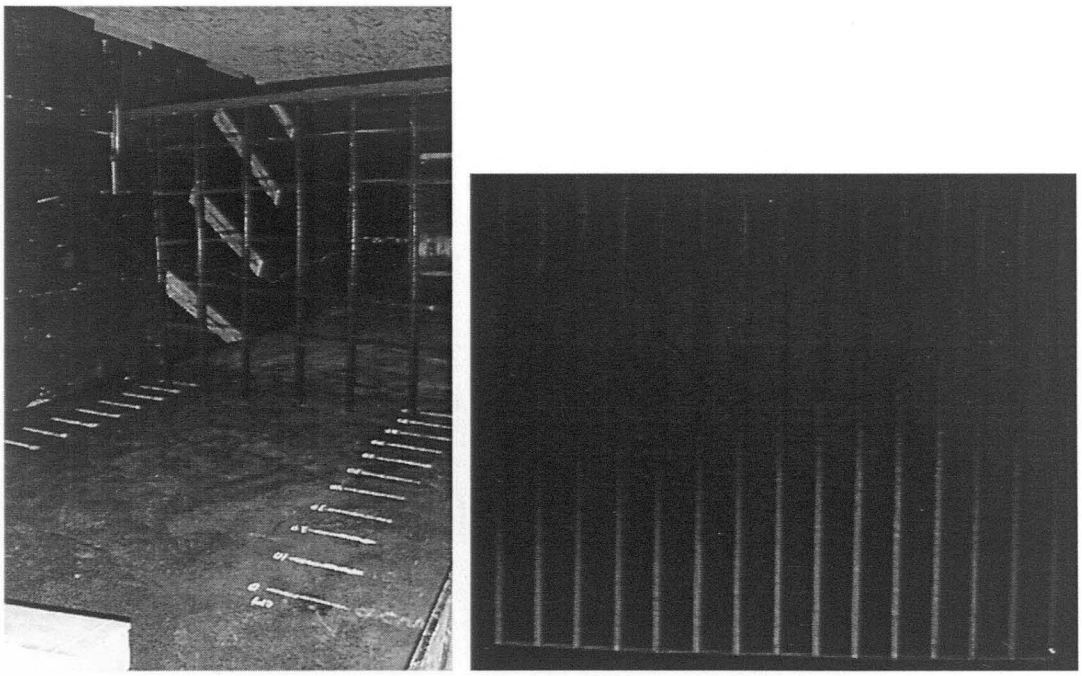

Figure 7: The vertical collector, Left) placement in the wind tunnel, Right) result after test

The vertical data was intended provide insight into the vertical structure of the particulate entrainment. However, no noticeable difference was found for tests involving different parameters. Because the only available camera was employed photographing the area of interest on

the wind tunnel floor throughout the test, only one photo of the vertical collector could be taken for each test after it was finished. Also, to maintain the consistency of the photographic data collection, the camera could never be moved. So the vertical collector had to be moved from its test location to the front of the camera, and a background board placed behind it. Also, between every run, the surface of the collector had to be cleaned, the grease applied to it so the new particles would stick. Care had to be taken to be consistent in the grease application as not to cause any variance in color or the amount of particles that would stick. The final result of the whole vertical collector situation was that the method was difficult, time consuming, cumbersome, provided little information, and was eventually abandoned.

CHAPTER III: RESULTS AND DISCUSSION

This chapter will discuss the results the preceding experiments have yielded. Digital analysis of the photographic data, and the statistical analysis of the mass loss data are presented.

When reviewing the results and drawing conclusions about the data, it is important to note several accidental variations from the predetermined experiment schedule in order to consider how they may effect the usefulness of the results. In Table 2, Run 7 was actually performed using three rows of bushes instead of one. This does not effect the data taken, but has some impact on the completeness of the experiments, and slightly limits the conclusions that can be drawn from the statistical analysis. For the sake of accuracy, the actual experiment schedule performed is given in Table 4, and is repeated in Appendix A.

Other accidental variations from the planned experiment schedule consist of the loss of mass data for Run 17, and an anomaly in Run 12. The missing data for Run 17 can be overcome, because it is identical to Run 15. The only effect of this loss is the reduced ability to determine experimental noise. Run 12 mass data indicates that more mass was collected on the wind tunnel floor than left the model. Clearly a

Table 4: Experiment schedule with hedges

Run	Wind Speed (m/s)	Angle of Attack (°)	Number of Rows	Bush Height (cm)	Thickness (cm)
7	4	0	3	10	3
8	4	30	1	10	4.5
9	6	0	3	10	3
10	4	0	3	10	4.5
11	6	0	1	10	4.5
12	4	30	3	10	3
13	6	30	3	10	4.5
14	6	30	1	10	3
15	5	15	2	7.5	4.5
16	5	15	2	7.5	3
17	5	15	2	7.5	4.5
18	5	15	2	7.5	3
19	4	0	3	5	3
20	4	0	1	5	4.5
21	4	30	1	5	3
22	6	0	3	5	4.5
23	6	30	3	5	3
24	4	30	3	5	4.5
25	6	0	1	5	3
26	6	30	1	5	4.5

measurement error was made. However the mistake was not noticed until long after the completion of the experiments, and the run could not be repeated. As in the case of the Run 1 error, this mistake degrades the amount of useful information that can be concluded from the experiment.

The most important modeling aspect of this experiment that effects its overall usefulness, is the correct recreation of the atmospheric boundary layer. Appendix C shows the resulting boundary layer profile, which matches the planned boundary layer thickness of 20 cm, and has a

roughness height z_0 of 5 cm. Profiles after the addition of the model and bushes are also given in Appendix C.

Digital Photograph Analysis

In Figures 8, 9, and 10, comparison photos between runs with and without bushes are shown. In the tests with shelterbelts, the area between the model and the first bush indicates a deposition pattern that is similar to patterns found without any shelterbelts. There is a dramatic difference, however, down wind of the hedges. The hedges produce an even, wide spread particle distribution which extends across the length of the bush. It is clear that there is much more material on the floor when windbreaks are present. Photographs of each run taken after 15 minutes can be found in Appendix F.

In order to provide a quantitative analysis of the photographs, the following process was applied. The digital photograph files are converted to an ASCII gray scale format, which uses 0 as black and 255 as white. This conversion works well, since the light colored walnut shell dust provides contrast against the black wind tunnel. From the photograph, a cross section, approximately 3 cm long and nearly the width of the picture frame, is chosen at a reference length of 100 cm down stream of the model, which is called the area of interest. The location of this area is outlined in

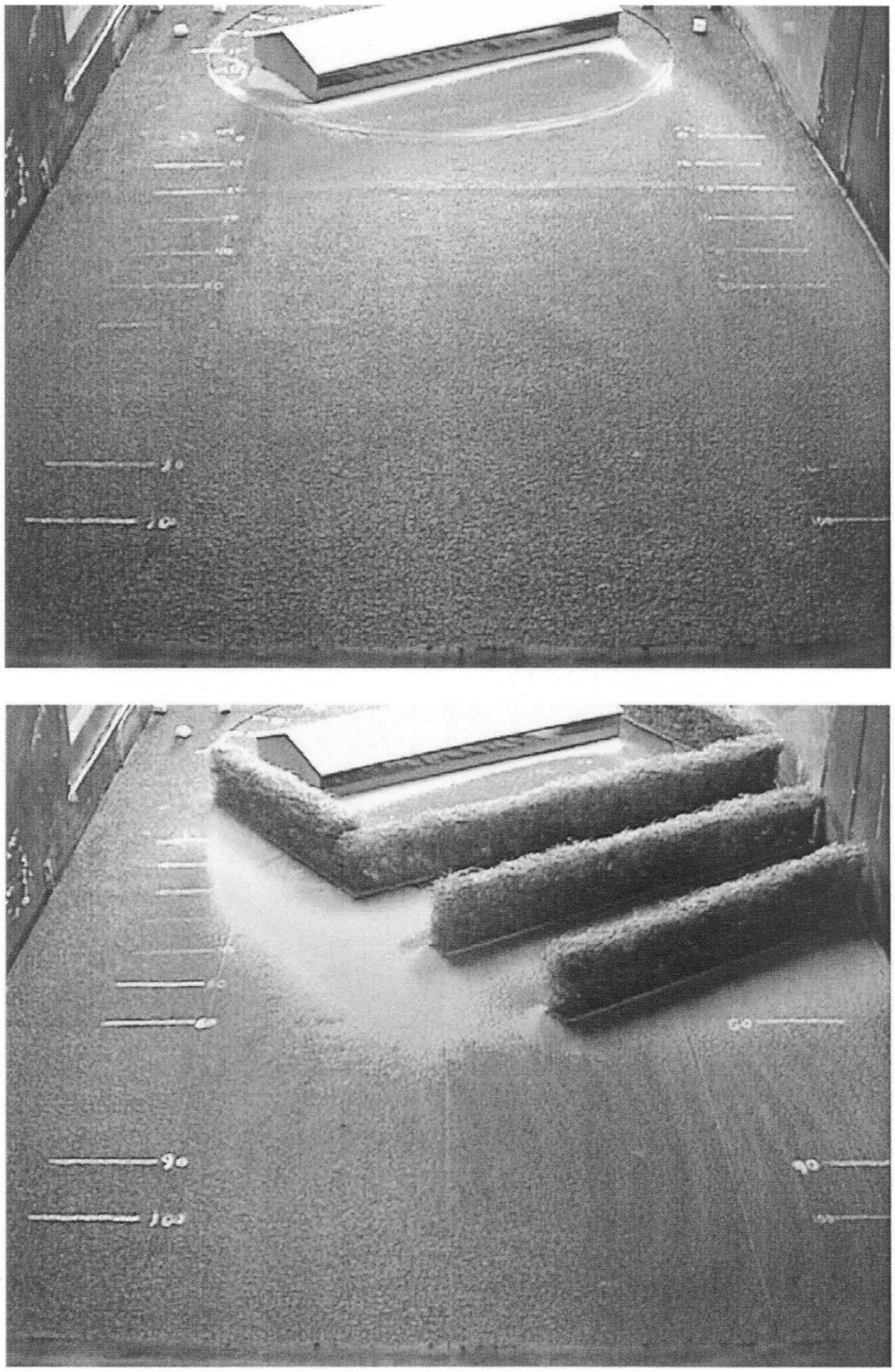

Figure 8: Wind speed 6m/s, angle of attack 30^0

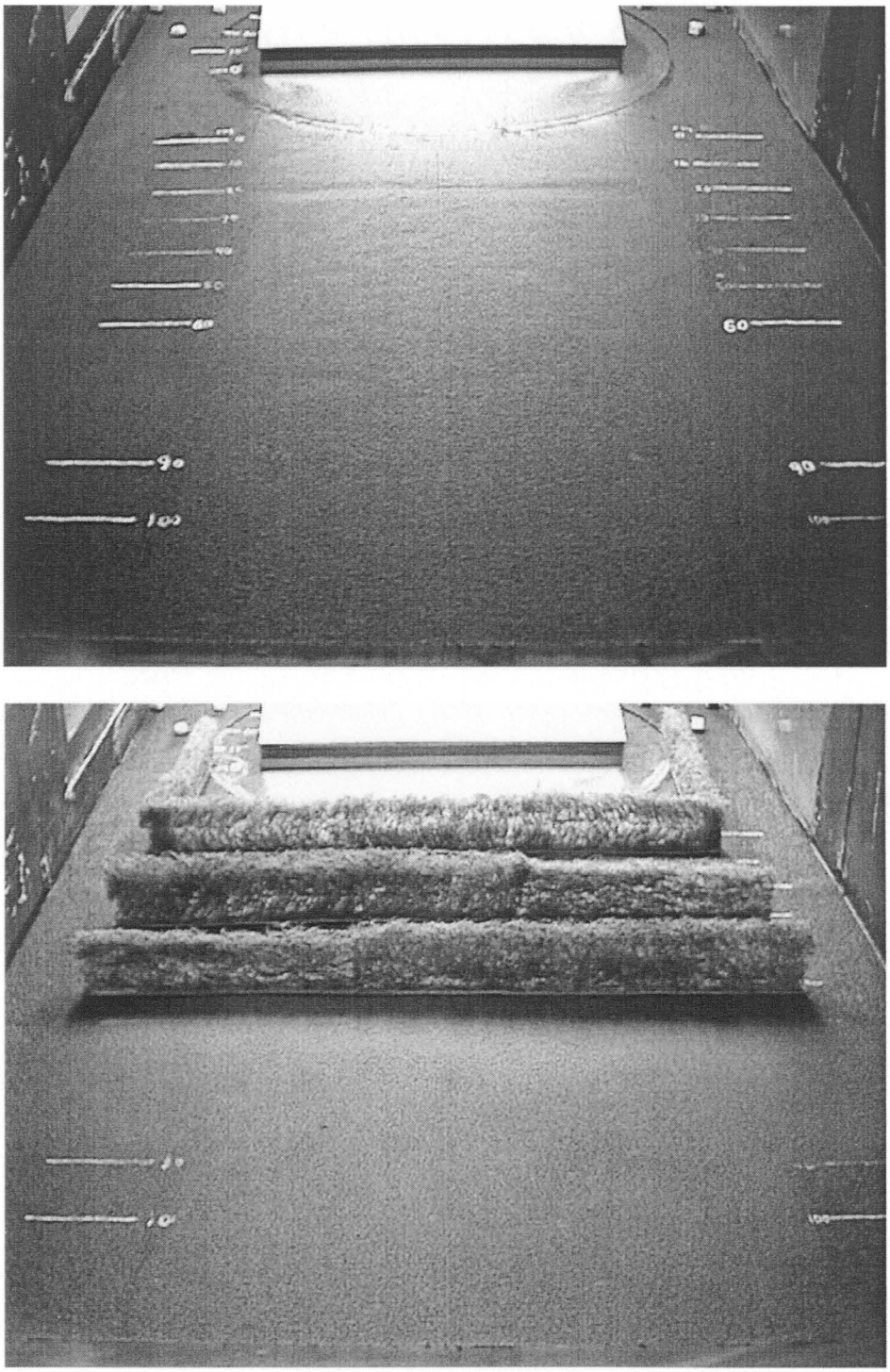

Figure 9: Wind speed 4m/s, angle of attack 0^0

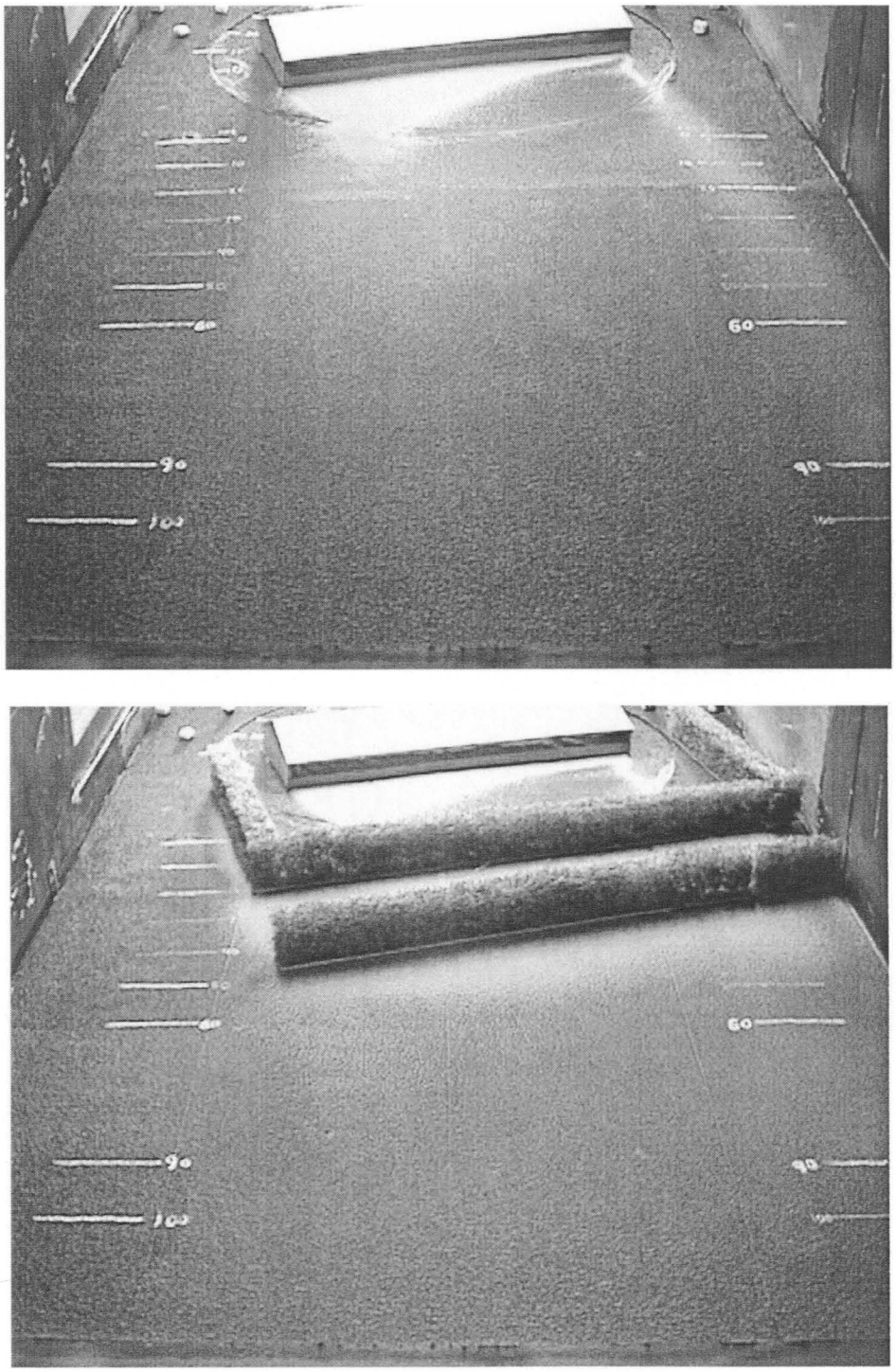

Figure 10: Wind speed 45m/s, angle of attack 15^0

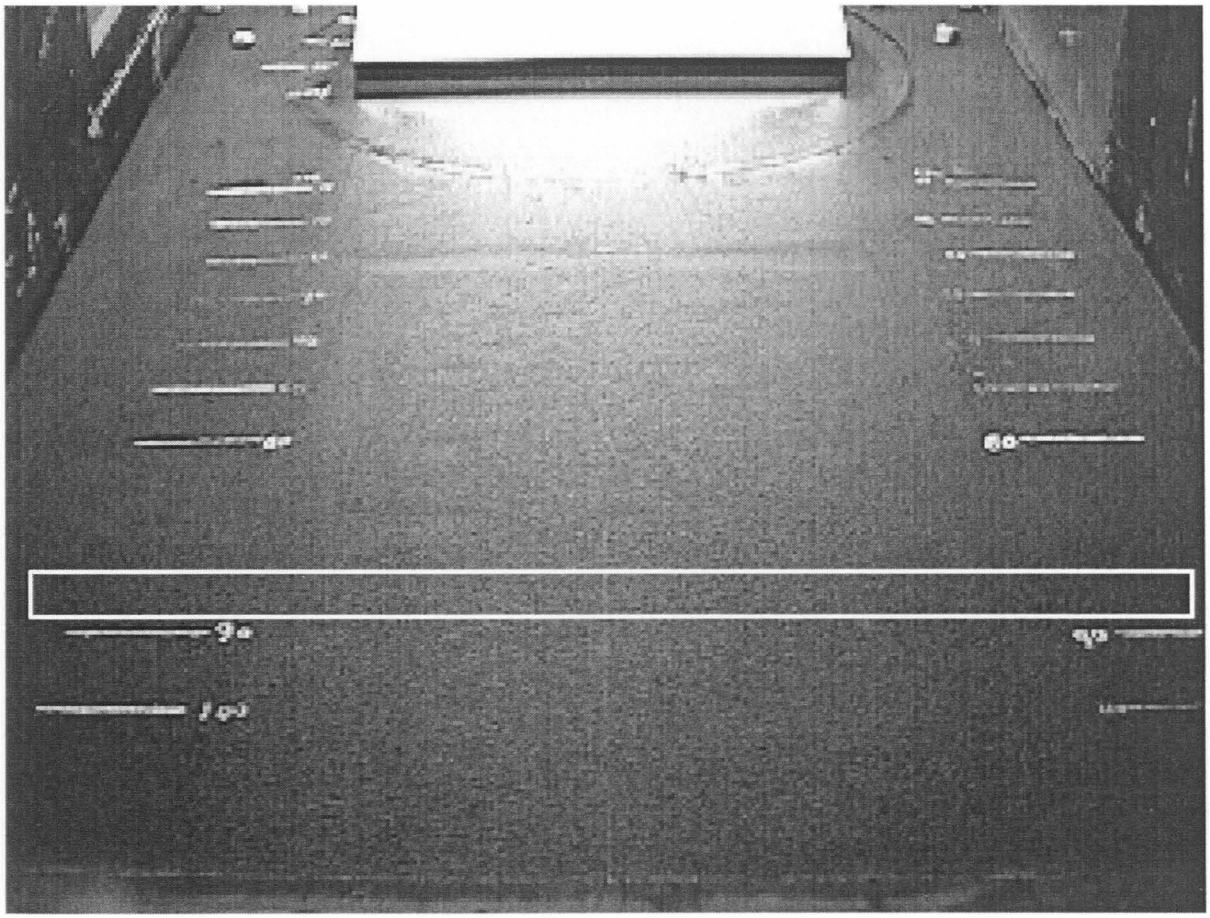

Figure 11: Typical photograph taken during a test run with area of interest outlined in white

white in Figure 11.

The gray scale intensity across this area of interest is averaged in the X direction as defined in Figure 1, to produce a set of values 1 pixel "long", and the same width of the area of interest. This averaging is intended to help filter out any anomalies may appear in some of the pixels. Throughout the experiment, the Y location is measured in pixels,

where 0 is the left side of the photograph. This procedure can performed using the FORTRAN computer code found in Appendix E. A picture of the clean floor is also taken before each test, and the cross sectional intensity resulting from this photo is subtracted from the others. This is to help reduce error from discoloration in the floor, so that the intensity will begin at 0 at all points, regardless of any "spots" on the floor. After taking a photograph and analyzing it as described, we obtain a plot like that shown in Figure 12 by plotting the intensity versus the Y location. As more of the light colored particles accumulate in the area of interest, the intensity increases. This type of plot shows the intensity across the area of interest, and thus directly reveals the amount of accumulation in the area.

As the test progresses, photographs are taken at different times, and this same photographic analysis is repeated. Figure 13 shows all of resultant curves in the same figure. Each curve directly corresponds to the particle accumulation in the area of interest at each time increment during the test. The figure clearly shows the increase of intensity with time throughout the experiment. This series of curves reveals not only the amount of deposit, but also suggests an accumulation rate. A sample of this comparison is shown in Figure 13. Next, each of these curves is integrated over Y, resulting in the total intensity across the entire cross section for each given time. This data is now used to make plots of

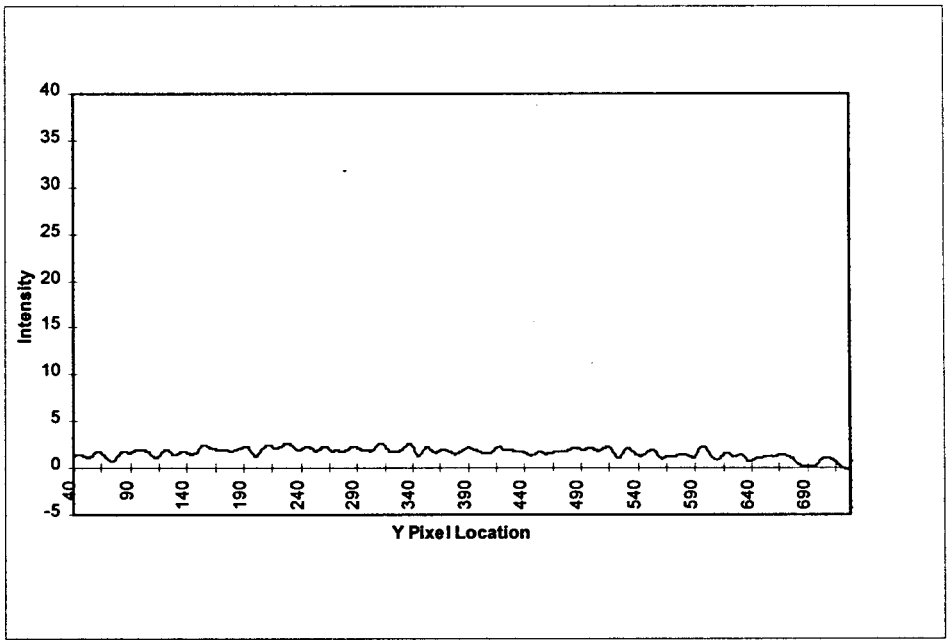

Figure 12: Typical plot of gray scale intensity vs. Y pixel location

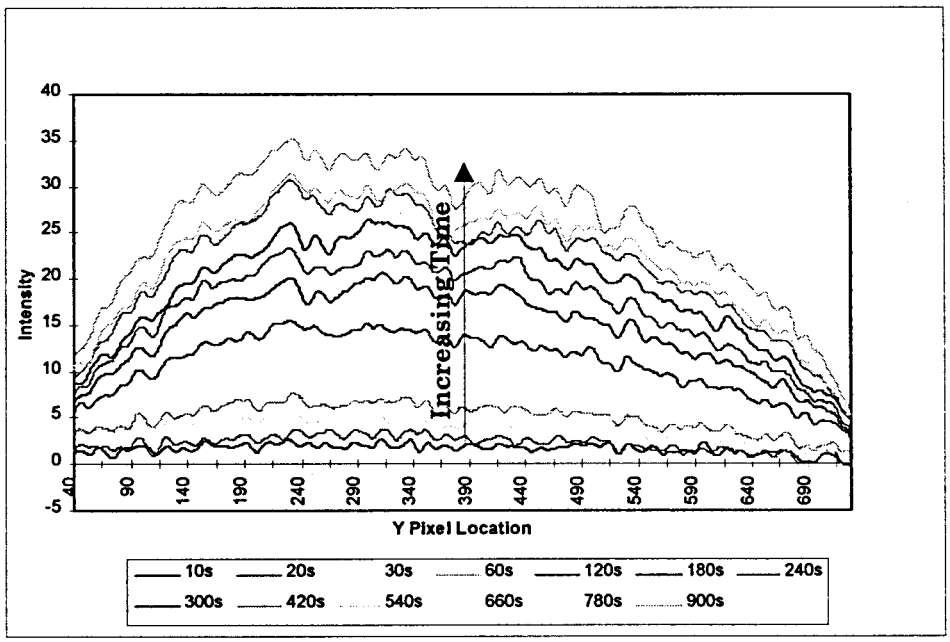

Figure 13: Intensity versus Y pixel location at varying times

total intensity across the area of interest as a function of time. The vertical axis of the chart indicates the total deposit at any time, and the slope of the curve indicates the rate of increase. An example of this curve is given in Figure 14.

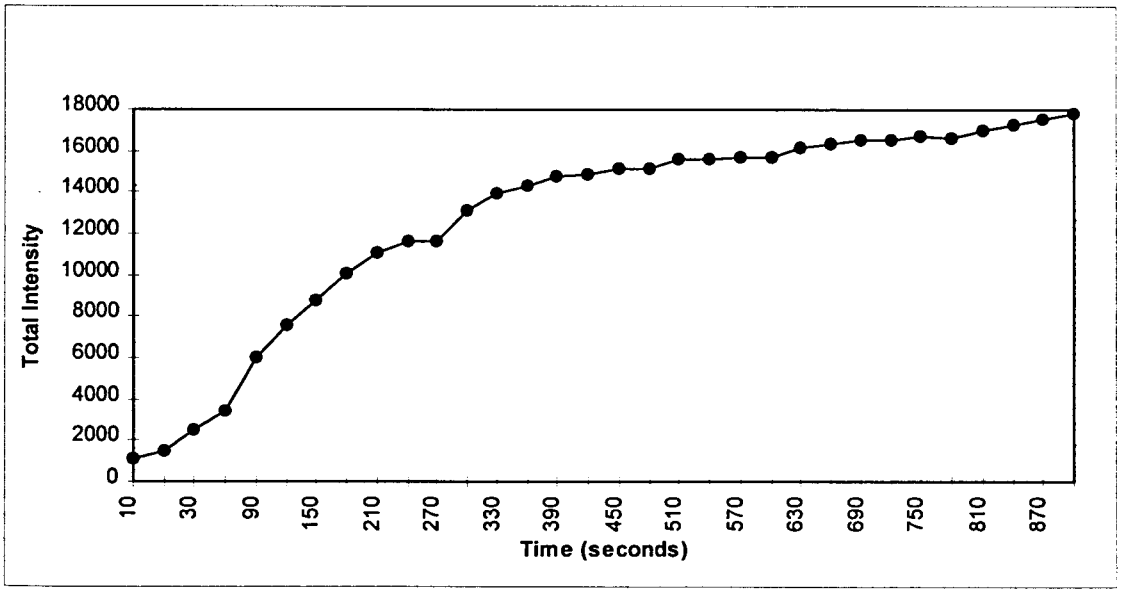

Figure 14: Typical plot of total intensity versus time

This final curve can be integrated, resulting in a simple number. This number represents the running total of all intensity (i.e. particle deposit) at all times. Thus, any difference in deposited amounts of dust and deposit rates will be reflected in this running total, and will allow a direct comparison between each of the tests.

Statistical Analysis of Mass Data

The objective of this analysis is to study the relationship between the percentage of mass lost downstream and the five experimental variables tested: angle of attack, number of bushes, bush height, bush thickness, and wind velocity. Twenty four data points on these factors and percentage of mass lost are recorded for analysis. The importance of these factors in determining the mass loss percentage are investigated.

In order to perform statistical analysis on the data a proposed model must describe the functional relationship between the percentage of mass lost and the five variables. Then the fit of the data to this model can be assessed. Let Y represent the mass loss percentage and ANGLE, BUSH, HT, THICK, and VEL represent the angle of attack, number of bushes, bush height, bush thickness, and wind velocity respectively. The model to be investigated is a polynomial regression model given by:

$$
\begin{aligned}
Y = \quad & \beta_0 + \beta_1(\text{ANGLE}) + \beta_2(\text{BUSH}) + \beta_3(\text{ANGLExBUSH}) + \beta_4(\text{HT}) + \\
& \beta_5(\text{ANGLExHT}) + \beta_6(\text{BUSHxHT}) + \beta_7(\text{THICK}) + \\
& \beta_8(\text{ANGLExTHICK}) + \beta_9(\text{BUSHxTHICK}) + \beta_{10}(\text{HTxTHICK}) + \\
& \beta_{11}(\text{VEL}) + \beta_{12}(\text{ANGLExVEL}) + \beta_{13}(\text{BUSHxVEL}) + \\
& \beta_{14}(\text{HTxVEL}) + \beta_{15}(\text{THICKxVEL}) + \varepsilon
\end{aligned}
$$

where the β_i's are unknown coefficients to be estimated from the data and the ε's are independent and identically distributed normal with mean 0 and variance σ^2. The ε's represent the random component due to noise, or experimental error. The model describes the linear dependence of Y on the five variables. The product terms are called linear-by-linear interaction terms between the five variables.

Estimation of the unknown coefficients in the model is performed using least-squares methods. Hypothesis tests of the form $H_0:\beta_i = 0$ are performed to study the importance of the corresponding effects. If there is evidence indicating that $\beta_i \neq 0$, then the corresponding effect (main or interaction) is important in determining the response Y, and the effect is said to be significant. The importance of the five variables can be judged by the significance of the respective coefficients, namely, β_1, β_2, β_4, β_7, β_{11}.

The data from the 26 runs consists of 24 separate test configurations using 24 combinations of values for ANGLE, BUSH, HT, THICK, and VEL. The first six runs are omitted for the analysis below because the factors are not independent, i.e. BUSH = 0 automatically means HT = THICK = 0.

Fitting the model given above to the data is done by least-squares methods, and this obtains $R^2 = 99.80\%$ and MSE = 4.51 with 2 degrees of

freedom (df). R^2 is called the coefficient of determination which is defined to be the proportion of variation in the percentage of mass lost measurements that is explained by the model that we fit. Values close to 100% are ideal and indicated that the model describes the data adequately. MSE stands for mean square error, an estimator of σ^2.

Table 5 gives the least-squares estimates of the coefficients $\beta_1, ..., \beta_{15}$. For each i, the hypothesis that $H_o:\beta_i = 0$ is tested. Each test yields a t-statistic and a p-value. The t-statistic gives a numerical summary of the test and the p-value is a probability that quantifies how unusual or extreme the t-statistic is, if $H_o:\beta_i = 0$ is indeed true. Unusual values of the t-statistic disagrees with the hypothesis, and rejects H_0. Small values of the p-value (e.g., < 0.05) indicate unusual t-statistic values. If p-value < α = 0.05, then the hypothesis is rejected at the $\alpha = 0.05$ level of significance, there is not enough evidence to support $\beta_i = 0$. Rejecting $H_o:\beta_i = 0$ suggests that $\beta_i \neq 0$ and the corresponding effect is important. Columns 3 and 4 of Table 5 give the t-statistics and the p-values for tests that model coefficients are zero. Tests significant at the 0.05 level are indicated by two asterisks.

Based on the t-tests in Table 5, velocity, bush height and the number of bushes are the most important of the five variables. The

Table 5: Coefficients estimates and results of hypothesis tests

Effect	Coefficient Estimate	t-statistic	p-value
INTERCEPT	53.49	50.93	0.0004**
ANGLE	-4.65	-2.01	0.1822
BUSH	-5.03	-4.48	0.0463**
ANGLE*BUSH	-0.07	-0.07	0.9475
HT	-4.19	-4.83	0.0403**
ANGLE*HT	-1.19	-1.25	0.3384
BUSH*HT	-8.31	-3.69	0.0662
THICK	0.37	0.50	0.6655
ANGLE*THICK	1.91	1.99	0.1845
BUSH*THICK	7.22	3.21	0.0849
HT*THICK	-3.83	-3.08	0.0911
VEL	16.59	19.14	0.0027**
ANGLE*VEL	6.27	6.55	0.0225**
BUSH*VEL	5.99	2.66	0.1171
HT*VEL	-4.29	-3.45	0.0746
THICK*VEL	2.73	2.20	0.1592

appropriate hypothesis tests for the coefficients of these factors are significant at the 0.05 level. Thickness appears to be the least important of the five variables.

The results of mass loss measurements are listed in Appendix A, and are graphed in the following figures. Figure 15 is a plot of the percentage of mass lost downstream versus the angle of attack. The line segments connect mean responses at each value of ANGLE. Figures 16, 17, 18, and 19 are similar plots for BUSH, HT, THICK, and VEL respectively. These plots indicate that THICK does not have strong effect on the response and that the effects of BUSH and HT are more

pronounced at the higher levels. It is clear from these plots that VEL is important in determining the mass lost. These plots indicate what has been concluded about the five factors from the hypothesis tests above.

The results in Table 5 are used to obtain a smaller, more manageable model. It is common practice to eliminate from the polynomial model the least important (highest p-value) of the highest degree terms at each step. In the analysis above, ANGLExBUSH should be deleted first. After a few steps, the equation becomes:

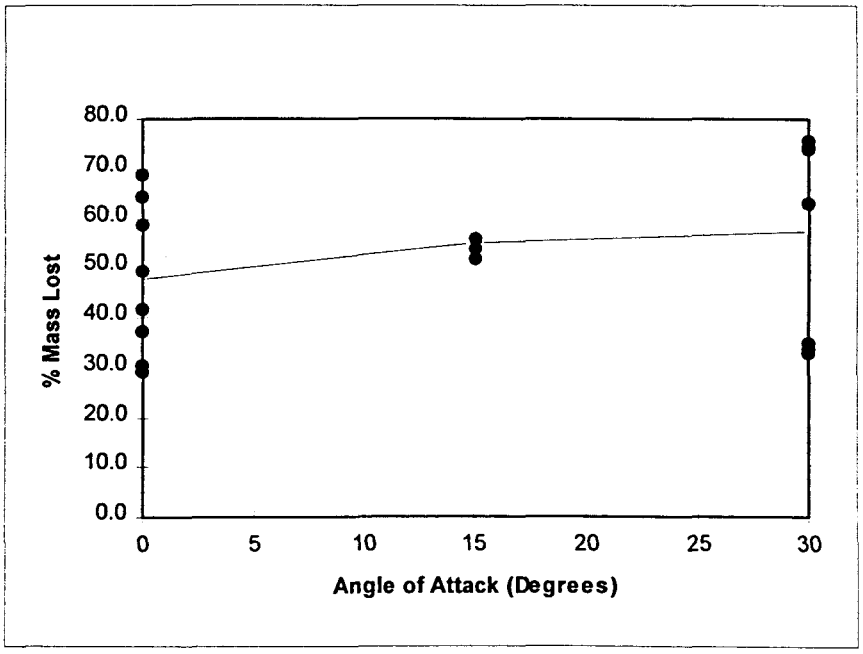

Figure 15: Plot of % mass lost versus angle of attack

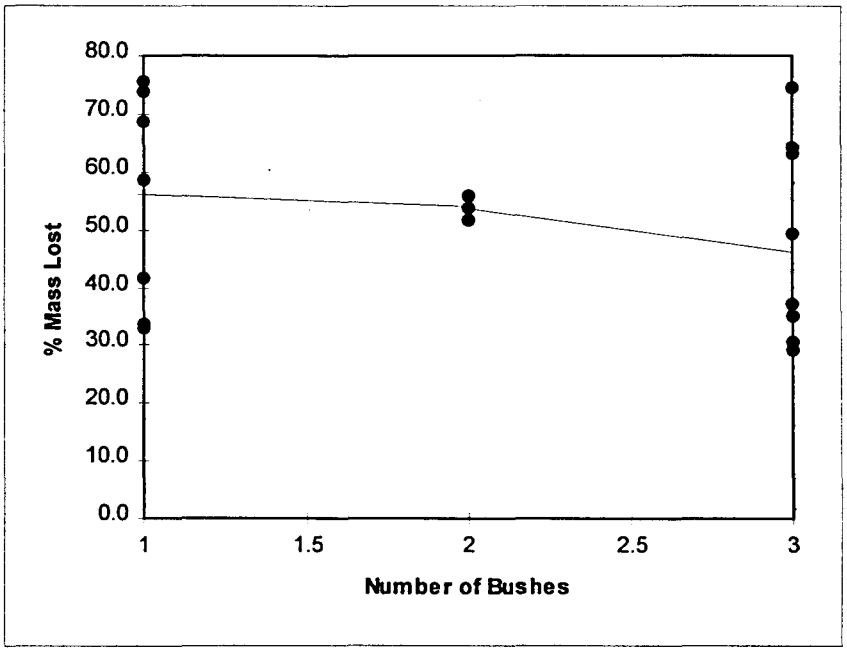

Figure 16: Plot of % mass lost versus number of bushes

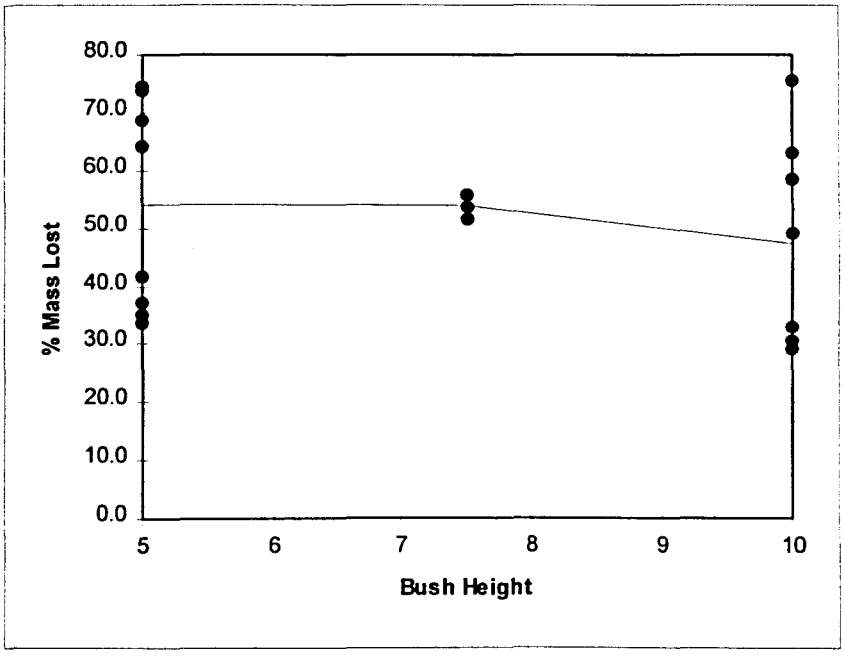

Figure 17: Plot of % mass lost versus bush height

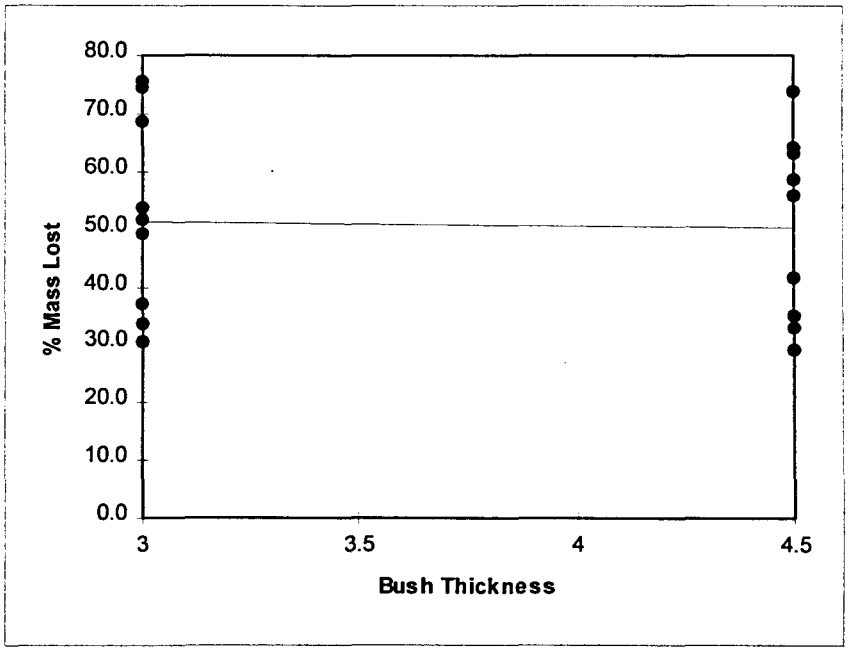

Figure 18: Plot of % mass lost versus bush thickness

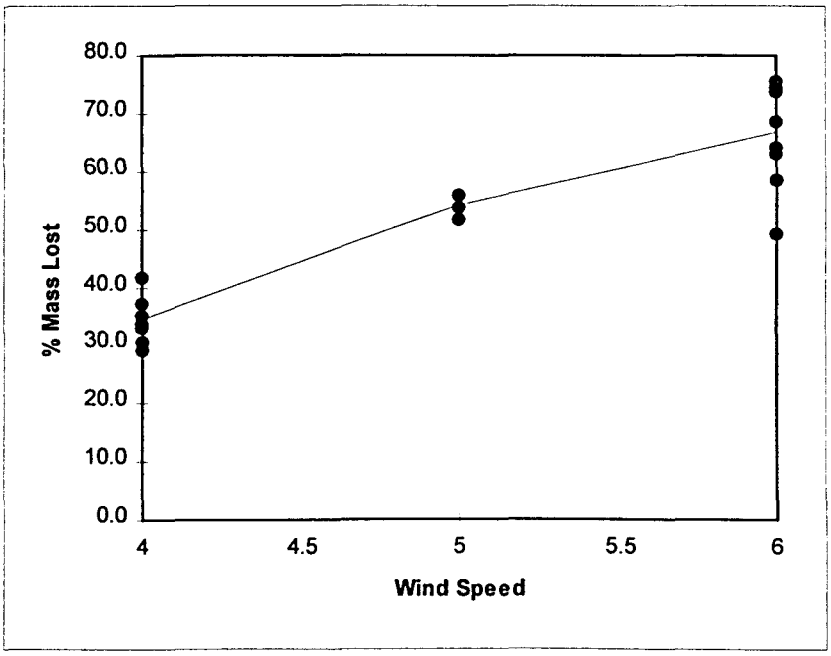

Figure 19: Plot of % mass lost versus bush wind speed

$$\hat{Y} = 51.60 = 0.35(\text{ANGLE}) - 3.29(\text{BUSH}) - 3.59(\text{HT}) - 3.94(\text{BUSHxHT}) - 0.03(\text{THICK}) + 2.85(\text{BUSHxTHICK}) - 1.56(\text{HTxTHICK}) + 15.99(\text{VEL}) + 4.84(\text{ANGLExVEL}) + 1.61(\text{BUSHxVEL}) - 2.02(\text{HTxVEL})$$

Here, $R^2 = 99.13$ %. Further simplifications are possible. The final fitted version is:

$$\hat{Y} = 50.25 + 2.24(\text{ANGLE}) - 2.82(\text{BUSH}) - 3.22(\text{HT}) + 15.62(\text{VEL}) + 4.23(\text{ANGLExVEL})$$

Here, $R^2 = 96.59\%$.

CHAPTER IV: CONCLUSIONS

The overall purpose of this project is to use a wind tunnel model to investigate the emission of dust from swine production facilities. The focus of this thesis is the design, construction, and testing of an appropriate wind tunnel configuration to model the full scale facilities and to conduct initial tests concerning how the dust is carried downstream.

The particular model and test conditions used are detailed in the main body and the appendices of this thesis. One of the goals was to determine how much of the dust that is blown from the building is deposited near the building and how much actually travels farther downstream where it could produce unwanted odors. The following conclusions were reached.

From the photographic data gathered, it is determined that the use of bushes causes an increase of deposit on the wind tunnel floor. This corresponds to a decrease of particle flow out of the wind tunnel. These facts are reinforced by the mass loss data, clearly indicating the differences with and without bushes. A highlight of the mass data showing the best case (minimum) percentage of mass lost using the shelterbelts is given in Table 6.

Table 6: Mass comparison with and without bushes

Wind Speed (m/s)	Angle of Attack (°)	% Lost Without Bushes	Best Case % Lost Using Bushes	% Reduction of % lost
4	0	57.4	29.1	49.3
4	30	75.3	32.8	56.4
5	15	80.0	51.7	35.4
6	0	81.9	49.3	39.8
6	30	96.4	63.0	34.6

Knowing that full scale conditions have been properly modeled, it can be concluded that the results would be similar around an actual hog production building. A successful reduction in mass transport far down stream, ranging from 35% to 56%, would provide a substantial reduction in the offensiveness of odor in surrounding areas.

However, the model is known to be distorted, since not all similarity properties could be met. Also, values found using the digital photograph analysis procedure such as intensity and total intensity can indicate the differences between test runs, but their exact meaning and usefulness in the full scale is unknown. For these reasons, to make the information gathered useful for full scale applications, it remains necessary to perform a small amount of full scale testing. Then, a comparison can be made between the full scale and wind tunnel results.

This comparison can be used to provide the exact relationship between the model and full scale, enabling model results to be directly applicable.

Use of the digital photographic analysis technique has not yet proven successful. Errors in the pictures taken may be caused if any photographic aspect is changed during the experiment, including camera position, shutter speed, aperture, and lighting. In the beginning of the research, it was noticed that the camera mount vibrated in the wind, and a more rigid mount was used to remedy this problem of camera motion. However, inspection of the photographs shows that the brightness in many of the pictures is different, indicating a change of one or more of these photographic factors. In an effort to refine the results and investigate these errors, a scheme to correct the data taken is being undertaken. This method involves using an inert area of the photographs and correcting the intensity of this area to match in all of the photographs. Data corrected using this method will be presented in an upcoming thesis on the same wind tunnel topic by S. Magnus Thernelius.

Based on the statistical analyses of the mass data, it is suggested that velocity, number of bushes, and height of bushes are the most important of the five experimental variables used. Thickness does not have a strong effect, if any, on the mass lost. Velocity appears to be the most important of the five variables. Its effect on the amount of mass lost

downstream may interfere with detection of the significance of other factors, and of interactions between factors. Further experimental runs with velocity kept constant may reveal the importance of these effects. These results can be used to plan future runs based on a smaller set of factors. These runs will reveal not only on the main effects of test variables but also on their interactions effects.

APPENDIX A: EXPERIMENTAL CONDITIONS, VELOCITY, AND MASS DATA

Experiment schedule without hedges

Run	Wind Speed (m/s)	Angle of Attack (o)	% Mass Lost
1	4	0	57.4
2	4	30	75.3
3	5	15	67.5
4	6	0	81.9
5	6	30	96.4
6	5	15	80.0

Experiment schedule with hedges

Run	Wind Speed (m/s)	Angle of Attack (°)	Number of Rows	Bush Height (cm)	Thickness (cm)	% Mass Lost
7	4	0	3	10	3	30.5
8	4	30	1	10	4.5	32.8
9	6	0	3	10	3	49.3
10	4	0	3	10	4.5	29.1
11	6	0	1	10	4.5	58.6
12	4	30	3	10	3	-57.7
13	6	30	3	10	4.5	63.0
14	6	30	1	10	3	75.4
15	5	15	2	7.5	4.5	55.8
16	5	15	2	7.5	3	53.8
17	5	15	2	7.5	4.5	No Data
18	5	15	2	7.5	3	51.7
19	4	0	3	5	3	37.1
20	4	0	1	5	4.5	41.5
21	4	30	1	5	3	33.6
22	6	0	3	5	4.5	64.2
23	6	30	3	5	3	74.4
24	4	30	3	5	4.5	34.9
25	6	0	1	5	3	68.5
26	6	30	1	5	4.5	73.9

Run 1

Conditions:	
Temperature (deg. C):	-3
Pressure (kPa):	98.23192
Number of Samples Collected Per Reading:	5000

Velocity:	
Desired Average Velocity (m/s):	4.00
Actual Average Velocity (m/s):	4.11

Test Information:	
Number of Bushes:	0
Angle of Attack (deg.):	0
Height of Bush(es):	0
Thickness of Bush(es)	0

Mass Relationships:	
Mass Leaving the Model (g):	171.1
Mass Recovered (g):	72.9
Mass Lost Downstream (g):	98.1
Percent Lost Downstream (%):	57.4

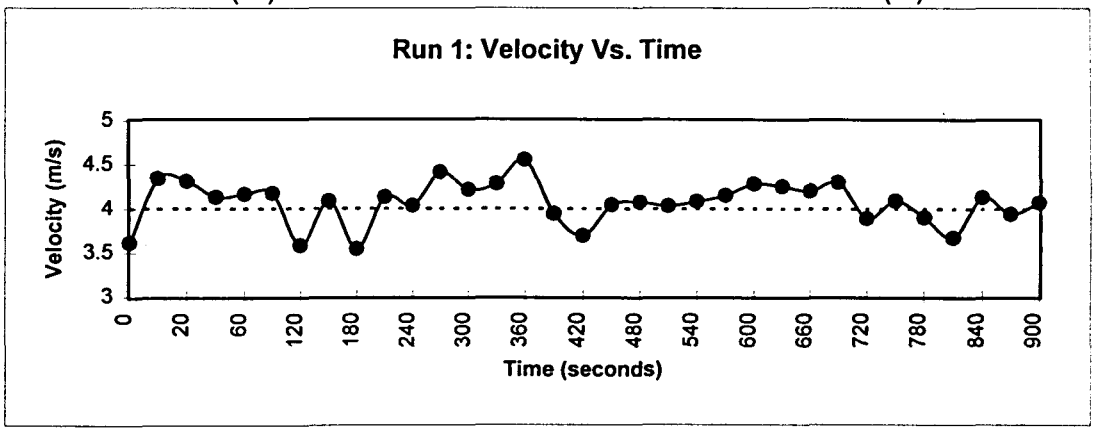

Run 2

Conditions:	
Temperature (deg. C):	-3
Pressure (kPa):	98.09859
Number of Samples Collected Per Reading:	5000

Velocity:	
Desired Average Velocity (m/s):	4.00
Actual Average Velocity (m/s) :	4.11

Test Information:	
Number of Bushes:	0
Angle of Attack (deg.):	30
Height of Bush(es):	0
Thickness of Bush(es):	0

Mass Relationships:	
Mass Leaving the Model (g):	122.0
Mass Recovered (g):	30.2
Mass Lost Downstream (g):	91.8
Percent Lost Downstream (%):	75.3

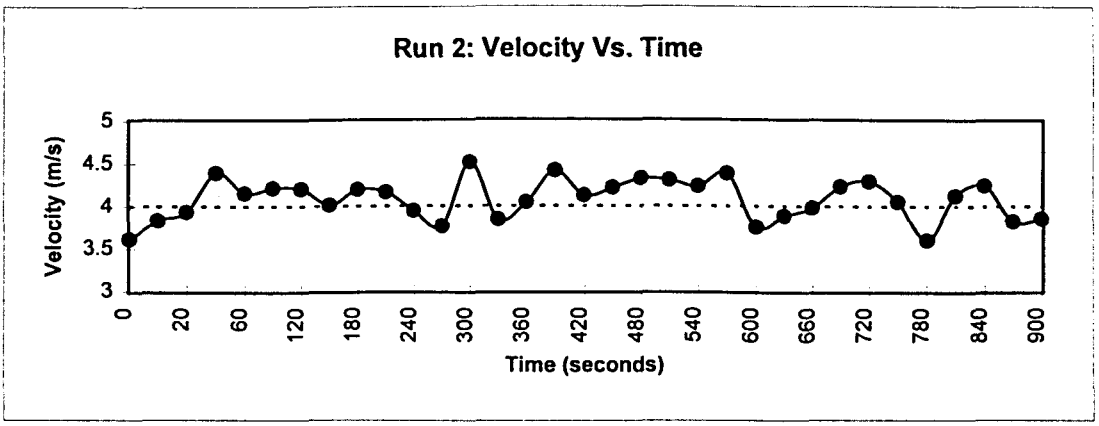

Run 3

Conditions:	
Temperature (deg. C):	0
Pressure (kPa):	97.27200
Number of Samples Collected Per Reading:	5000

Velocity:	
Desired Average Velocity (m/s):	5.00
Actual Average Velocity (m/s):	4.87

Test Information:	
Number of Bushes:	0
Angle of Attack (deg.):	15
Height of Bush(es):	0
Thickness of Bush(es):	0

Mass Relationships:	
Mass Leaving the Model (g):	526.5
Mass Recovered (g):	171.1
Mass Lost Downstream (g):	355.5
Percent Lost Downstream (%):	67.5

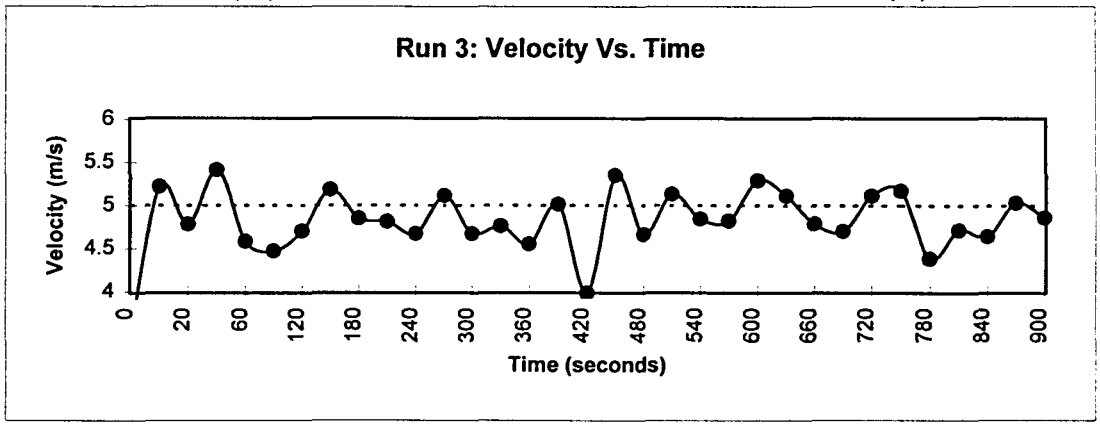

Run 4

Conditions:	
Temperature (deg. C):	-6
Pressure (kPa):	98.79188
Number of Samples Collected per Reading:	5000

Velocity:	
Desired Average Velocity (m/s):	6.00
Actual Average Velocity (m/s) :	6.01

Test Information:	
Number of Bushes:	0
Angle of Attack (deg.):	0
Height of Bush(es):	0
Thickness of Bush(es):	0

Mass Relationships:	
Mass Leaving the Model (g):	984.3
Mass Recovered (g):	178.3
Mass Lost Downstream (g):	806.0
Percent Lost Downstream (%):	81.9

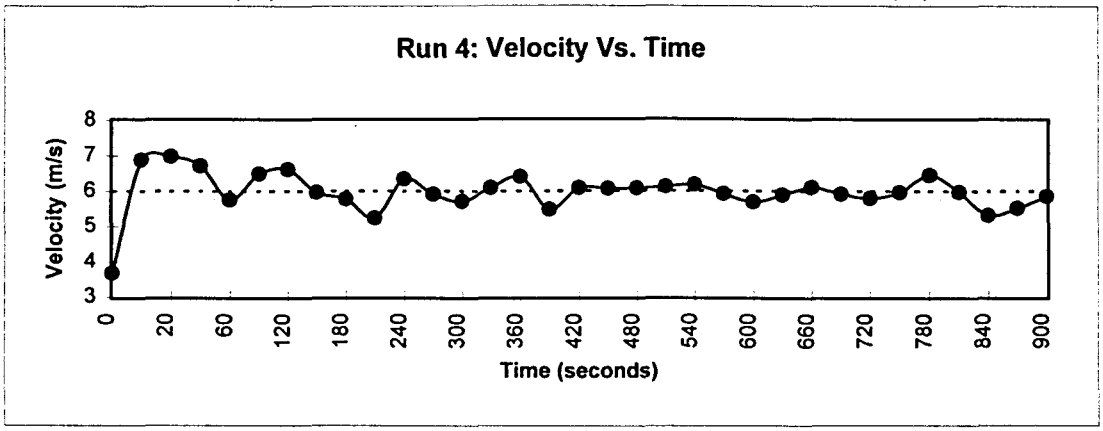

Run 5

Conditions:	
Temperature (deg. C):	-5
Pressure (kPa):	100.48510
Number of Samples Collected per Reading:	5000

Velocity:	
Desired Average Velocity (m/s):	6.00
Actual Average Velocity (m/s):	6.16

Test Information:	
Number of Bushes:	0
Angle of Attack (deg.):	30
Height of Bush(es):	0
Thickness of Bush(es):	0

Mass Relationships:	
Mass Leaving the Model (g):	1047.2
Mass Recovered (g):	37.5
Mass Lost Downstream (g):	1009.7
Percent Lost Downstream (%):	96.4

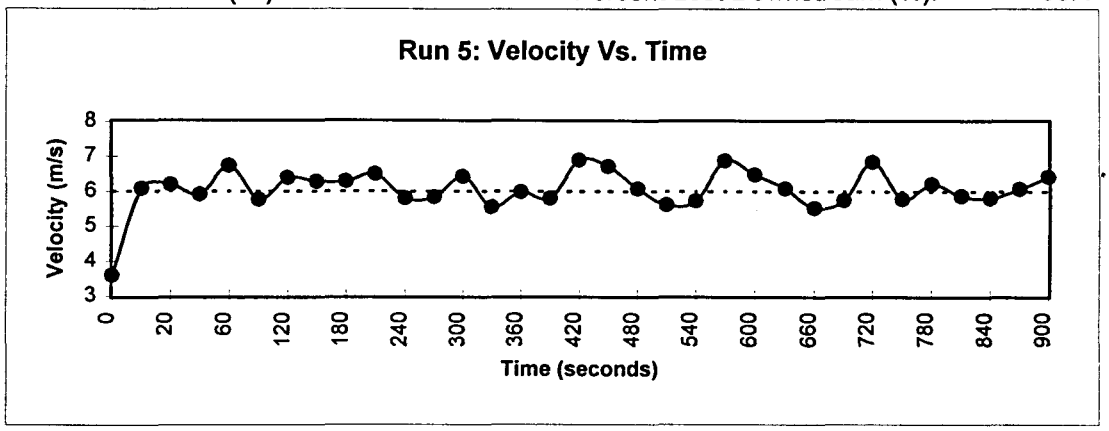

Run 6

Conditions:	
Temperature (deg. C):	-10
Pressure (kPa):	100.44510
Number of Samples Collected per Reading:	5000

Velocity:	
Desired Average Velocity (m/s):	5.00
Actual Average Velocity (m/s):	5.11

Test Information:	
Number of Bushes:	0
Angle of Attack (deg.):	15
Height of Bush(es):	0
Thickness of Bush(es):	0

Mass Relationships:	
Mass Leaving the Model (g):	570.3
Mass Recovered (g):	114.0
Mass Lost Downstream (g):	456.3
Percent Lost Downstream (%):	80.0

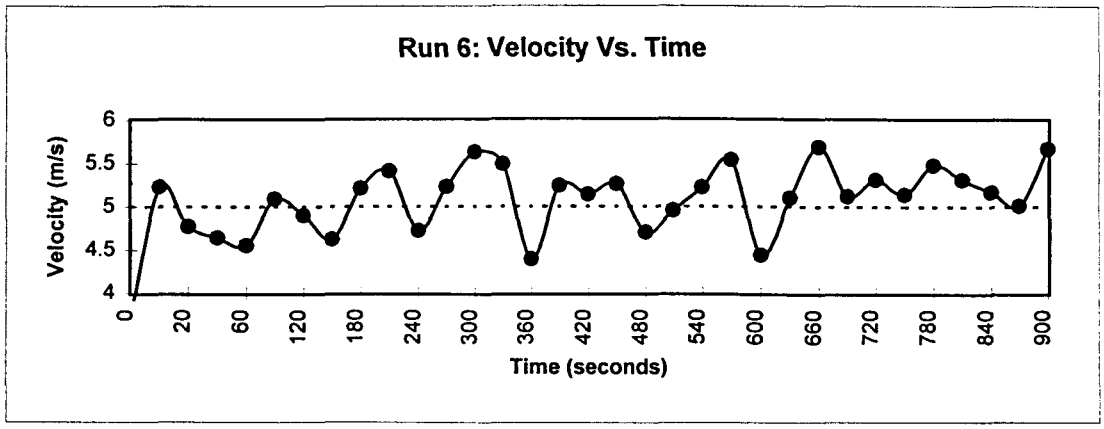

Run 7

Conditions:	
Temperature (deg. C):	-7
Pressure (kPa):	100.36510
Number of Samples Collected per Reading:	5000

Velocity:	
Desired Average Velocity (m/s):	4.00
Actual Average Velocity (m/s):	4.03

Test Information:	
Number of Bushes:	3
Angle of Attack (deg.):	0
Height of Bush(es):	10
Thickness of Bush(es):	3

Mass Relationships:	
Mass Leaving the Model (g):	127.8
Mass Recovered (g):	88.8
Mass Lost Downstream (g):	39.0
Percent Lost Downstream (%):	30.5

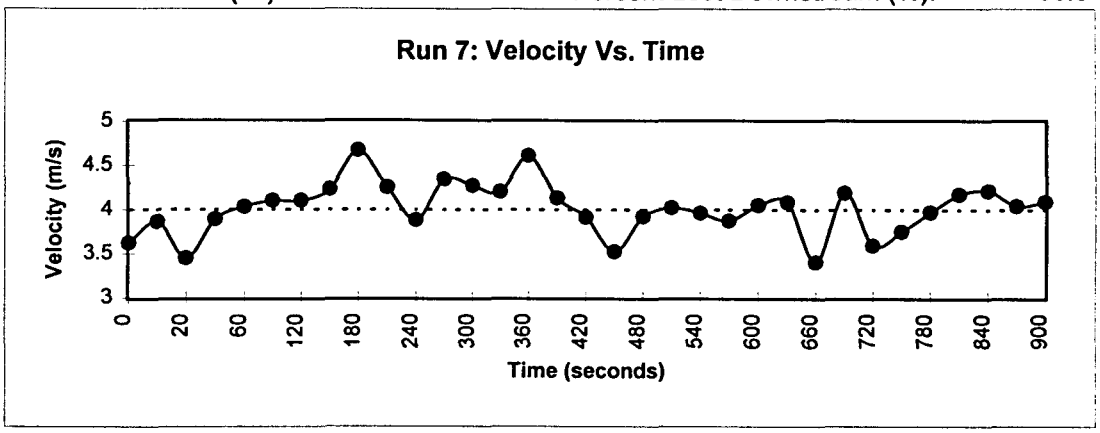

Run 8

Conditions:	
Temperature (deg. C):	-3
Pressure (kPa):	97.25867
Number of Samples Collected per Reading:	5000

Velocity:	
Desired Average Velocity (m/s):	4.00
Actual Average Velocity (m/s) :	4.06

Test Information:	
Number of Bushes:	1
Angle of Attack (deg.):	30
Height of Bush(es):	10
Thickness of Bush(es):	4.5

Mass Relationships:	
Mass Leaving the Model (g):	73.9
Mass Recovered (g):	49.6
Mass Lost Downstream (g):	24.2
Percent Lost Downstream (%):	32.8

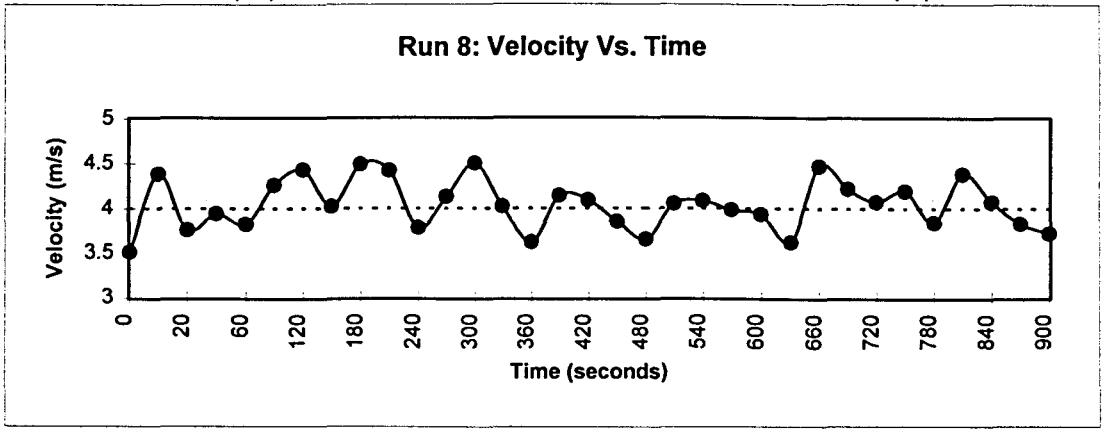

Run 9

Conditions:	
Temperature (deg. C):	-2
Pressure (kPa):	99.24517
Number of Samples Collected per Reading:	5000

Velocity:	
Desired Average Velocity (m/s):	6.00
Actual Average Velocity (m/s):	6.03

Test Information:	
Number of Bushes:	3
Angle of Attack (deg.):	0
Height of Bush(es):	10
Thickness of Bush(es):	3

Mass Relationships:	
Mass Leaving the Model (g):	1027.2
Mass Recovered (g):	520.7
Mass Lost Downstream (g):	506.5
Percent Lost Downstream (%):	49.3

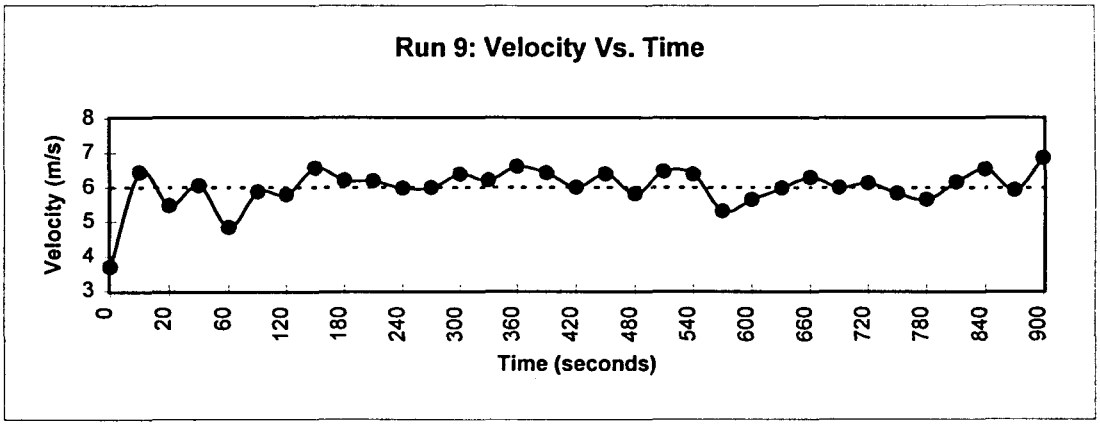

Run 10

Conditions:	
Temperature (deg. C):	0
Pressure (kPa):	96.65872
Number of Samples Collected per Reading:	5000

Velocity:	
Desired Average Velocity (m/s):	4.00
Actual Average Velocity (m/s):	3.95

Test Information:	
Number of Bushes:	3
Angle of Attack (deg.):	0
Height of Bush(es):	10
Thickness of Bush(es):	4.5

Mass Relationships:	
Mass Leaving the Model (g):	74.5
Mass Recovered (g):	52.8
Mass Lost Downstream (g):	21.7
Percent Lost Downstream (%):	29.1

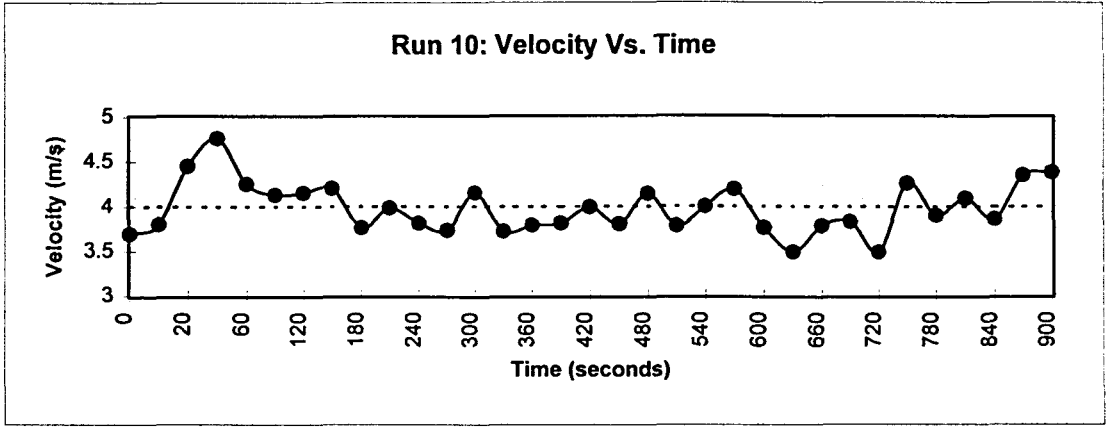

Run 11

Conditions:	
Temperature (deg. C):	-7
Pressure (kPa):	99.99178
Number of Samples Collected per Reading:	5000

Velocity:	
Desired Average Velocity (m/s):	6.00
Actual Average Velocity (m/s):	6.06

Test Information:	
Number of Bushes:	1
Angle of Attack (deg.):	0
Height of Bush(es):	10
Thickness of Bush(es):	4.5

Mass Relationships:	
Mass Leaving the Model (g):	1004.4
Mass Recovered (g):	415.4
Mass Lost Downstream (g):	588.9
Percent Lost Downstream (%):	58.6

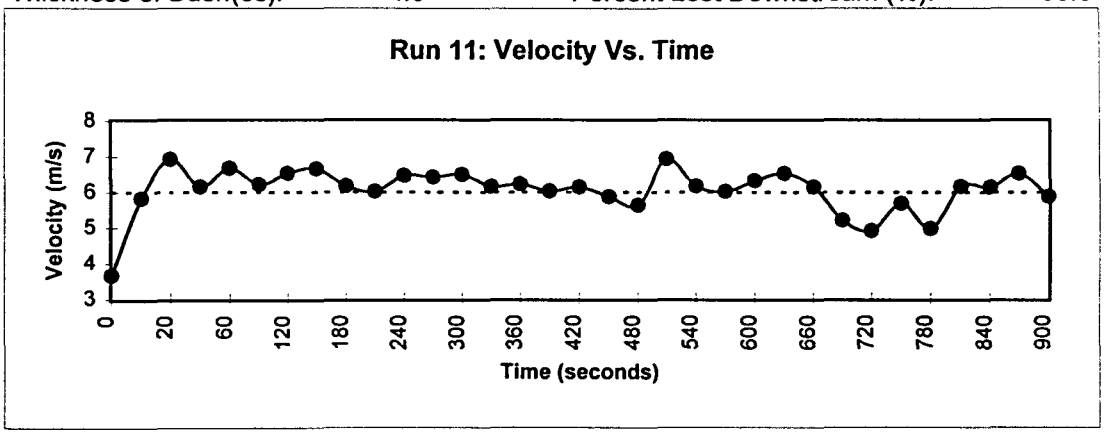

Run 12

Conditions:	
Temperature (deg. C):	-4
Pressure (kPa):	97.32533
Number of Samples Collected per Reading:	5000

Velocity:	
Desired Average Velocity (m/s):	4.00
Actual Average Velocity (m/s):	3.97

Test Information:	
Number of Bushes:	3
Angle of Attack (deg.):	30
Height of Bush(es):	10
Thickness of Bush(es):	3

Mass Relationships:	
Mass Leaving the Model (g):	53.2
Mass Recovered (g):	83.9
Mass Lost Downstream (g):	-30.7
Percent Lost Downstream (%):	-57.7

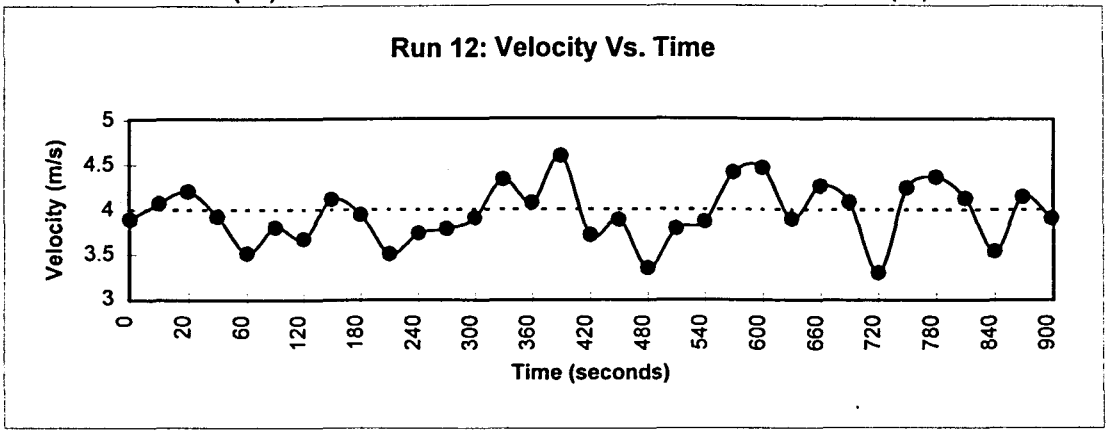

Run 13

Conditions:	
Temperature (deg. C):	-7
Pressure (kPa):	99.59181
Number of Samples Collected per Reading:	5000

Velocity:	
Desired Average Velocity (m/s):	6.00
Actual Average Velocity (m/s):	6.03

Test Information:	
Number of Bushes:	3
Angle of Attack (deg.):	30
Height of Bush(es):	10
Thickness of Bush(es):	4.5

Mass Relationships:	
Mass Leaving the Model (g):	782.3
Mass Recovered (g):	289.7
Mass Lost Downstream (g):	492.6
Percent Lost Downstream (%):	63.0

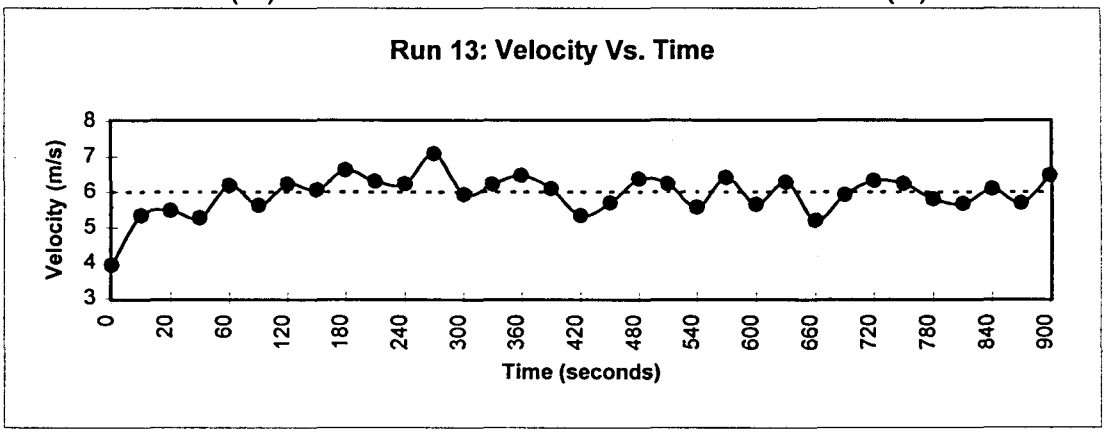

Run 14

Conditions:	
Temperature (deg. C):	-12
Pressure (kPa):	99.59181
Number of Samples Collected per Reading:	5000

Velocity:	
Desired Average Velocity (m/s):	6.00
Actual Average Velocity (m/s):	6.11

Test Information:	
Number of Bushes:	1
Angle of Attack (deg.):	30
Height of Bush(es):	10
Thickness of Bush(es):	3

Mass Relationships:	
Mass Leaving the Model (g):	870.1
Mass Recovered (g):	214.2
Mass Lost Downstream (g):	655.9
Percent Lost Downstream (%):	75.4

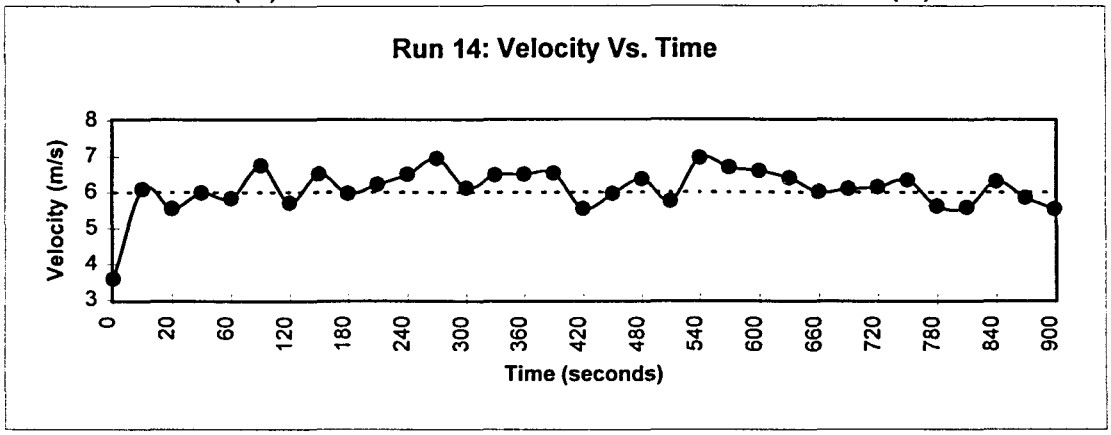

Run 15

Conditions:	
Temperature (deg. C):	-10
Pressure (kPa):	99.56514
Number of Samples Collected per Reading:	5000

Velocity:	
Desired Average Velocity (m/s):	5.00
Actual Average Velocity (m/s):	5.02

Test Information:	
Number of Bushes:	2
Angle of Attack (deg.):	15
Height of Bush(es):	7.5
Thickness of Bush(es):	4.5

Mass Relationships:	
Mass Leaving the Model (g):	471.8
Mass Recovered (g):	208.7
Mass Lost Downstream (g):	263.1
Percent Lost Downstream (%):	55.8

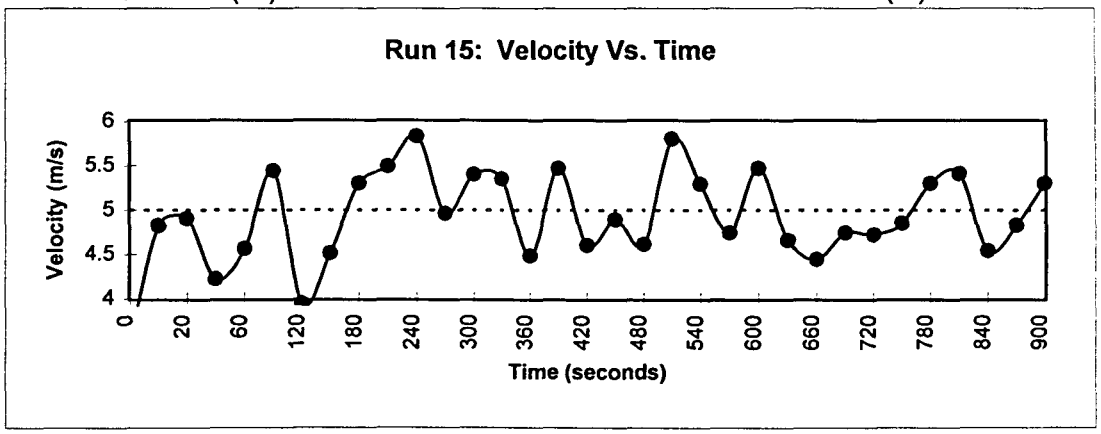

Run 16

Conditions:	
Temperature (deg. C):	-10
Pressure (kPa):	99.19184
Number of Samples Collected per Reading:	5000

Velocity:	
Desired Average Velocity (m/s):	5.00
Actual Average Velocity (m/s):	5.02

Test Information:	
Number of Bushes:	2
Angle of Attack (deg.):	15
Height of Bush(es):	7.5
Thickness of Bush(es):	3

Mass Relationships:	
Mass Leaving the Model (g):	420.6
Mass Recovered (g):	194.3
Mass Lost Downstream (g):	226.3
Percent Lost Downstream (%):	53.8

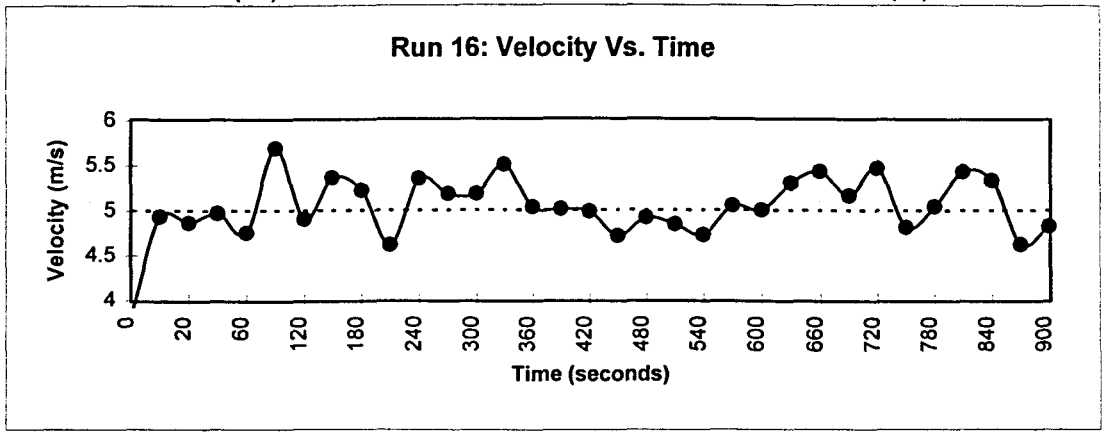

Run 17

Conditions:	
Temperature (deg. C):	No Data
Pressure (kPa):	No Data
Number of Samples Collected per Reading:	No Data

Velocity:	
Desired Average Velocity (m/s):	5.00
Actual Average Velocity (m/s):	No Data

Test Information:	
Number of Bushes:	2
Angle of Attack (deg.):	15
Height of Bush(es):	7.5
Thickness of Bush(es):	4.5

Mass Relationships:	
Mass Leaving the Model (g):	No Data
Mass Recovered (g):	No Data
Mass Lost Downstream (g):	No Data
Percent Lost Downstream (%):	No Data

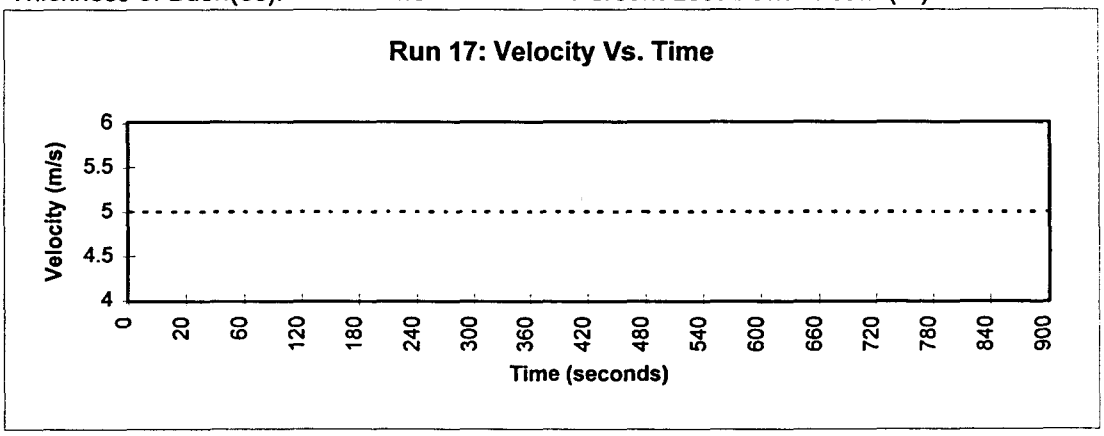

Run 18

Conditions:	
Temperature (deg. C):	-10
Pressure (kPa):	99.19184
Number of Samples Collected per Reading:	5000

Velocity:	
Desired Average Velocity (m/s):	5.00
Actual Average Velocity (m/s):	5.04

Test Information:	
Number of Bushes:	2
Angle of Attack (deg.):	15
Height of Bush(es):	7.5
Thickness of Bush(es):	3

Mass Relationships:	
Mass Leaving the Model (g):	436.0
Mass Recovered (g):	210.5
Mass Lost Downstream (g):	225.5
Percent Lost Downstream (%):	51.7

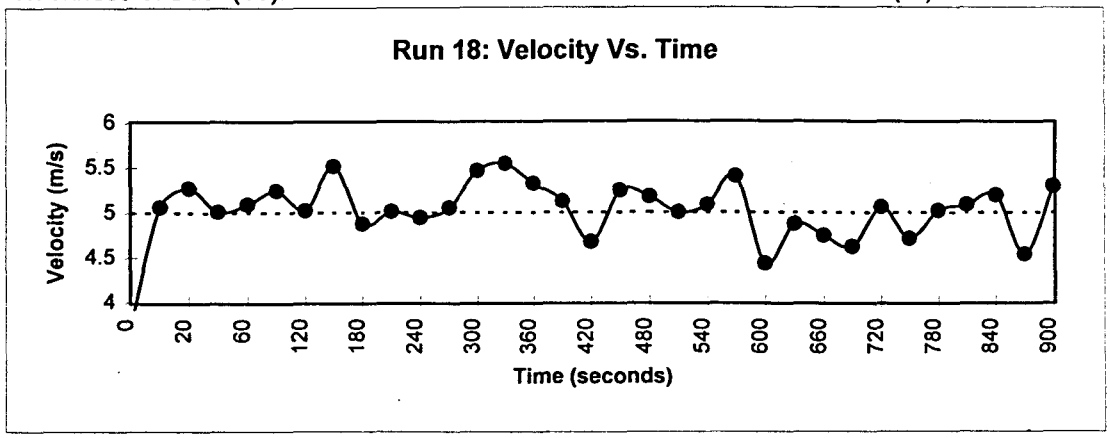

Run 19

Conditions:	
Temperature (deg. C):	-6
Pressure (kPa):	99.40516
Number of Samples Collected per Reading:	5000

Velocity:	
Desired Average Velocity (m/s):	4.00
Actual Average Velocity (m/s):	4.08

Test Information:	
Number of Bushes:	3
Angle of Attack (deg.):	0
Height of Bush(es):	5
Thickness of Bush(es):	3

Mass Relationships:	
Mass Leaving the Model (g):	66.3
Mass Recovered (g):	41.8
Mass Lost Downstream (g):	24.6
Percent Lost Downstream (%):	37.1

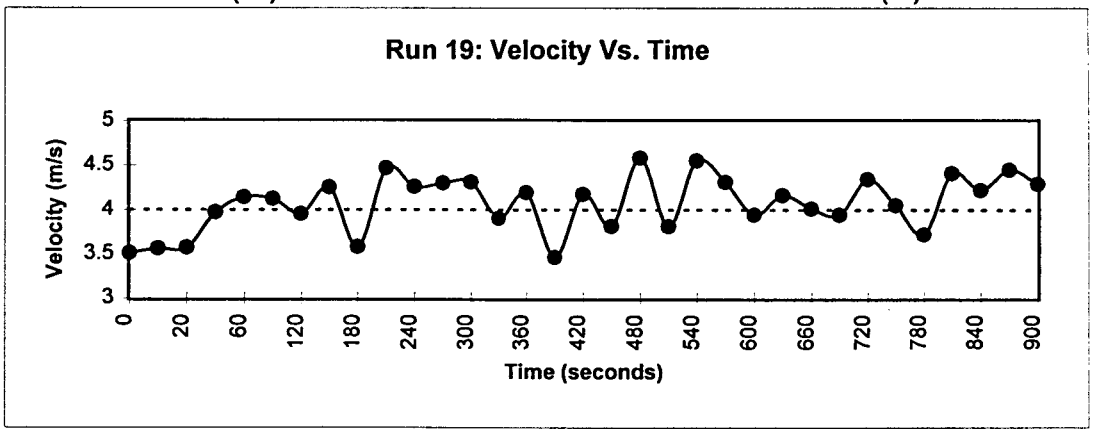

Run 20

Conditions:	
Temperature (deg. C):	-10
Pressure (kPa):	99.12518
Number of Samples Collected per Reading:	5000

Velocity:	
Desired Average Velocity (m/s):	4.00
Actual Average Velocity (m/s):	4.03

Test Information:	
Number of Bushes:	1
Angle of Attack (deg.):	0
Height of Bush(es):	5
Thickness of Bush(es):	4.5

Mass Relationships:	
Mass Leaving the Model (g):	51.8
Mass Recovered (g):	30.3
Mass Lost Downstream (g):	21.5
Percent Lost Downstream (%):	41.5

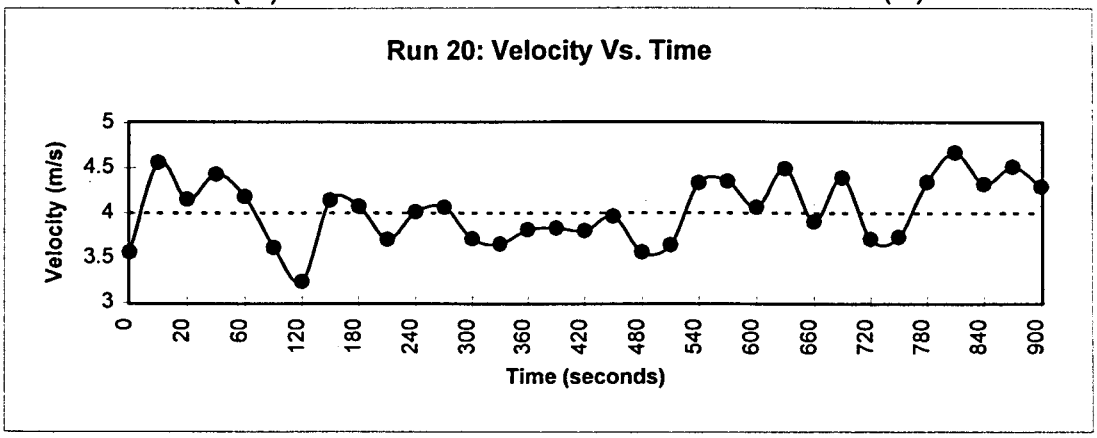

Run 21

Conditions:	
Temperature (deg. C):	-14
Pressure (kPa):	99.40516
Number of Samples Collected per Reading:	5000

Velocity:	
Desired Average Velocity (m/s):	4.00
Actual Average Velocity (m/s):	4.03

Test Information:	
Number of Bushes:	1
Angle of Attack (deg.):	30
Height of Bush(es):	5
Thickness of Bush(es):	3

Mass Relationships:	
Mass Leaving the Model (g):	48.6
Mass Recovered (g):	32.3
Mass Lost Downstream (g):	16.3
Percent Lost Downstream (%):	33.6

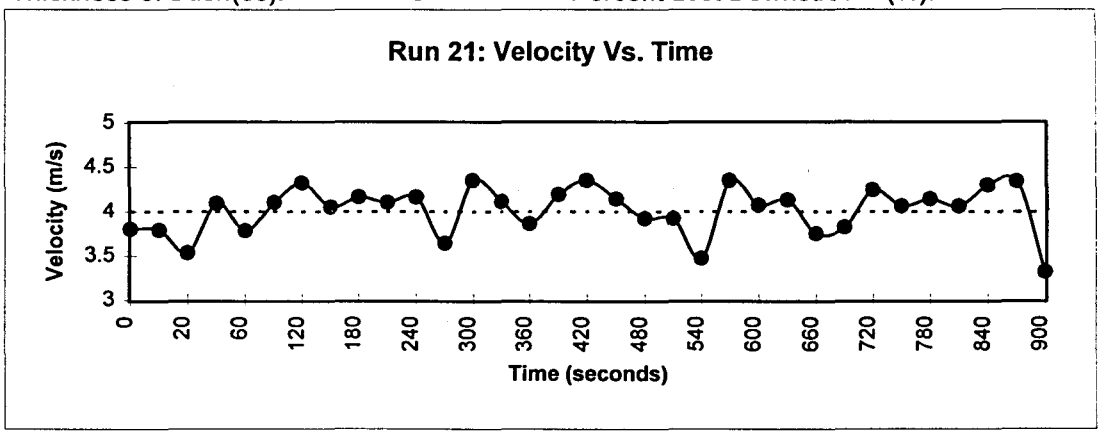

Run 22

Conditions:	
Temperature (deg. C):	-4
Pressure (kPa):	98.48524
Number of Samples Collected per Reading:	5000

Velocity:	
Desired Average Velocity (m/s):	6.00
Actual Average Velocity (m/s):	5.96

Test Information:	
Number of Bushes:	1
Angle of Attack (deg.):	0
Height of Bush(es):	5
Thickness of Bush(es):	4.5

Mass Relationships:	
Mass Leaving the Model (g):	754.8
Mass Recovered (g):	269.9
Mass Lost Downstream (g):	484.9
Percent Lost Downstream (%):	64.2

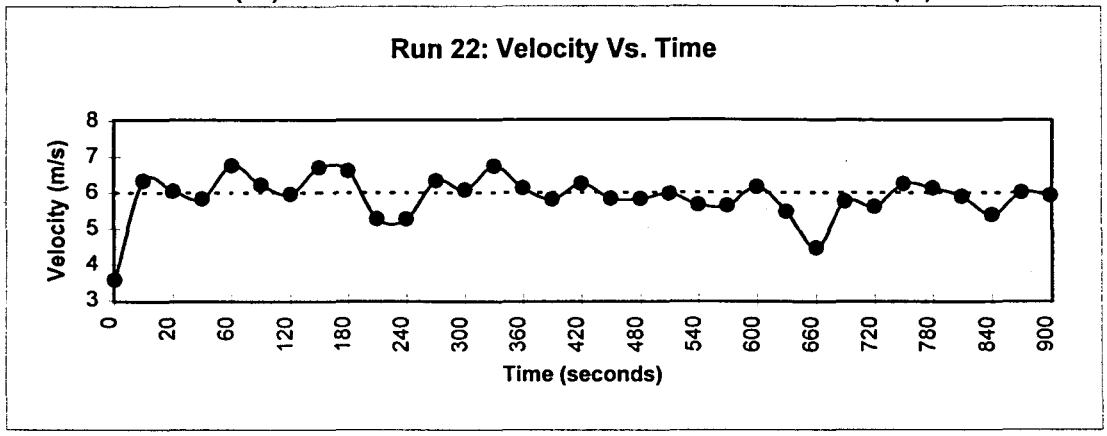

Run 23

Conditions:	
Temperature (deg. C):	-4
Pressure (kPa):	98.48524
Number of Samples Collected per Reading:	5000

Velocity:	
Desired Average Velocity (m/s):	6.00
Actual Average Velocity (m/s):	5.92

Test Information:	
Number of Bushes:	3
Angle of Attack (deg.):	30
Height of Bush(es):	5
Thickness of Bush(es):	3

Mass Relationships:	
Mass Leaving the Model (g):	630.9
Mass Recovered (g):	161.6
Mass Lost Downstream (g):	469.2
Percent Lost Downstream (%):	74.4

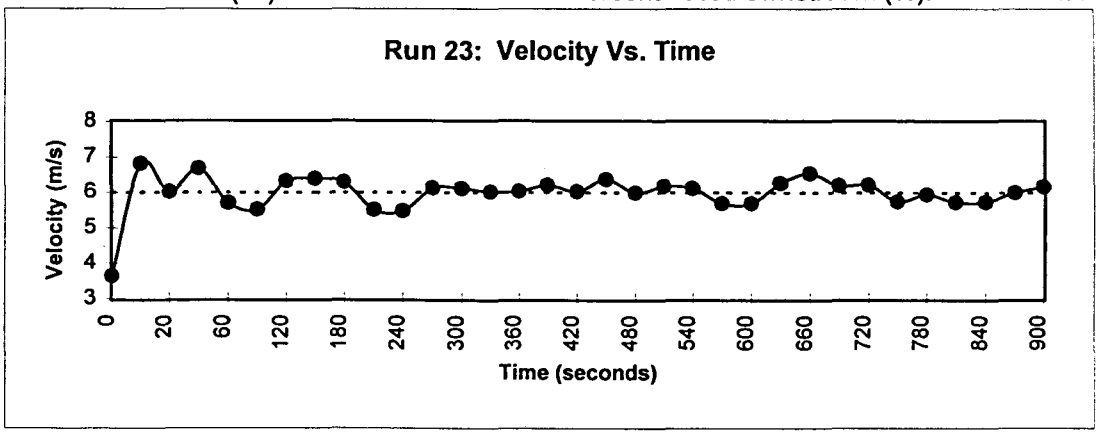

Run 24

Conditions:	
Temperature (deg. C):	-14
Pressure (kPa):	99.40516
Number of Samples Collected per Reading:	5000

Velocity:	
Desired Average Velocity (m/s):	4.00
Actual Average Velocity (m/s):	4.06

Test Information:	
Number of Bushes:	3
Angle of Attack (deg.):	30
Height of Bush(es):	5
Thickness of Bush(es):	4.5

Mass Relationships:	
Mass Leaving the Model (g):	88.3
Mass Recovered (g):	57.5
Mass Lost Downstream (g):	30.8
Percent Lost Downstream (%):	34.9

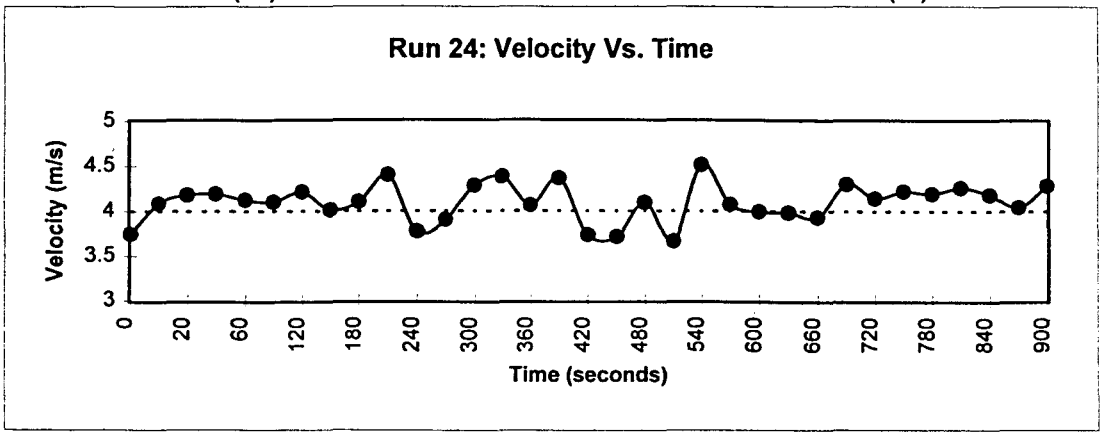

Run 25

Conditions:	
Temperature (deg. C):	-6
Pressure (kPa):	98.20525
Number of Samples Collected per Reading:	5000

Velocity:	
Desired Average Velocity (m/s):	6.00
Actual Average Velocity (m/s):	6.15

Test Information:	
Number of Bushes:	1
Angle of Attack (deg.):	0
Height of Bush(es):	5
Thickness of Bush(es):	3

Mass Relationships:	
Mass Leaving the Model (g):	800.5
Mass Recovered (g):	252.3
Mass Lost Downstream (g):	548.2
Percent Lost Downstream (%):	68.5

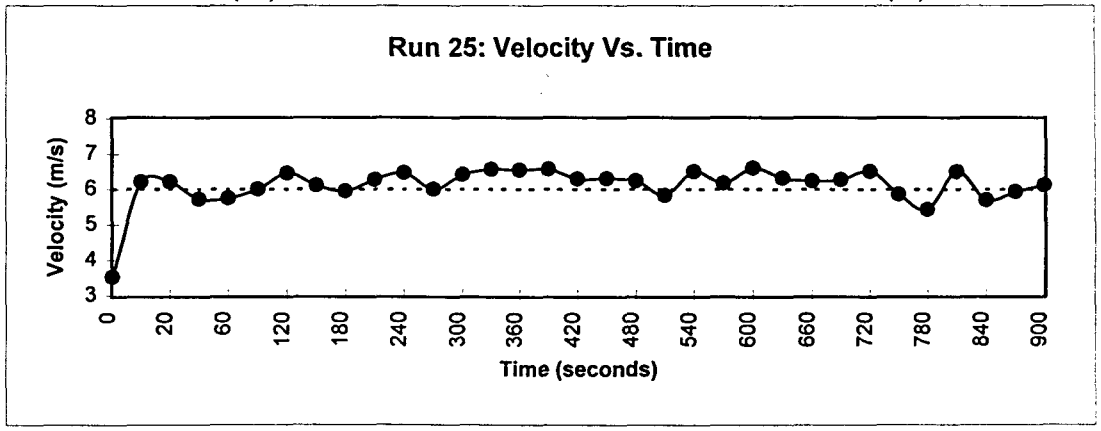

Run 26

Conditions:	
Temperature (deg. C):	-5
Pressure (kPa):	98.20525
Number of Samples Collected per Reading:	5000

Velocity:	
Desired Average Velocity (m/s):	6.00
Actual Average Velocity (m/s):	6.09

Test Information:	
Number of Bushes:	1
Angle of Attack (deg.):	30
Height of Bush(es):	5
Thickness of Bush(es):	4.5

Mass Relationships:	
Mass Leaving the Model (g):	741.6
Mass Recovered (g):	193.8
Mass Lost Downstream (g):	547.8
Percent Lost Downstream (%):	73.9

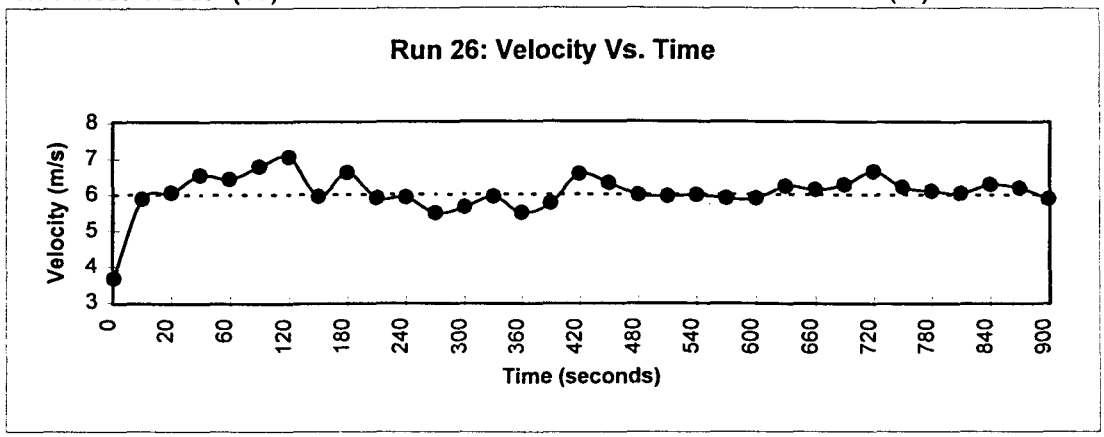

APPENDIX B: INTENSITY DATA

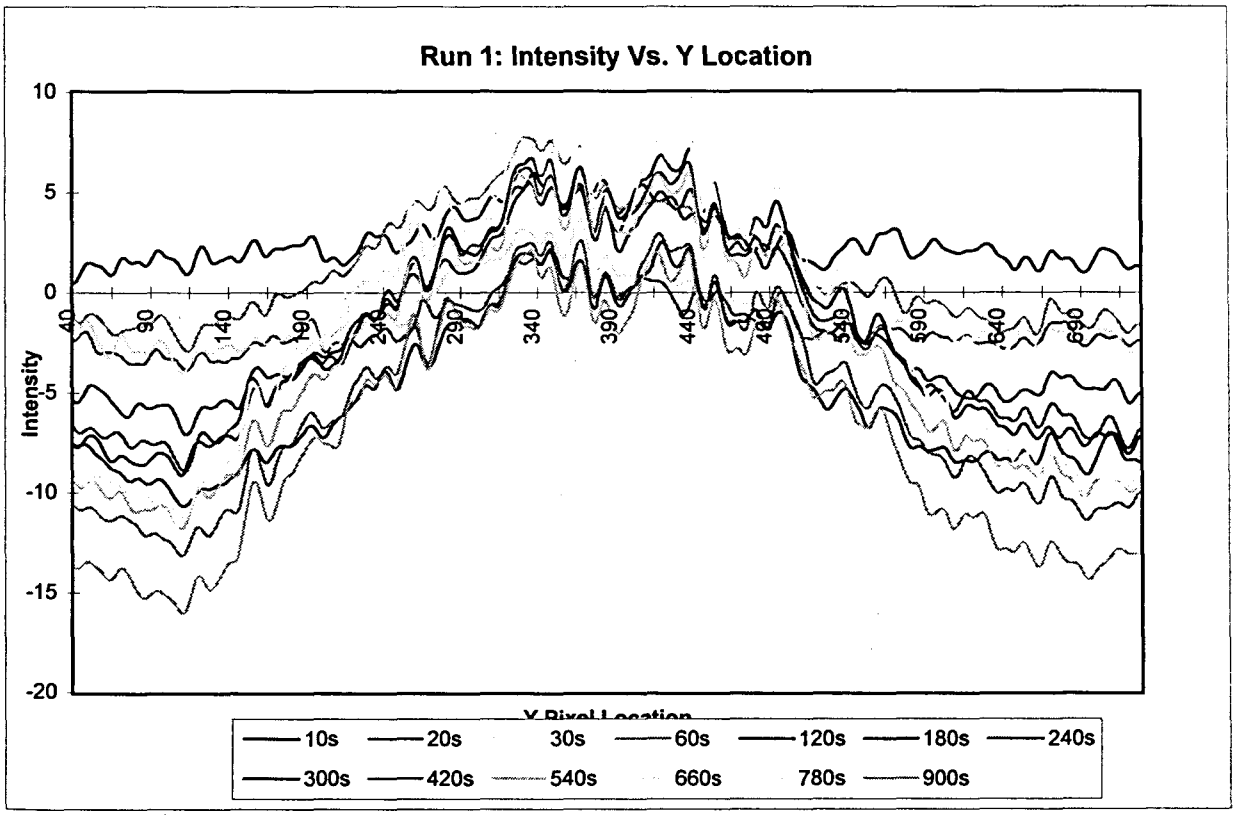
Run 1: Intensity Vs. Y Location
Intensity
10
5
0
-5
-10
-15
-20
40
90
140
190
240
290
340
390
440
490
540
590
640
690
10s
20s
30s
60s
120s
180s
240s
300s
420s
540s
660s
780s
900s

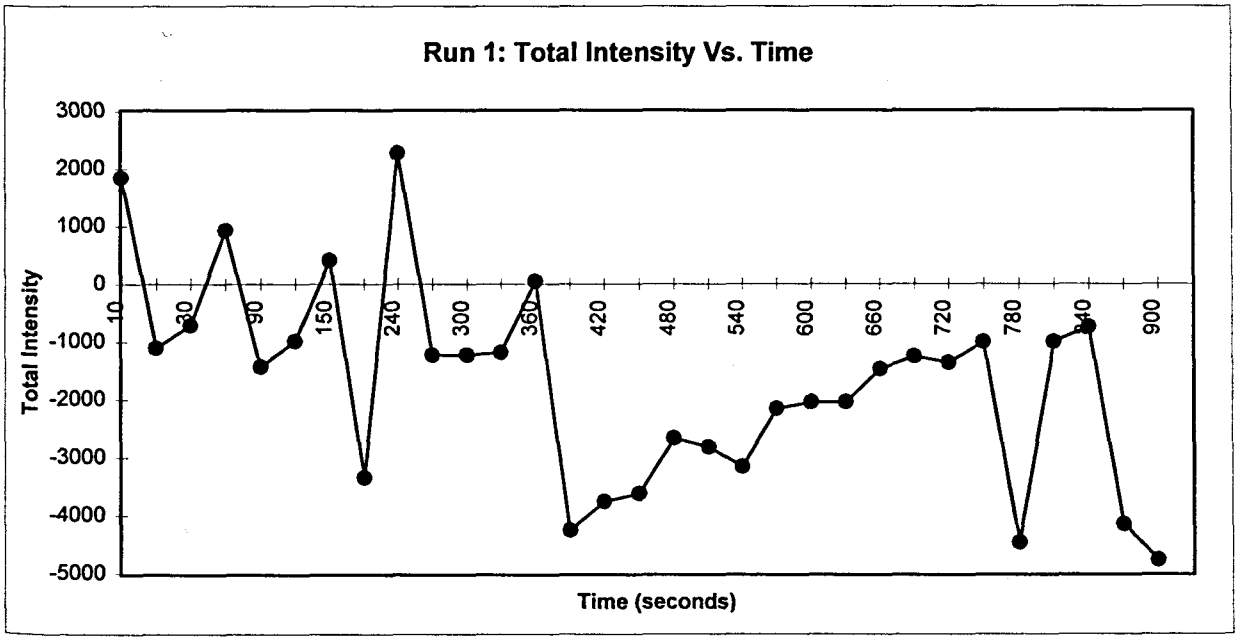
Run 1: Total Intensity Vs. Time
Total Intensity
3000
2000
1000
0
-1000
-2000
-3000
-4000
-5000
10
30
90
150
240
300
360
420
480
540
600
660
720
780
840
900
Time (seconds)

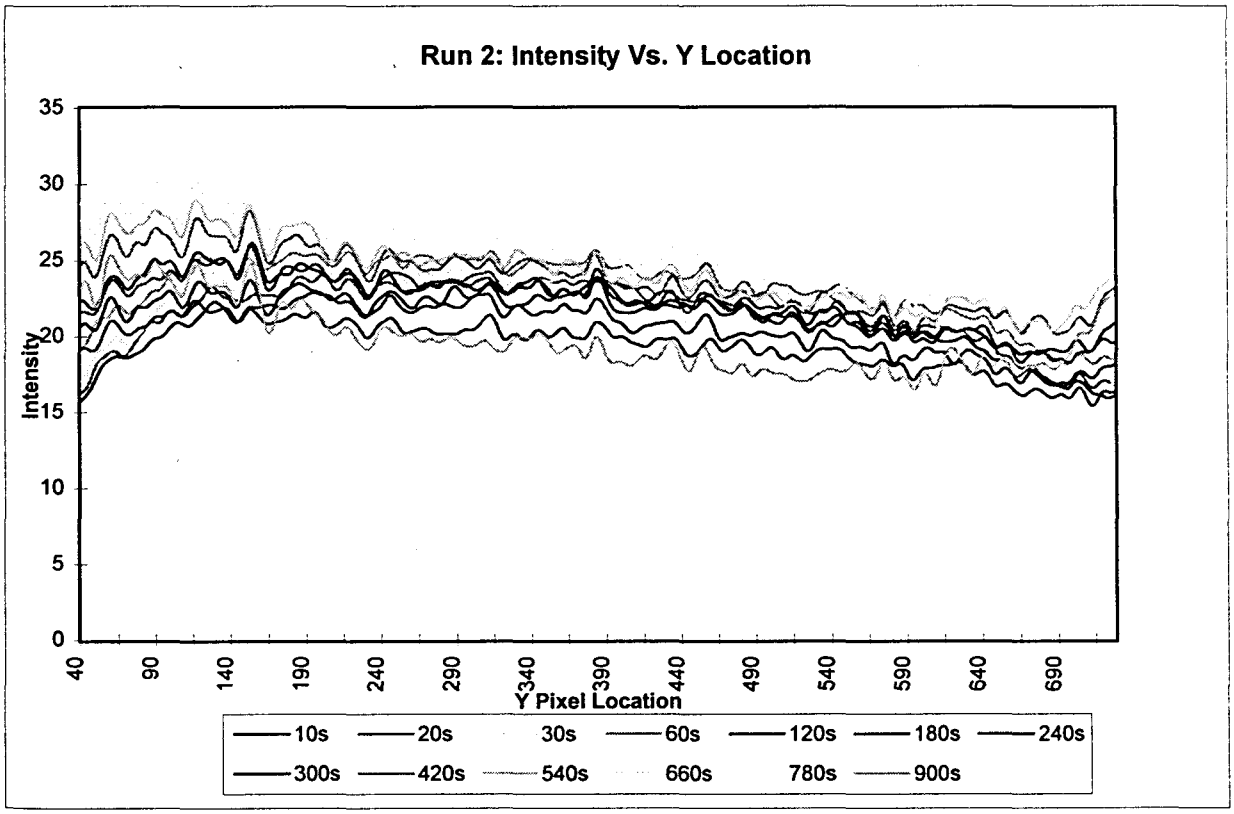
Run 2: Intensity Vs. Y Location
Intensity
35
30
25
20
15
10
5
0
40
90
140
190
240
290
340
390
440
490
540
590
640
690
Y Pixel Location
10s
20s
30s
60s
120s
180s
240s
300s
420s
540s
660s
780s
900s

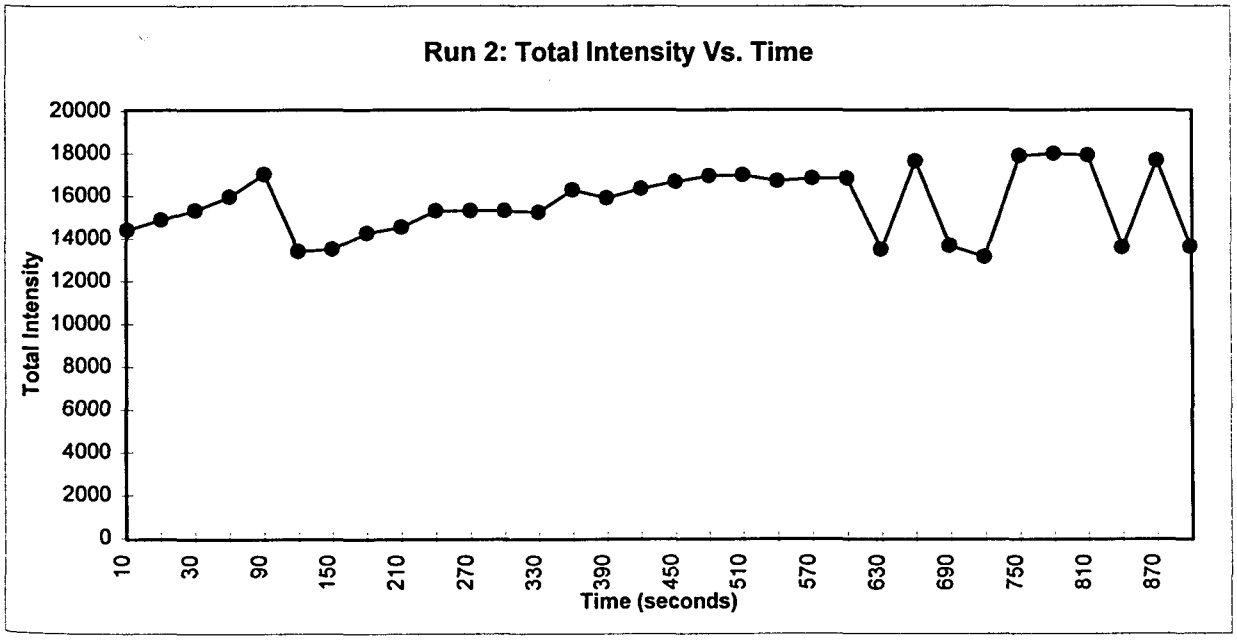
Run 2: Total Intensity Vs. Time
Total Intensity
20000
18000
16000
14000
12000
10000
8000
6000
4000
2000
0
10
30
90
150
210
270
330
390
450
510
570
630
690
750
810
870
Time (seconds)

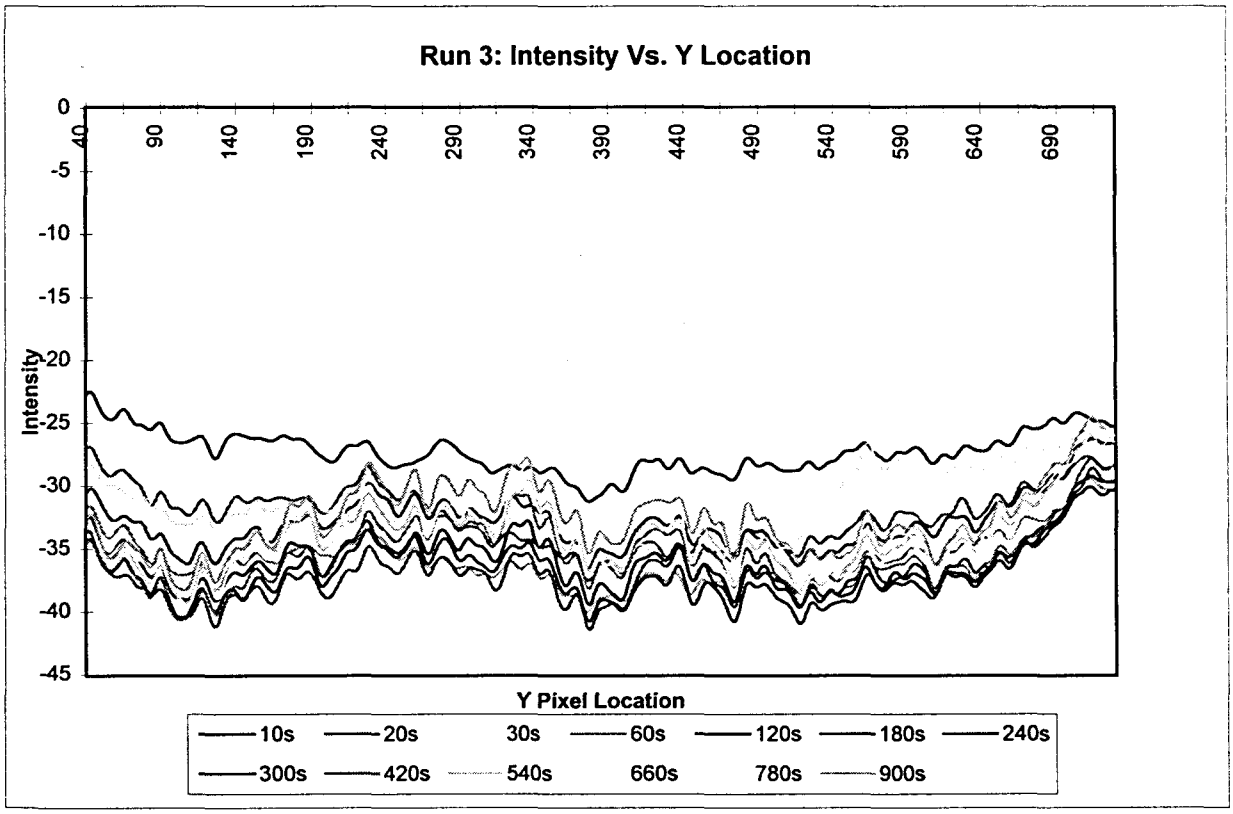
Run 3: Intensity Vs. Y Location
Intensity
0
-5
-10
-15
-20
-25
-30
-35
-40
-45
40
90
140
190
240
290
340
390
440
490
540
590
640
690
Y Pixel Location
10s
20s
30s
60s
120s
180s
240s
300s
420s
540s
660s
780s
900s

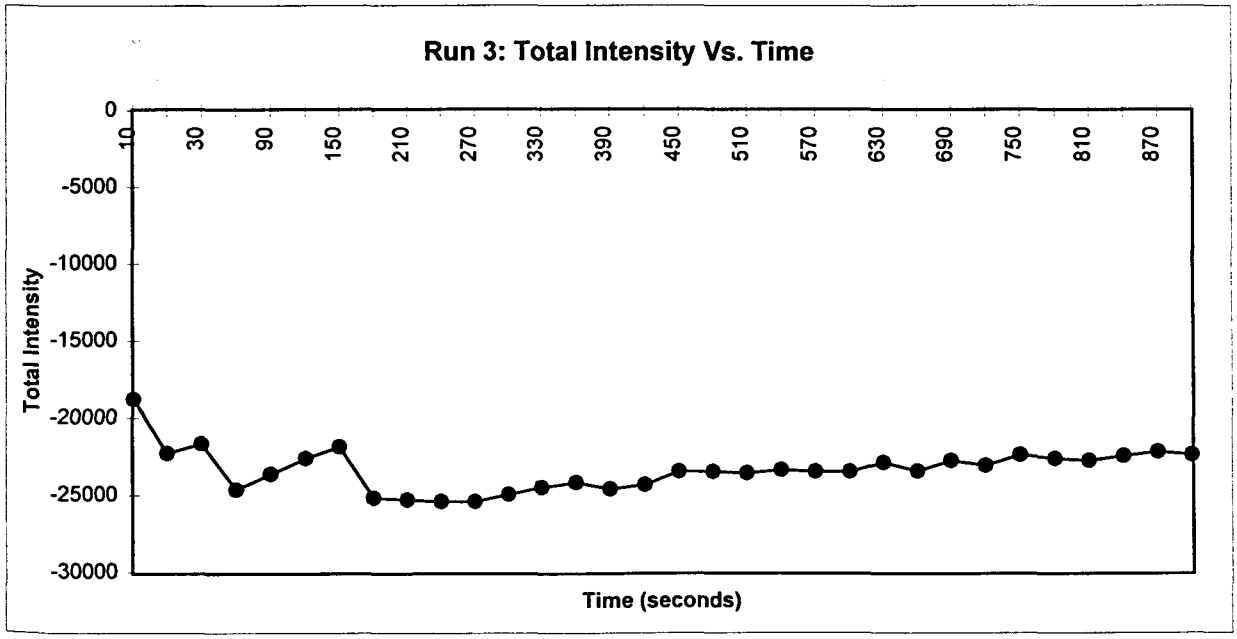
Run 3: Total Intensity Vs. Time
Total Intensity
0
-5000
-10000
-15000
-20000
-25000
-30000
10
30
90
150
210
270
330
390
450
510
570
630
690
750
810
870
Time (seconds)

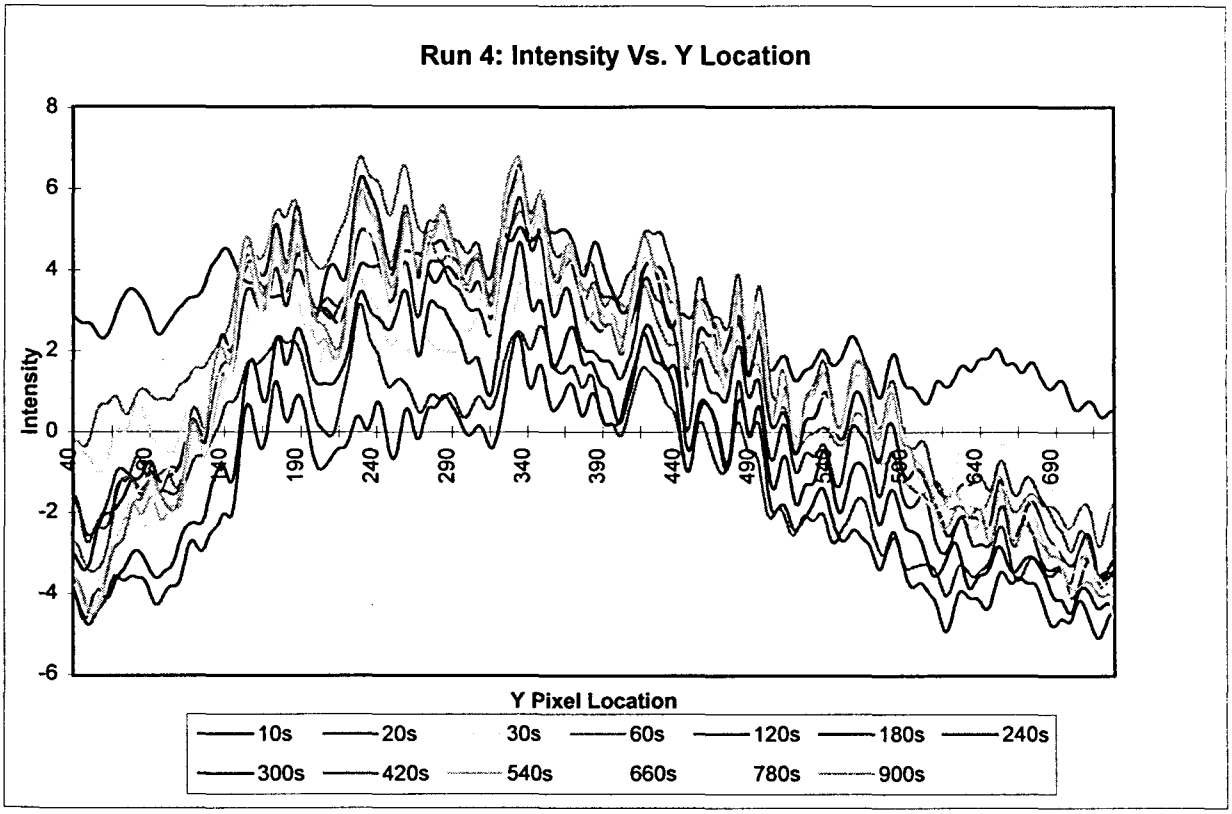
Run 4: Intensity Vs. Y Location
Intensity
8
6
4
2
0
-2
-4
-6
40
90
140
190
240
290
340
390
440
490
540
590
640
690
Y Pixel Location
10s
20s
30s
60s
120s
180s
240s
300s
420s
540s
660s
780s
900s

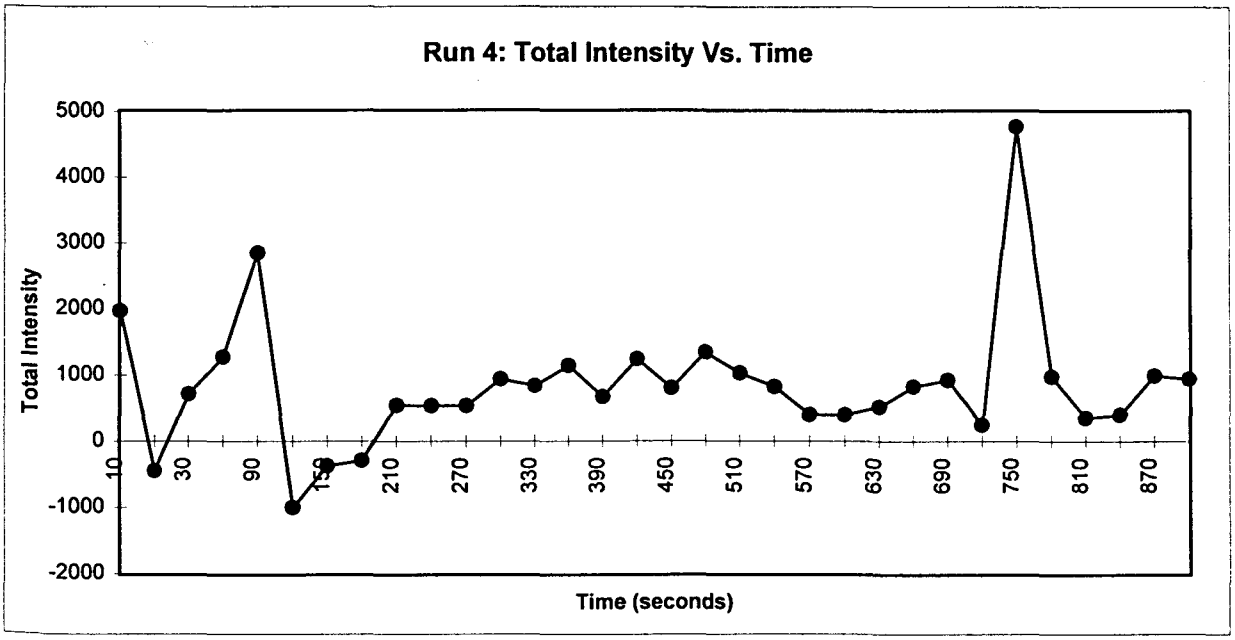
Run 4: Total Intensity Vs. Time
Total Intensity
5000
4000
3000
2000
1000
0
-1000
-2000
10
30
90
150
210
270
330
390
450
510
570
630
690
750
810
870
Time (seconds)

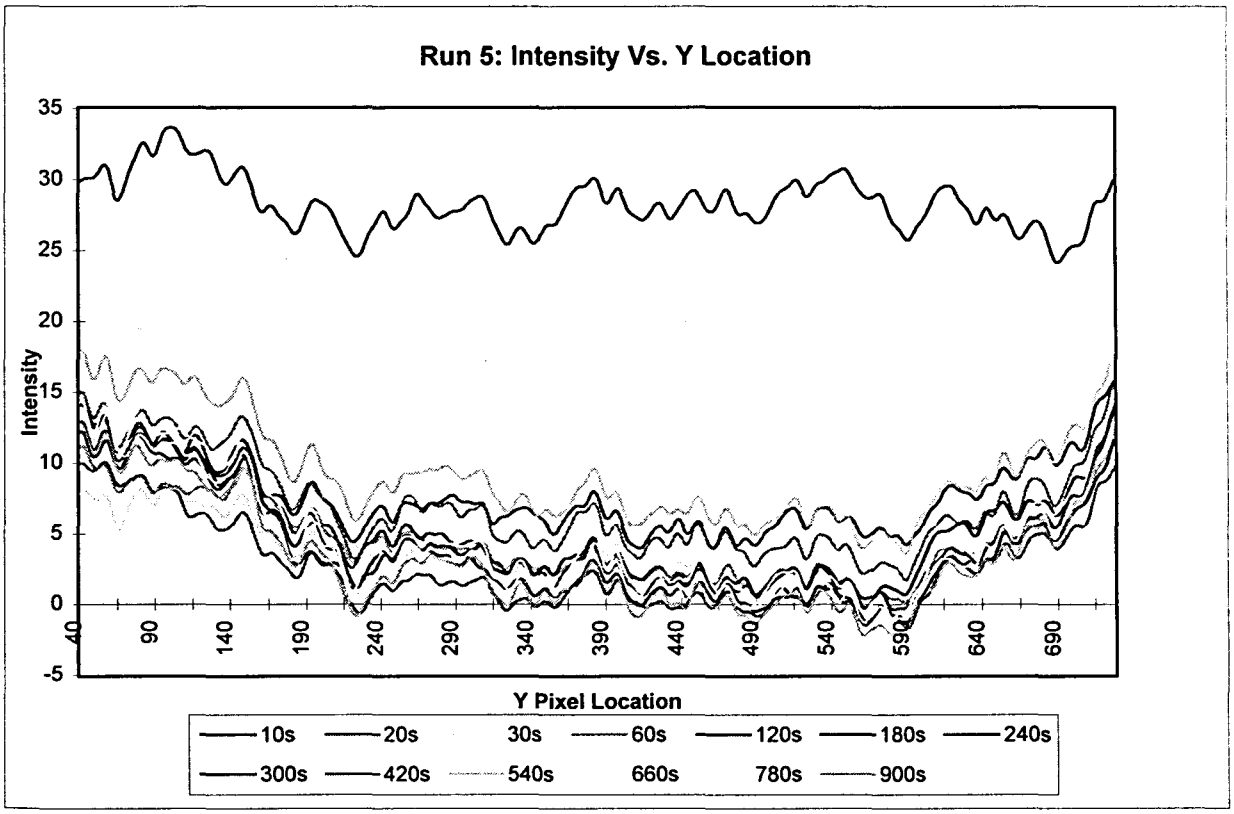
Run 5: Intensity Vs. Y Location
Intensity
35
30
25
20
15
10
5
0
-5
40
90
140
190
240
290
340
390
440
490
540
590
640
690
Y Pixel Location
10s
20s
30s
60s
120s
180s
240s
300s
420s
540s
660s
780s
900s

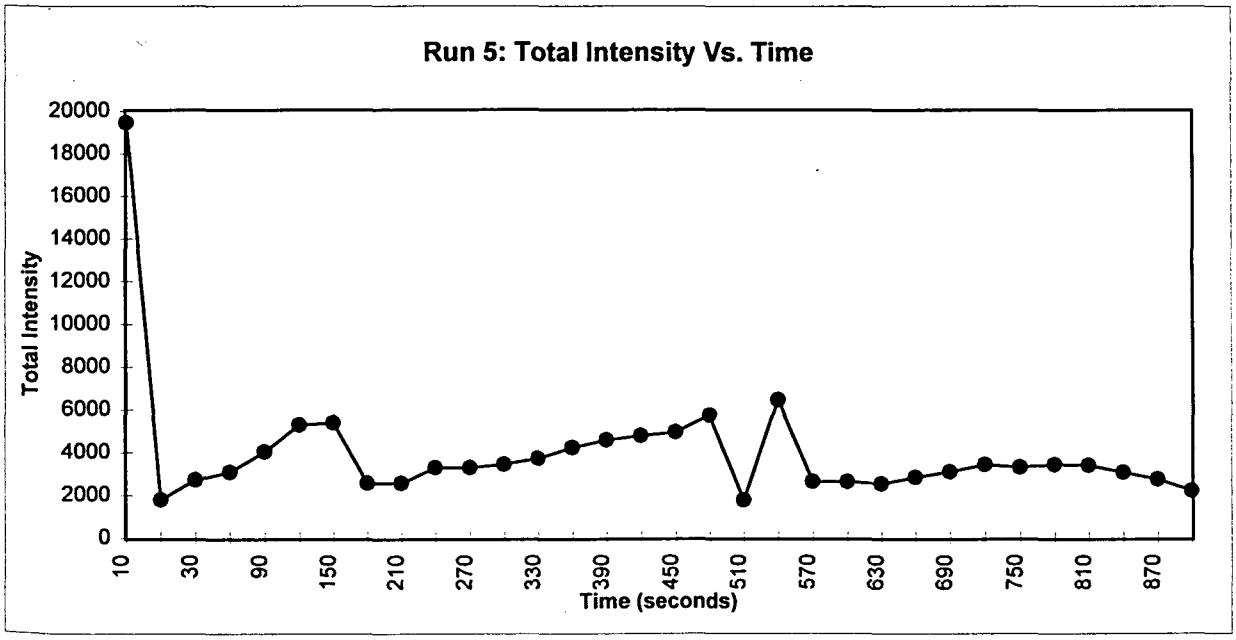
Run 5: Total Intensity Vs. Time
Total Intensity
20000
18000
16000
14000
12000
10000
8000
6000
4000
2000
0
10
30
90
150
210
270
330
390
450
510
570
630
690
750
810
870
Time (seconds)

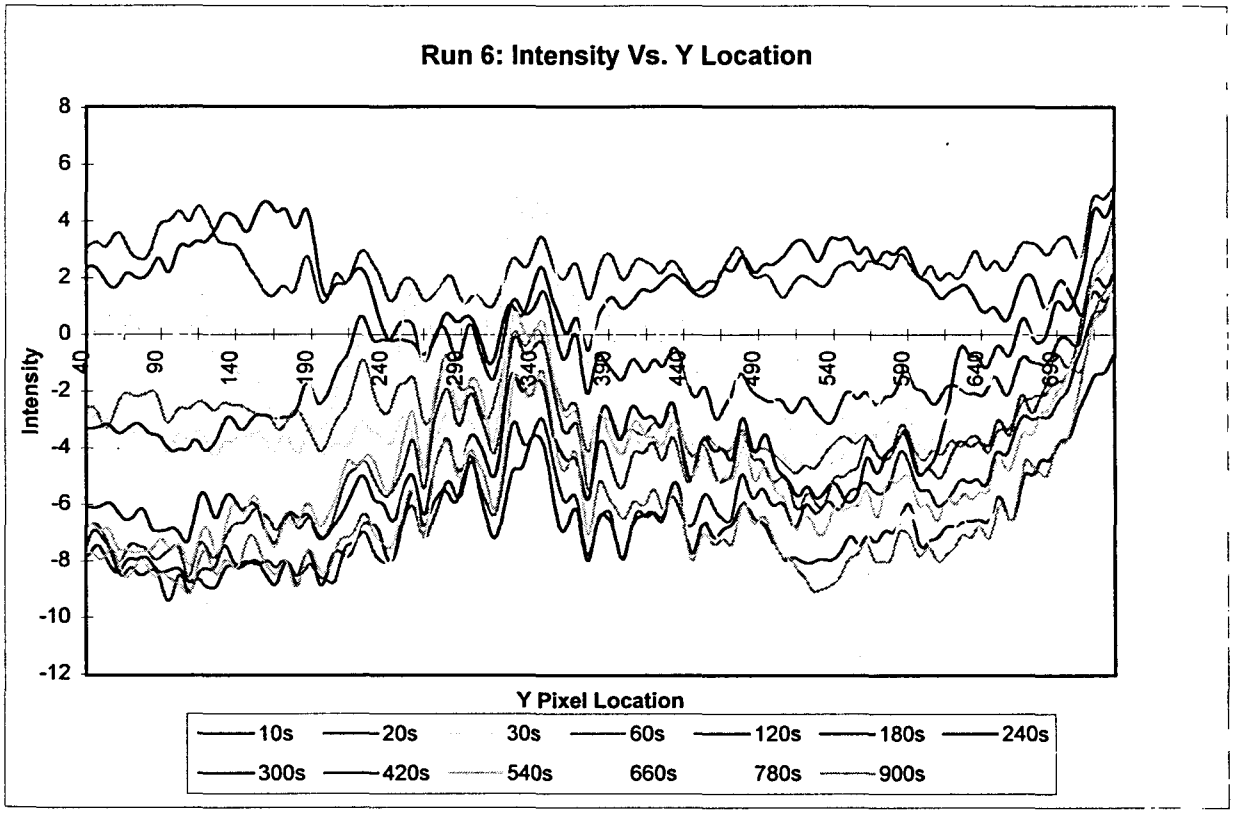
Run 6: Intensity Vs. Y Location
Intensity
Y Pixel Location
10s
20s
30s
60s
120s
180s
240s
300s
420s
540s
660s
780s
900s

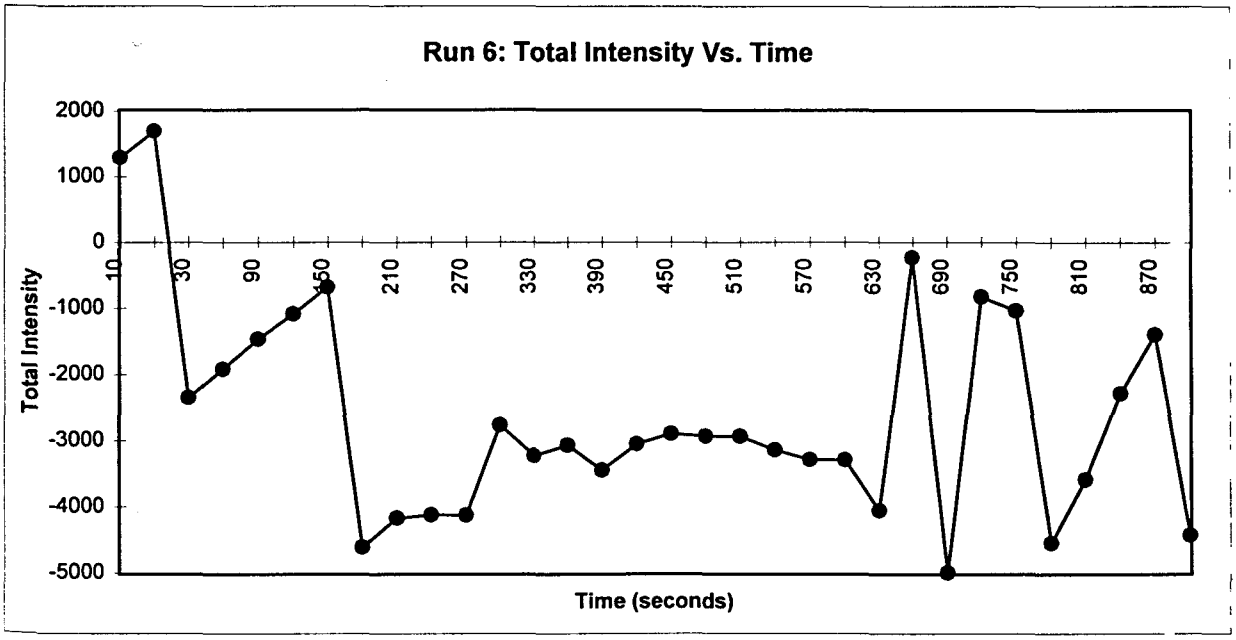
Run 6: Total Intensity Vs. Time
Total Intensity
Time (seconds)

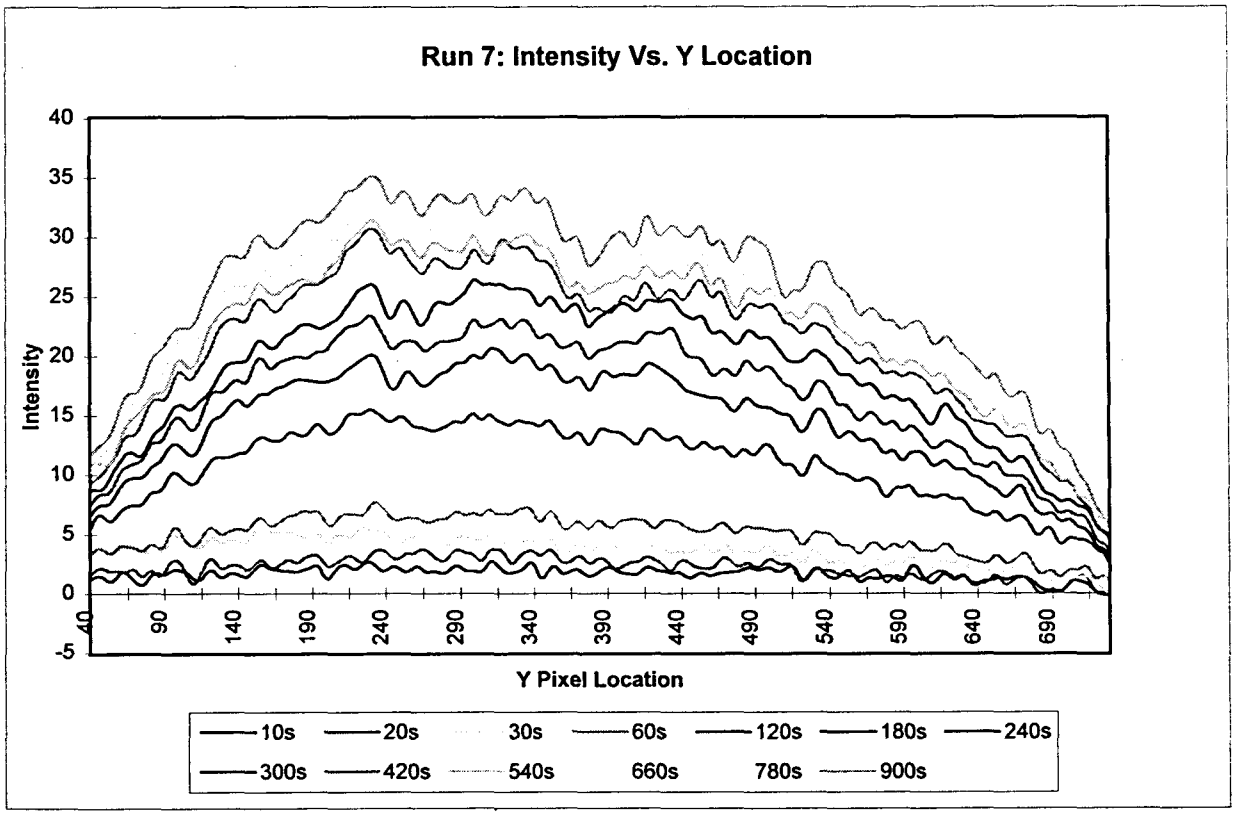
Run 7: Intensity Vs. Y Location
Intensity
Y Pixel Location
10s
20s
30s
60s
120s
180s
240s
300s
420s
540s
660s
780s
900s

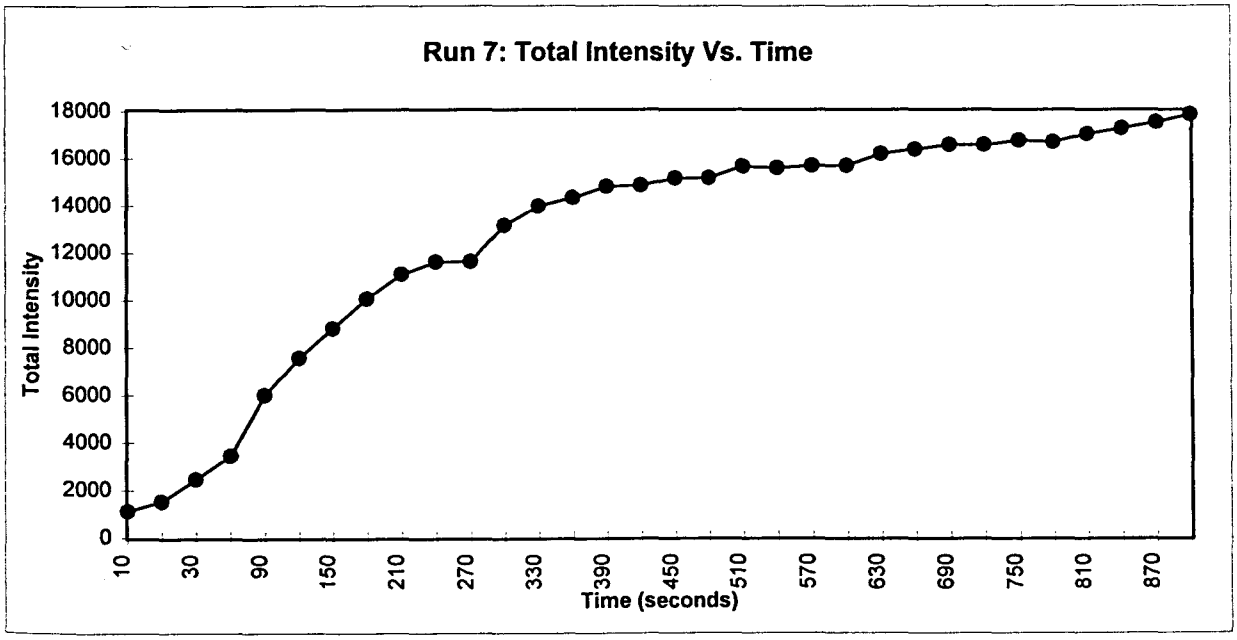
Run 7: Total Intensity Vs. Time
Total Intensity
Time (seconds)

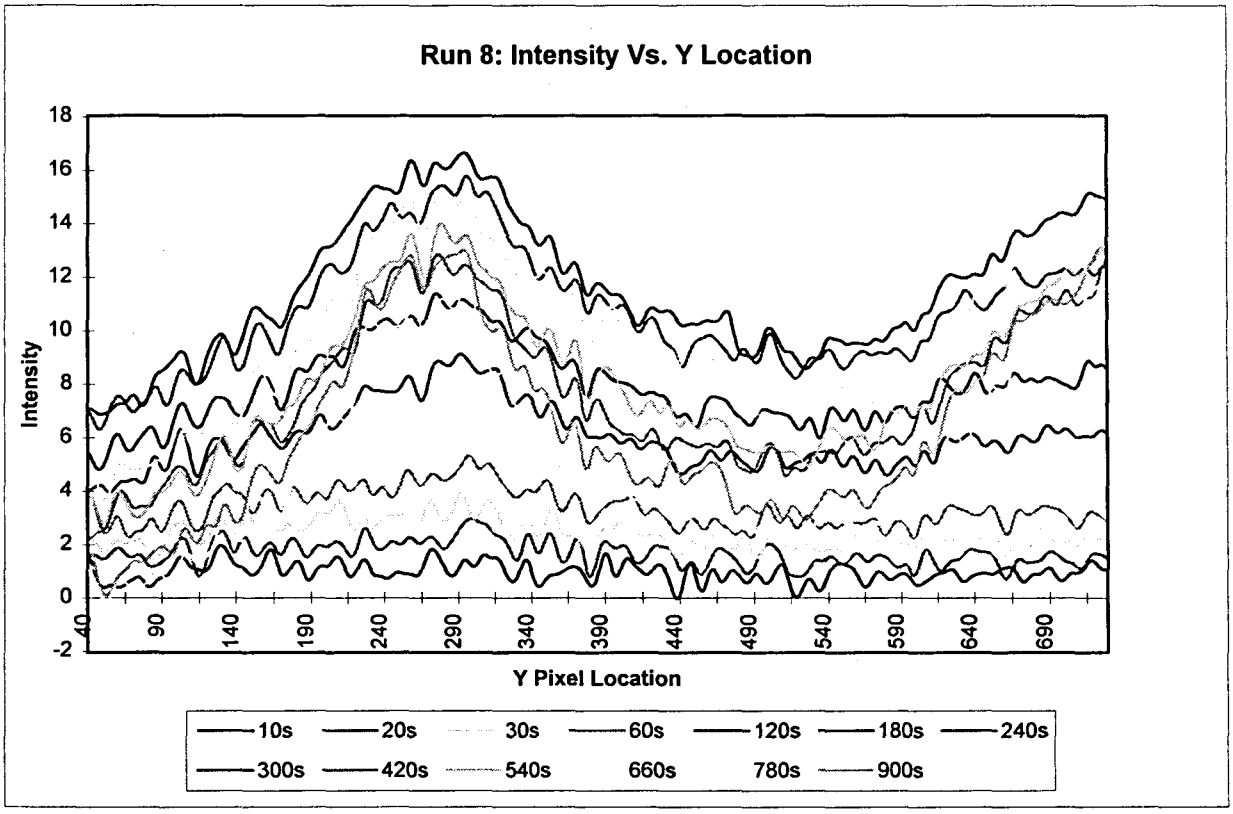
Run 8: Intensity Vs. Y Location
Intensity
18
16
14
12
10
8
6
4
2
0
-2
40
90
140
190
240
290
340
390
440
490
540
590
640
690
Y Pixel Location
10s
20s
30s
60s
120s
180s
240s
300s
420s
540s
660s
780s
900s

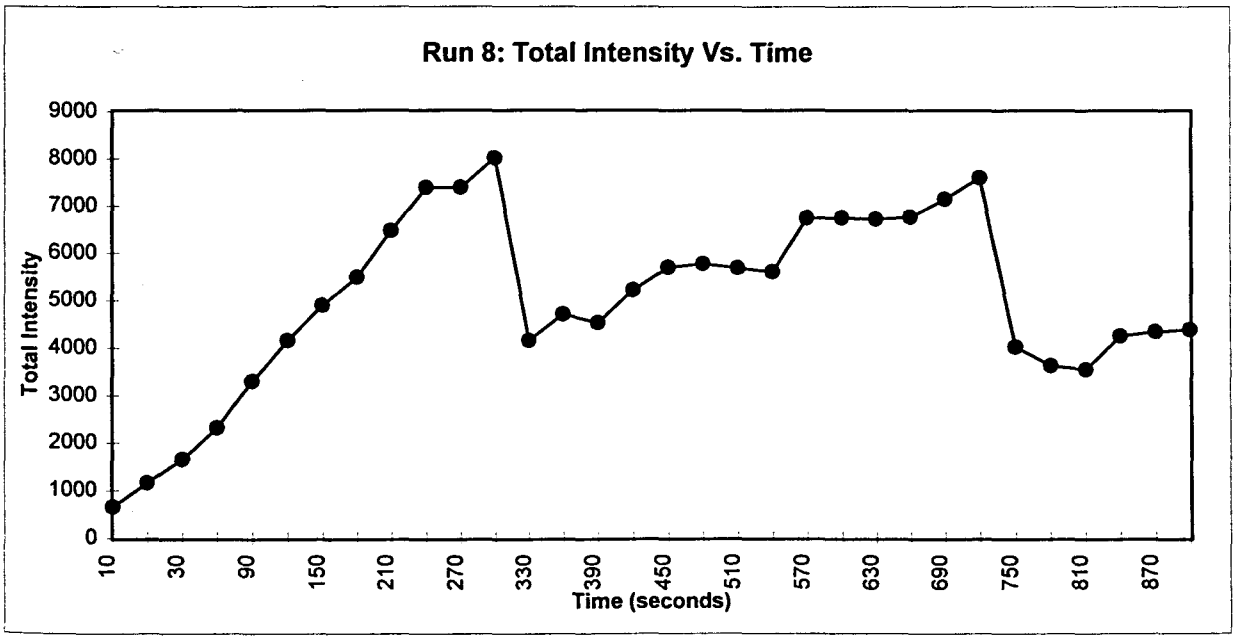
Run 8: Total Intensity Vs. Time
Total Intensity
9000
8000
7000
6000
5000
4000
3000
2000
1000
0
10
30
90
150
210
270
330
390
450
510
570
630
690
750
810
870
Time (seconds)

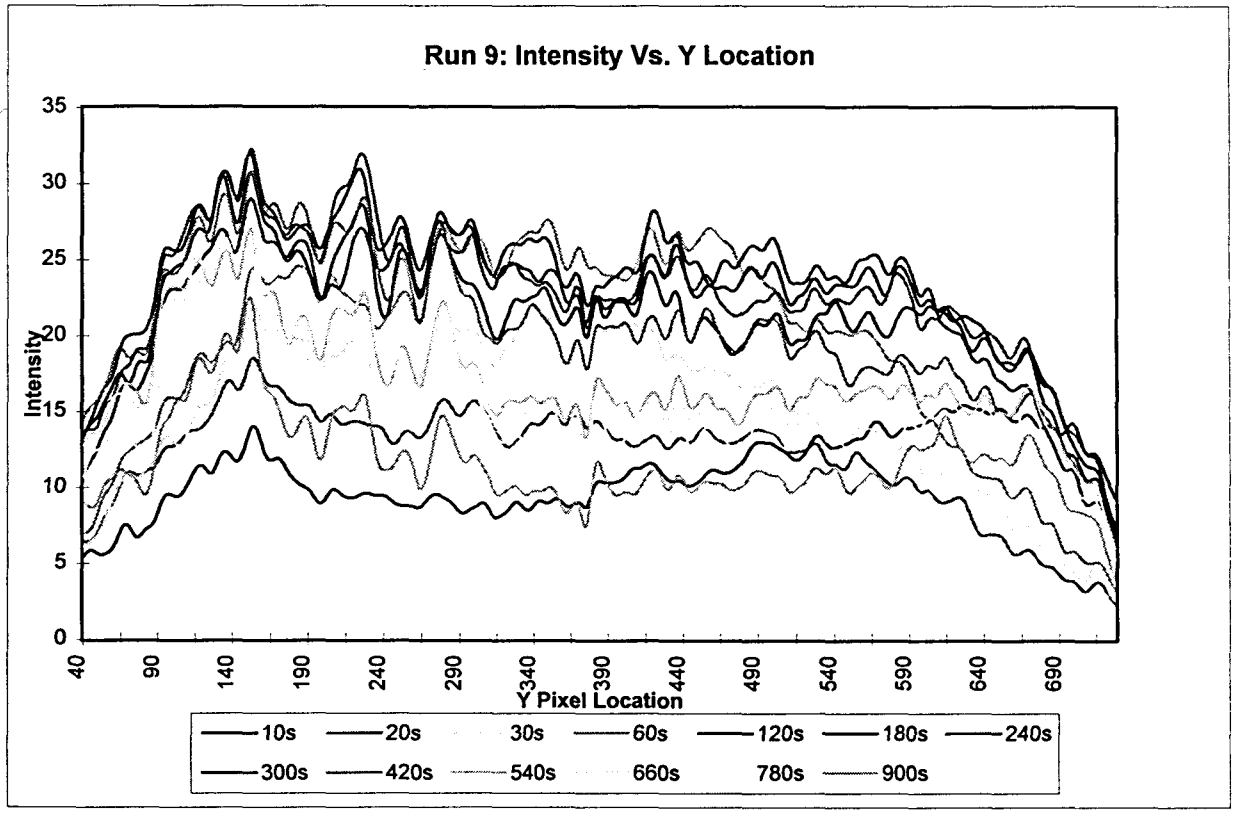
Run 9: Intensity Vs. Y Location
Intensity
Y Pixel Location
0
5
10
15
20
25
30
35
40
90
140
190
240
290
340
390
440
490
540
590
640
690
10s
20s
30s
60s
120s
180s
240s
300s
420s
540s
660s
780s
900s

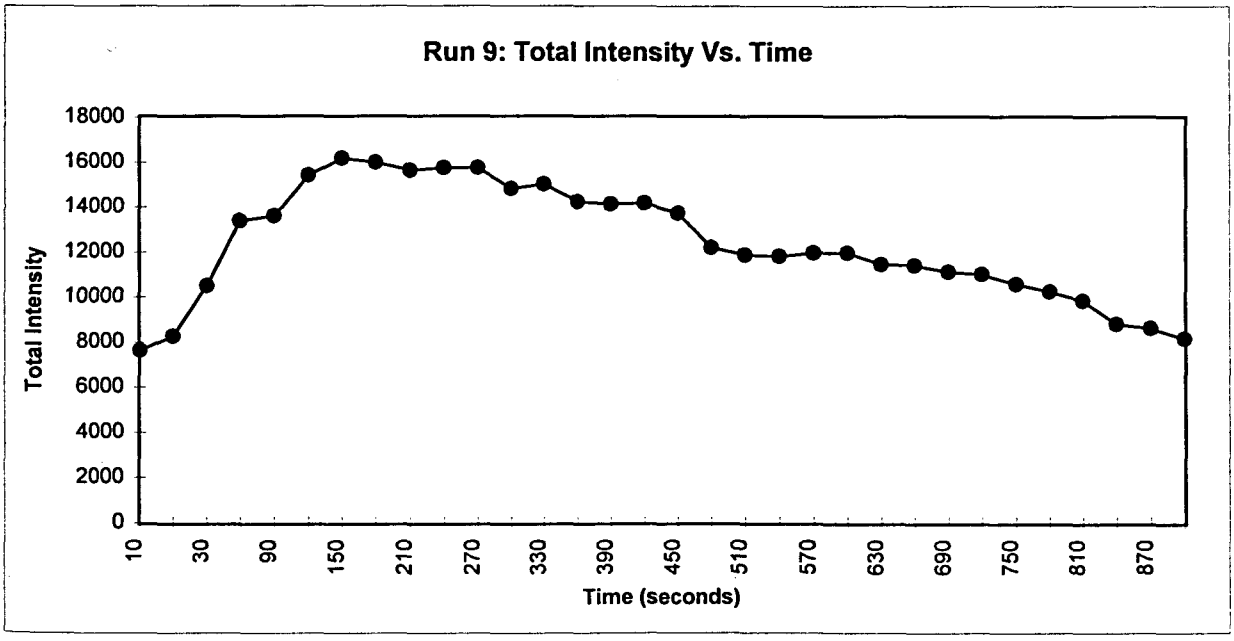
Run 9: Total Intensity Vs. Time
Total Intensity
Time (seconds)
0
2000
4000
6000
8000
10000
12000
14000
16000
18000
10
30
90
150
210
270
330
390
450
510
570
630
690
750
810
870

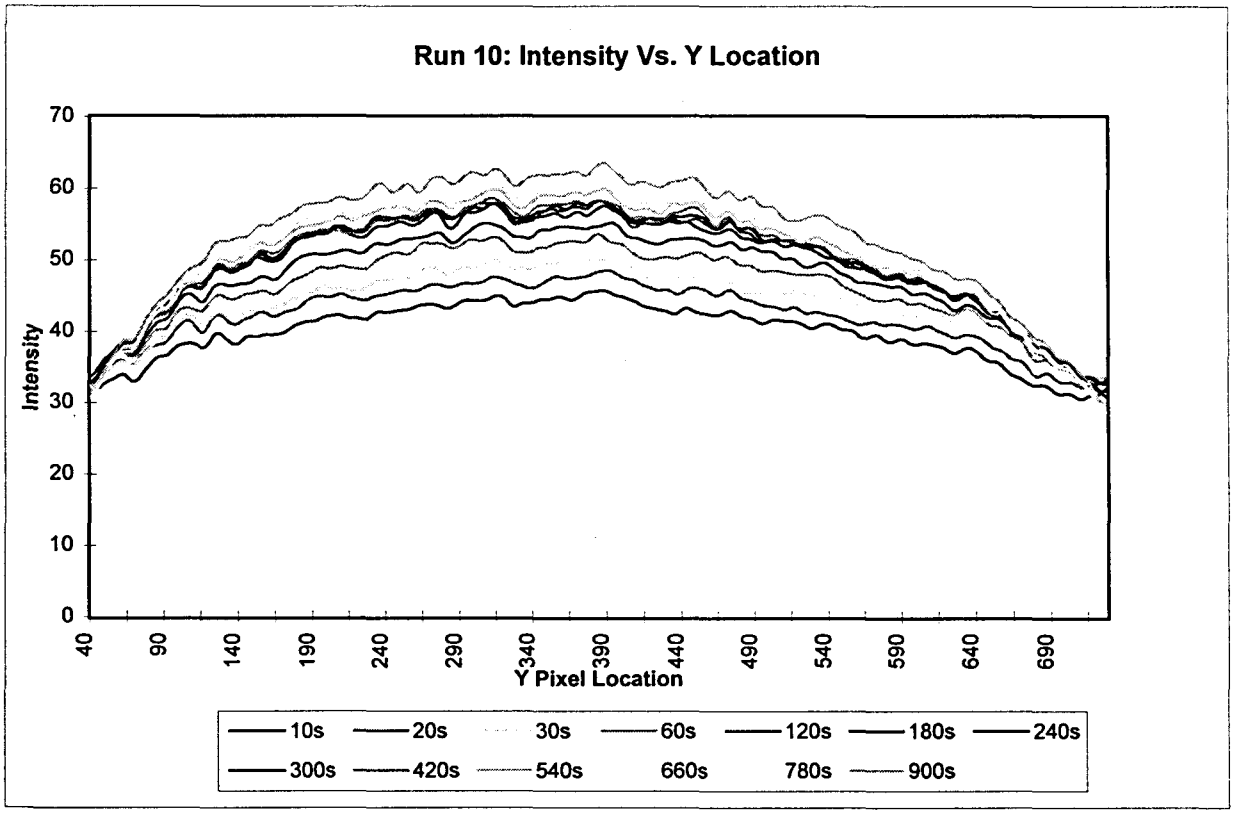
Run 10: Intensity Vs. Y Location
Intensity
70
60
50
40
30
20
10
0
40
90
140
190
240
290
340
390
440
490
540
590
640
690
Y Pixel Location
10s
20s
30s
60s
120s
180s
240s
300s
420s
540s
660s
780s
900s

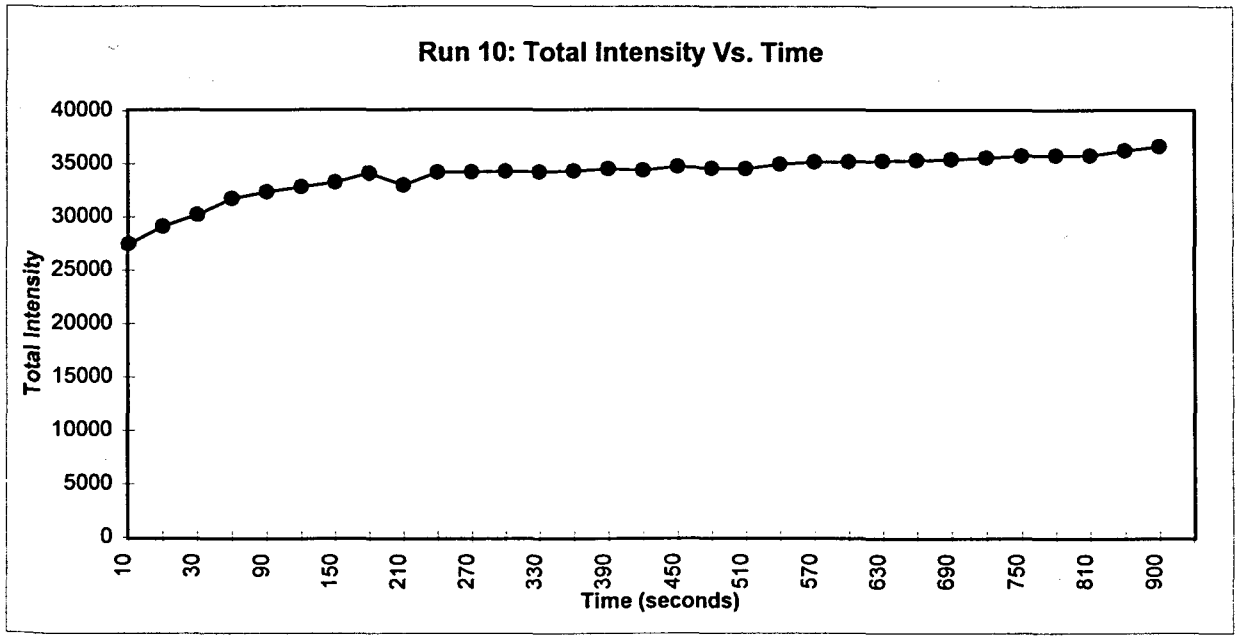
Run 10: Total Intensity Vs. Time
Total Intensity
40000
35000
30000
25000
20000
15000
10000
5000
0
10
30
90
150
210
270
330
390
450
510
570
630
690
750
810
900
Time (seconds)

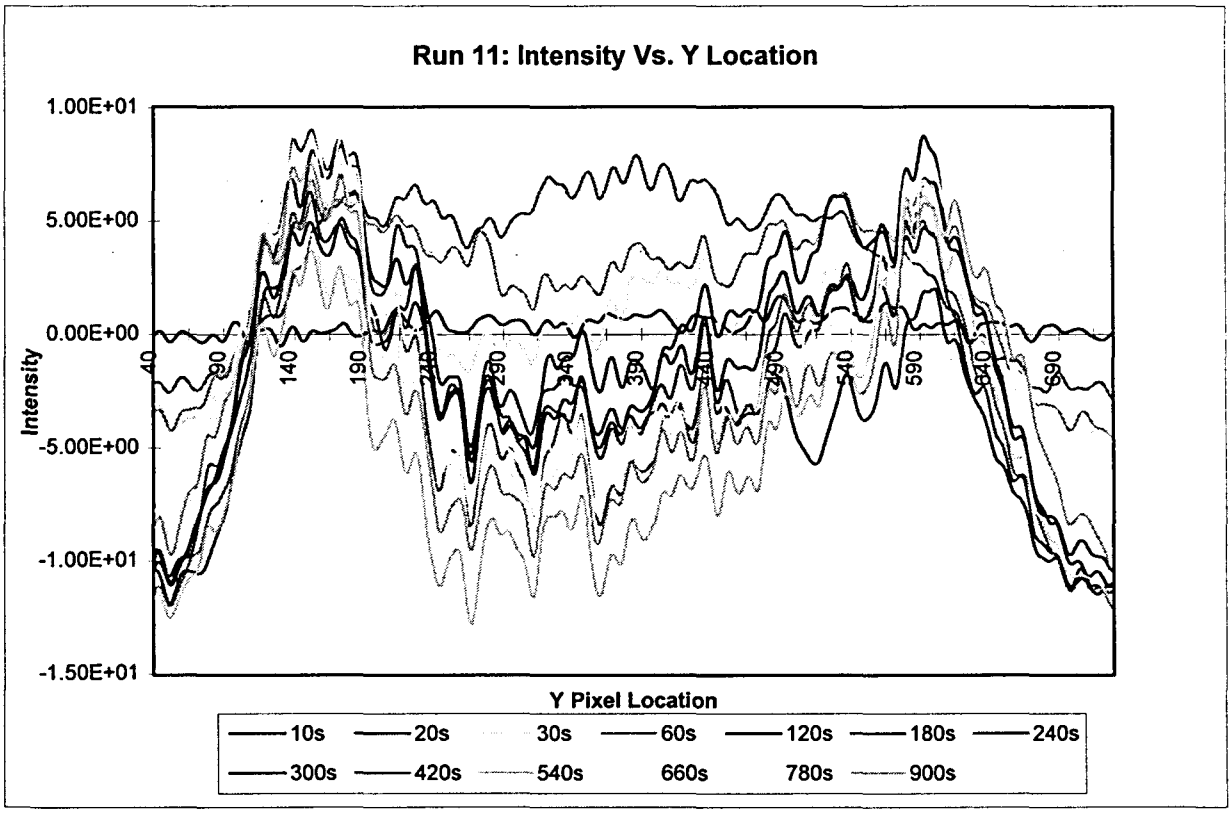
Run 11: Intensity Vs. Y Location
1.00E+01
5.00E+00
0.00E+00
-5.00E+00
-1.00E+01
-1.50E+01
Intensity
40
90
140
190
240
290
340
390
440
490
540
590
640
690
Y Pixel Location
10s
20s
30s
60s
120s
180s
240s
300s
420s
540s
660s
780s
900s

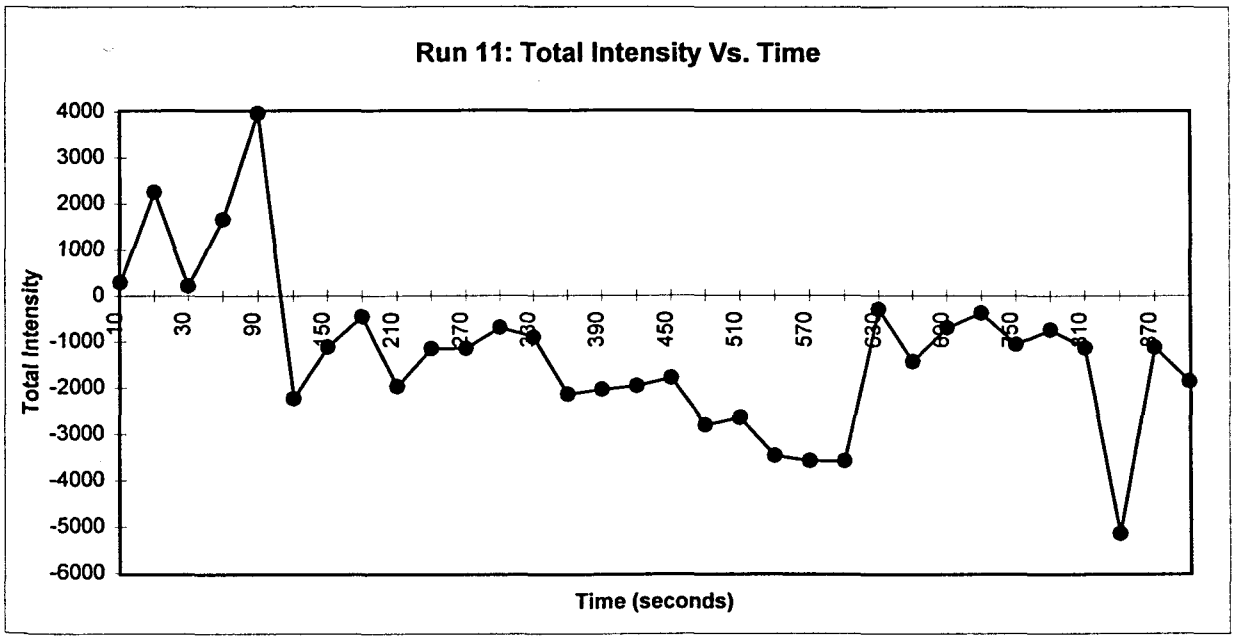
Run 11: Total Intensity Vs. Time
4000
3000
2000
1000
0
-1000
-2000
-3000
-4000
-5000
-6000
Total Intensity
10
30
90
150
210
270
330
390
450
510
570
630
690
750
810
870
Time (seconds)

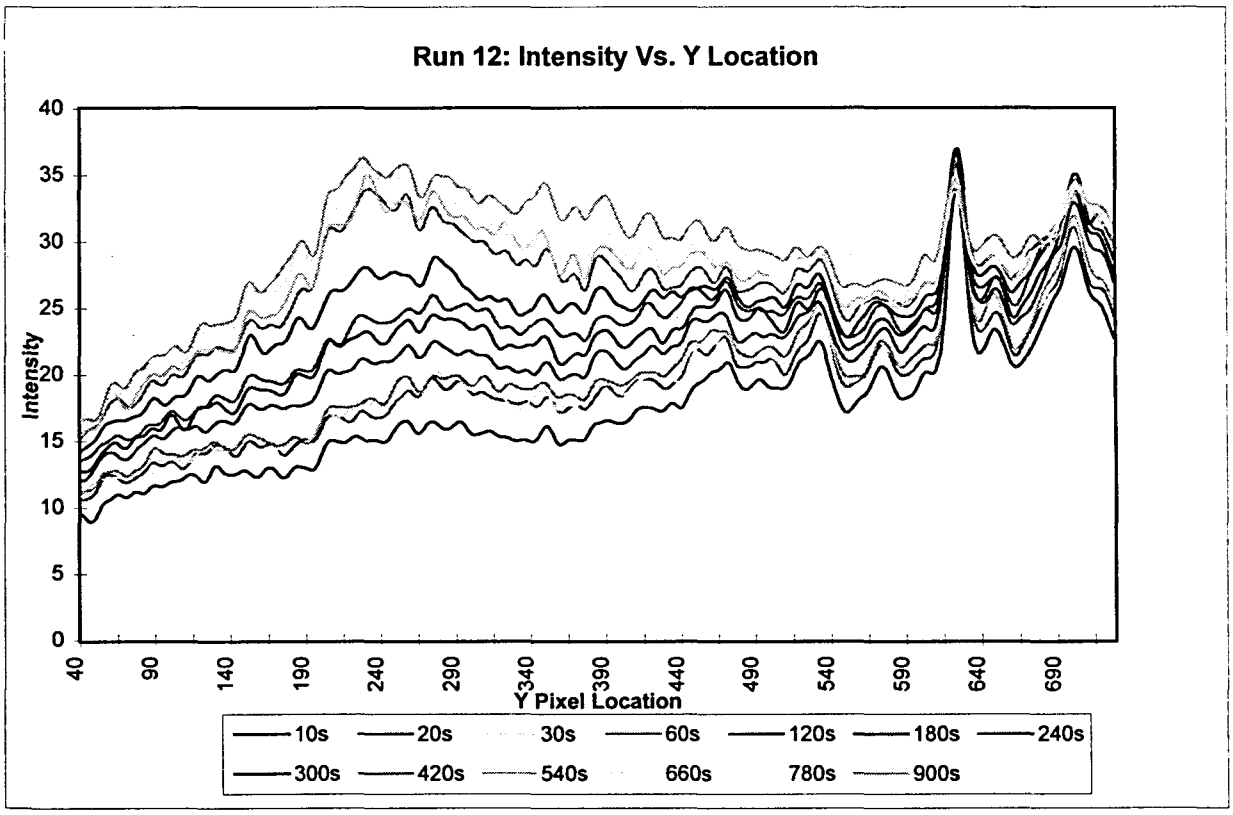
Run 12: Intensity Vs. Y Location
Intensity
Y Pixel Location
10s
20s
30s
60s
120s
180s
240s
300s
420s
540s
660s
780s
900s

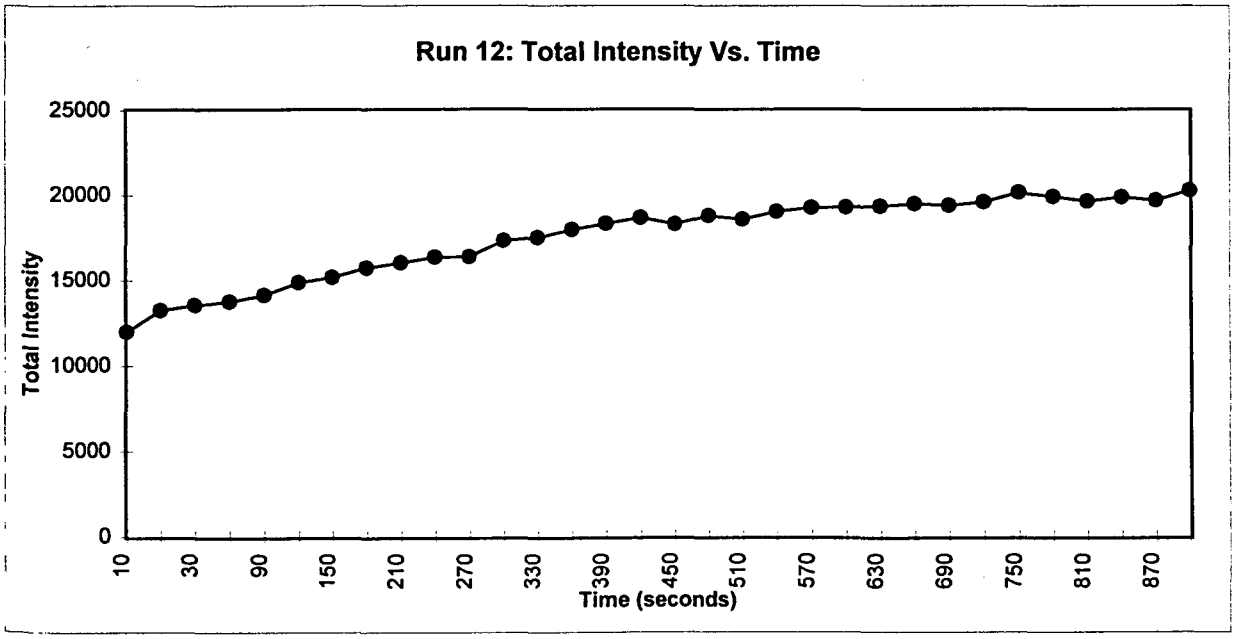
Run 12: Total Intensity Vs. Time
Total Intensity
Time (seconds)

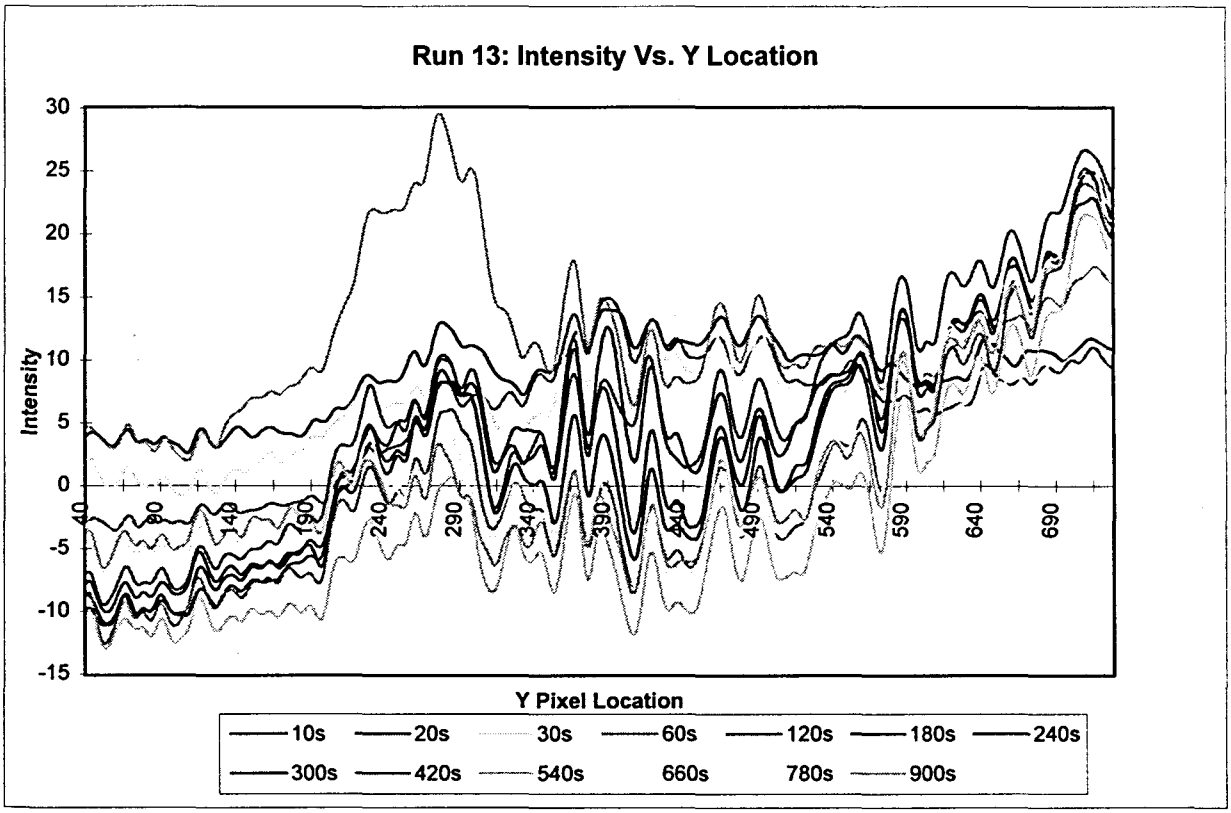
Run 13: Intensity Vs. Y Location
Intensity
30
25
20
15
10
5
0
-5
-10
-15
40
90
140
190
240
290
340
390
440
490
540
590
640
690
Y Pixel Location
10s
20s
30s
60s
120s
180s
240s
300s
420s
540s
660s
780s
900s

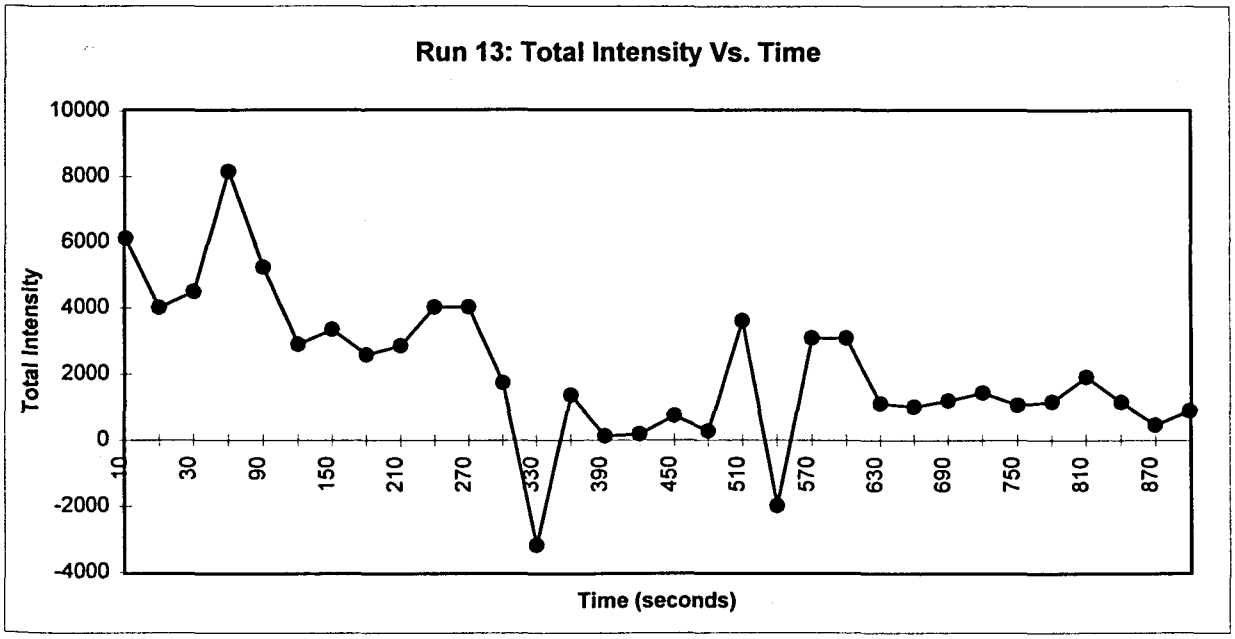
Run 13: Total Intensity Vs. Time
Total Intensity
10000
8000
6000
4000
2000
0
-2000
-4000
10
30
90
150
210
270
330
390
450
510
570
630
690
750
810
870
Time (seconds)

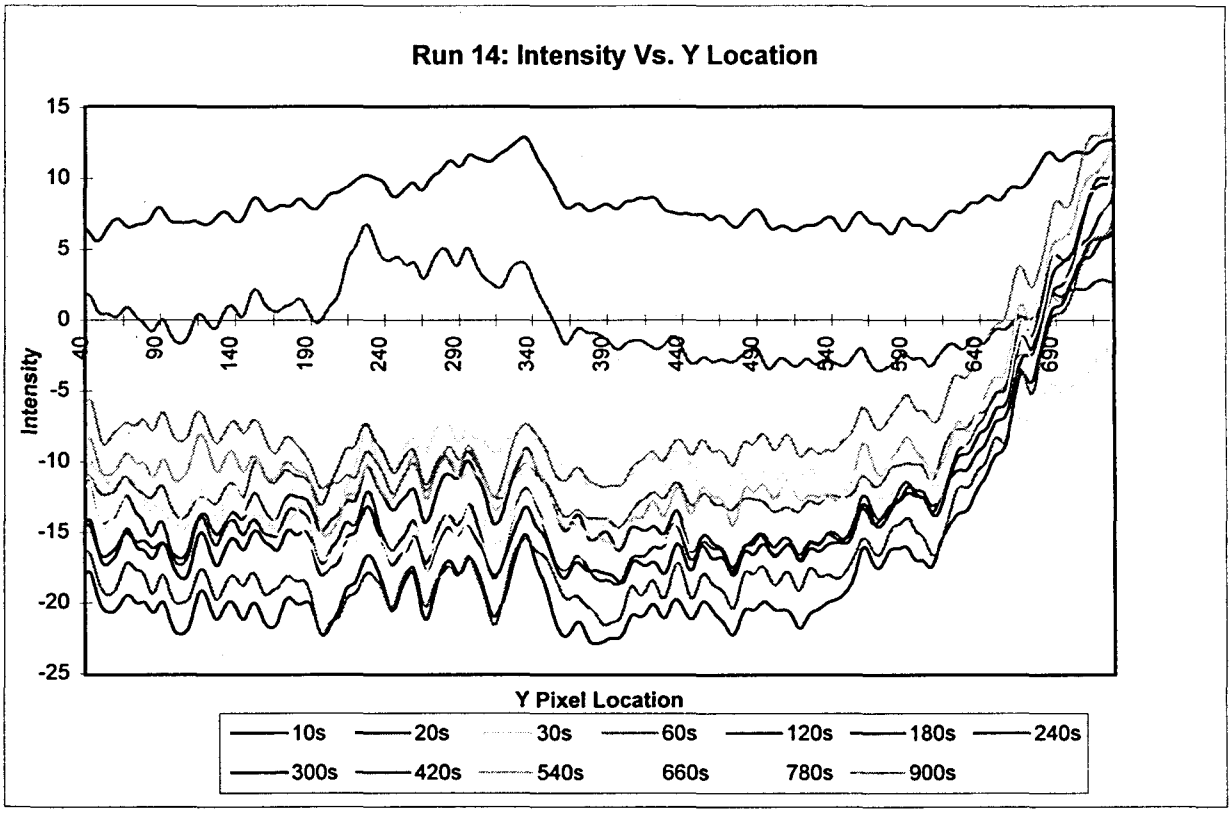
Run 14: Intensity Vs. Y Location
Intensity
Y Pixel Location
10s
20s
30s
60s
120s
180s
240s
300s
420s
540s
660s
780s
900s

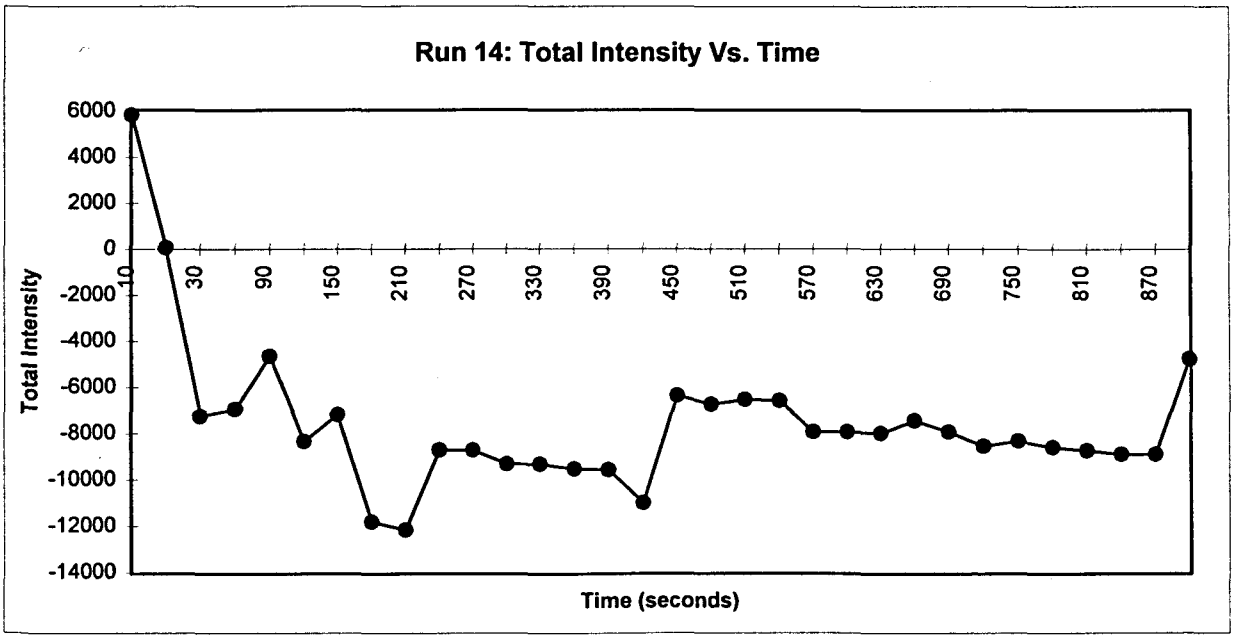
Run 14: Total Intensity Vs. Time
Total Intensity
Time (seconds)

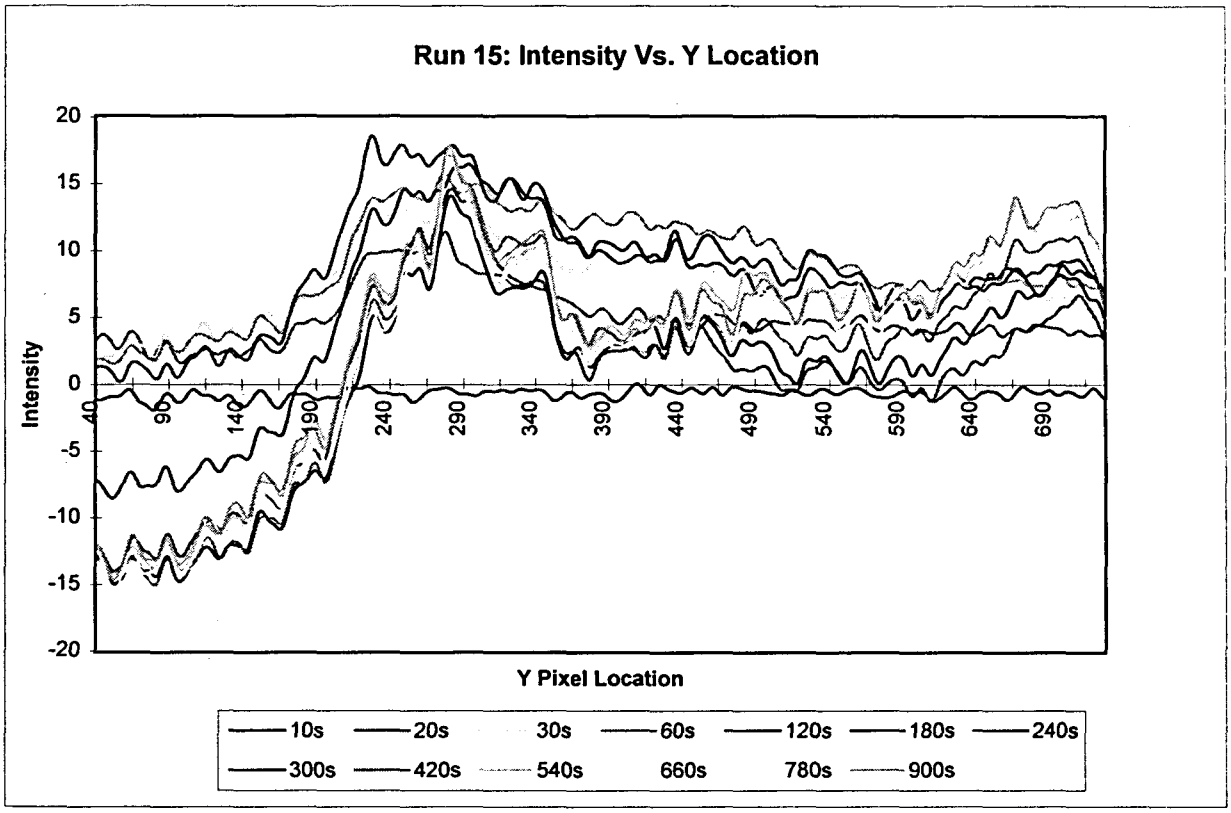
Run 15: Intensity Vs. Y Location
Intensity
Y Pixel Location
10s
20s
30s
60s
120s
180s
240s
300s
420s
540s
660s
780s
900s

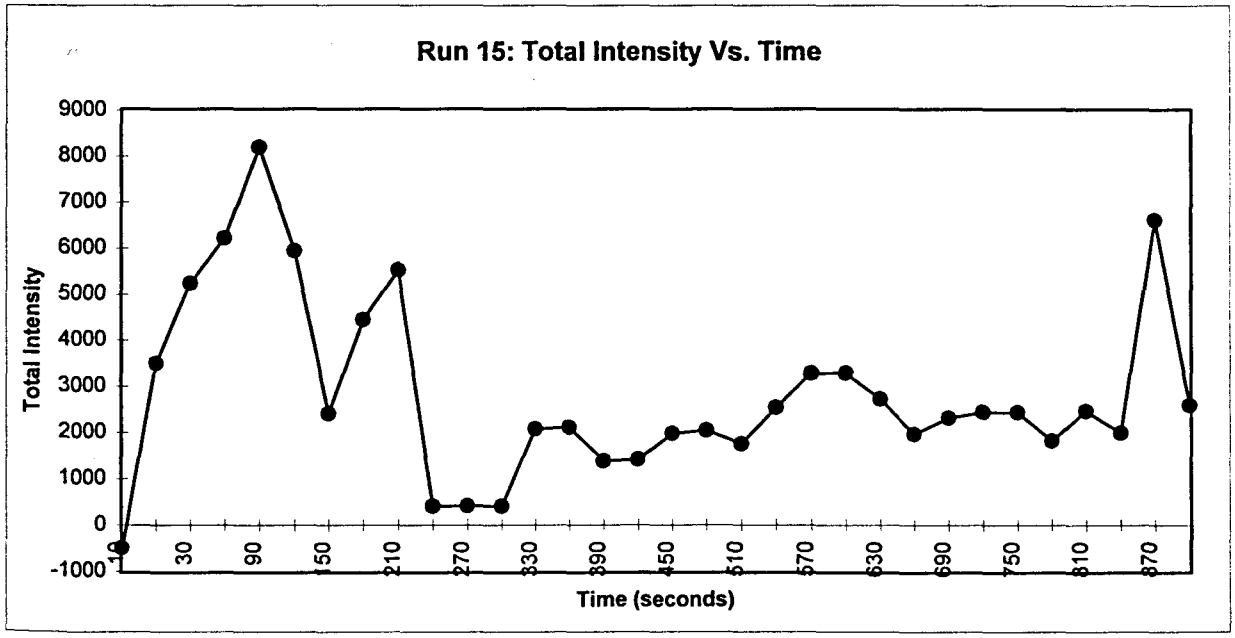
Run 15: Total Intensity Vs. Time
Total Intensity
Time (seconds)

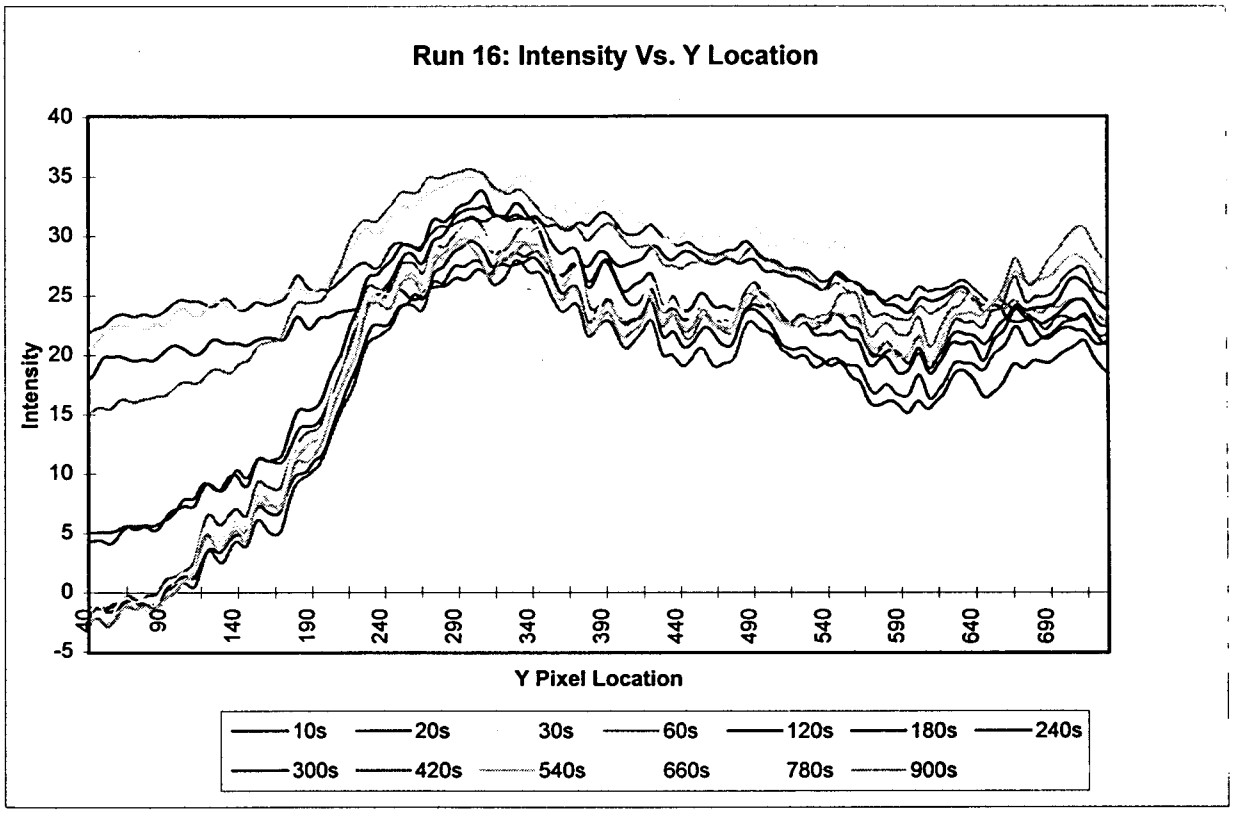
Run 16: Intensity Vs. Y Location
Intensity
Y Pixel Location
10s
20s
30s
60s
120s
180s
240s
300s
420s
540s
660s
780s
900s

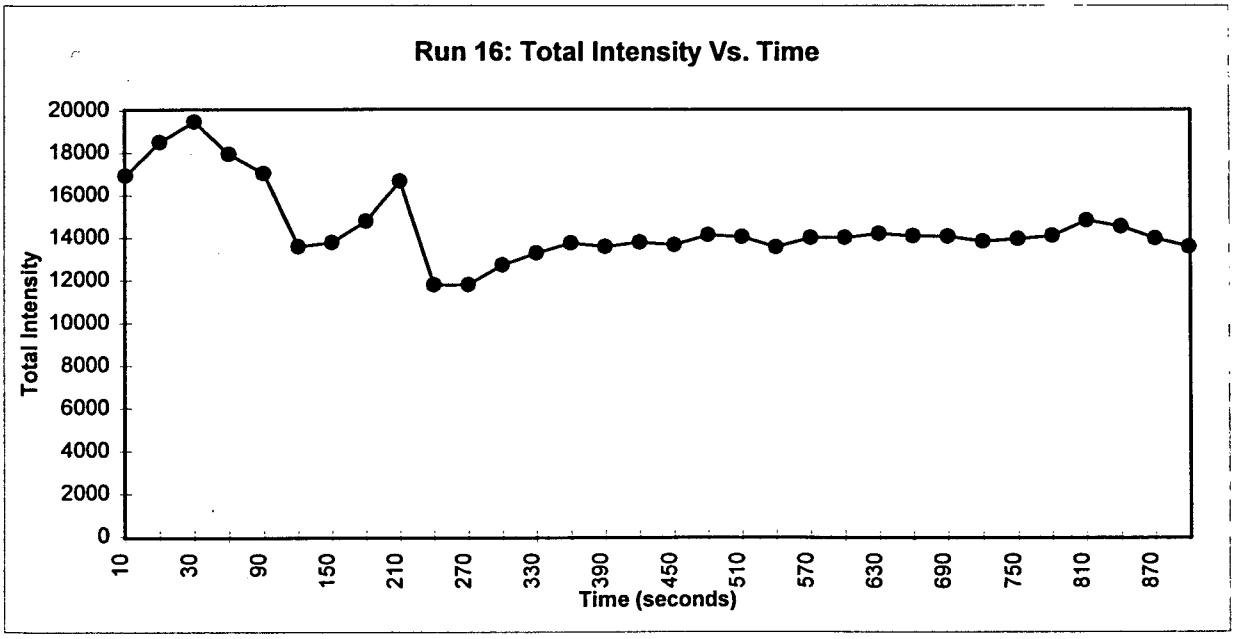
Run 16: Total Intensity Vs. Time
Total Intensity
Time (seconds)

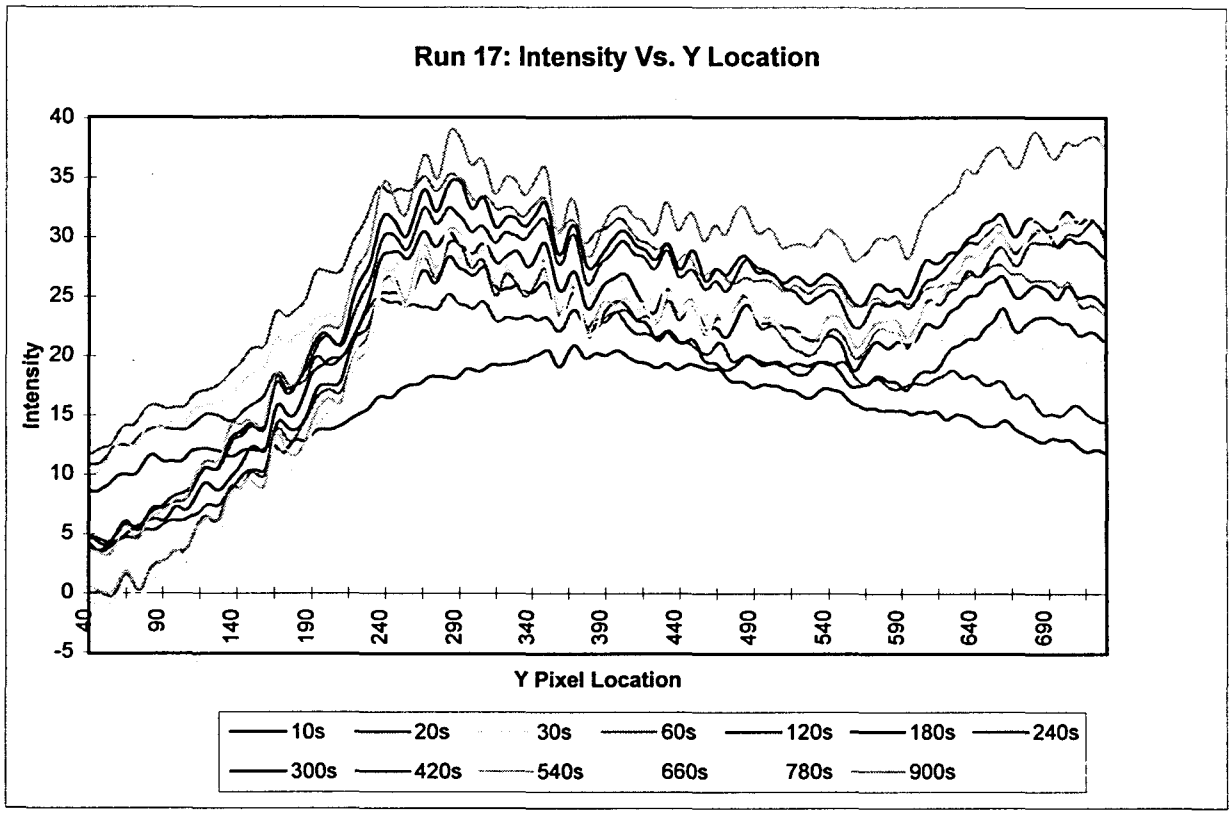
Run 17: Intensity Vs. Y Location
Intensity
Y Pixel Location
10s
20s
30s
60s
120s
180s
240s
300s
420s
540s
660s
780s
900s

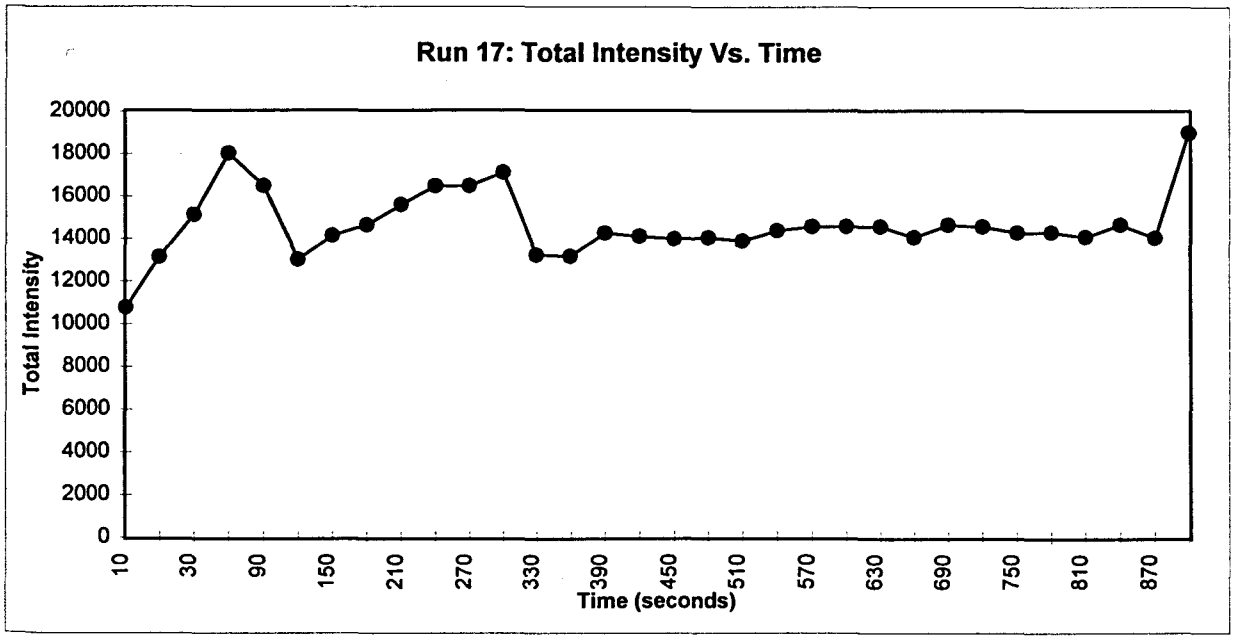
Run 17: Total Intensity Vs. Time
Total Intensity
Time (seconds)

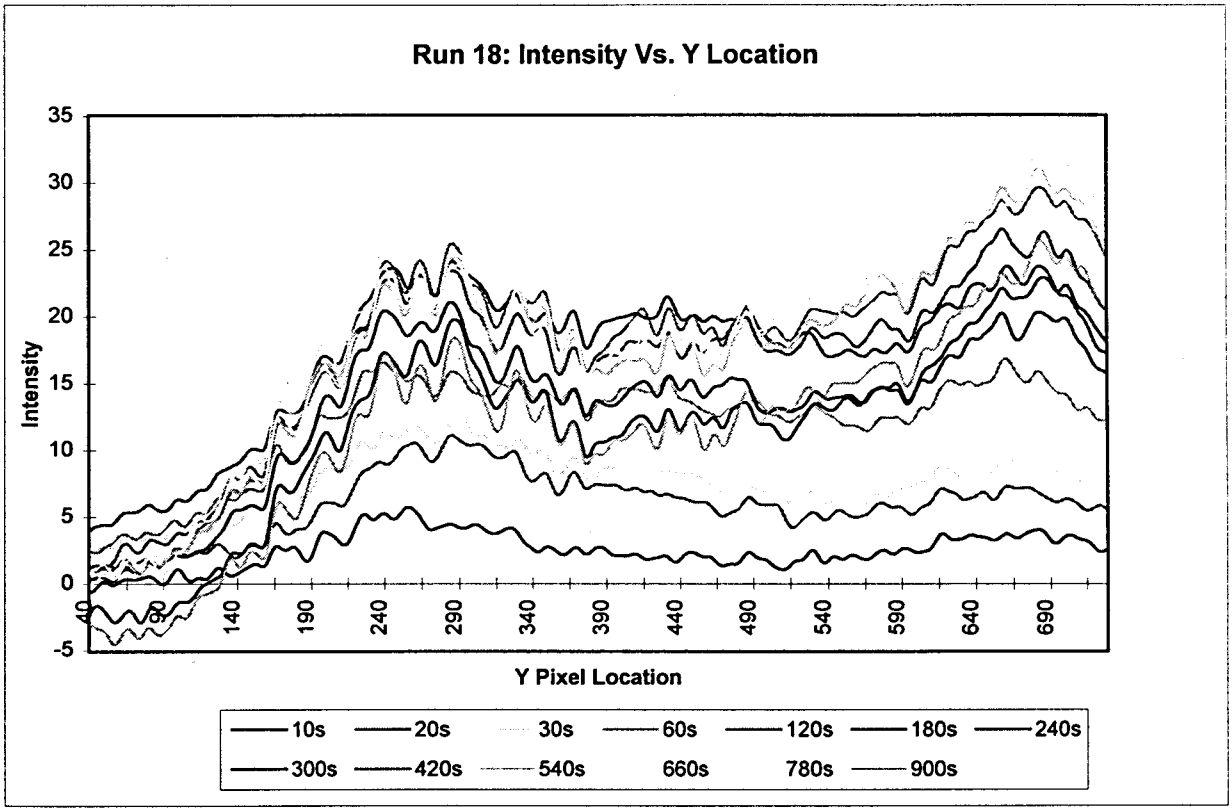
Run 18: Intensity Vs. Y Location
Intensity
35
30
25
20
15
10
5
0
-5
40
90
140
190
240
290
340
390
440
490
540
590
640
690
Y Pixel Location
10s
20s
30s
60s
120s
180s
240s
300s
420s
540s
660s
780s
900s

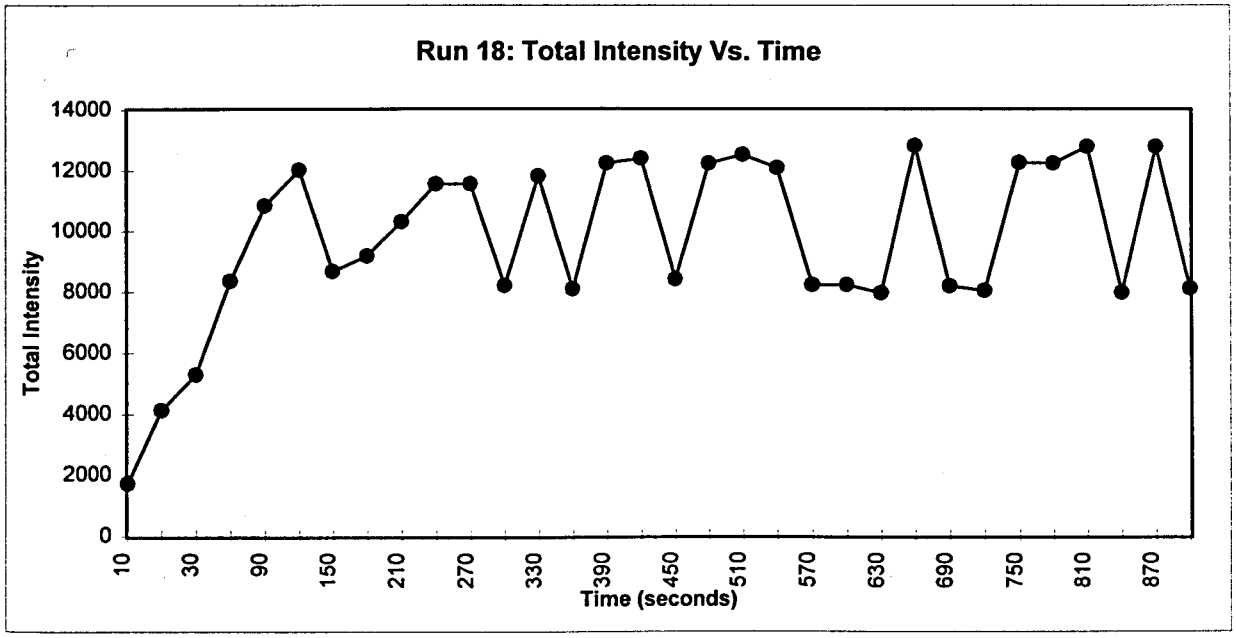
Run 18: Total Intensity Vs. Time
Total Intensity
14000
12000
10000
8000
6000
4000
2000
0
10
30
90
150
210
270
330
390
450
510
570
630
690
750
810
870
Time (seconds)

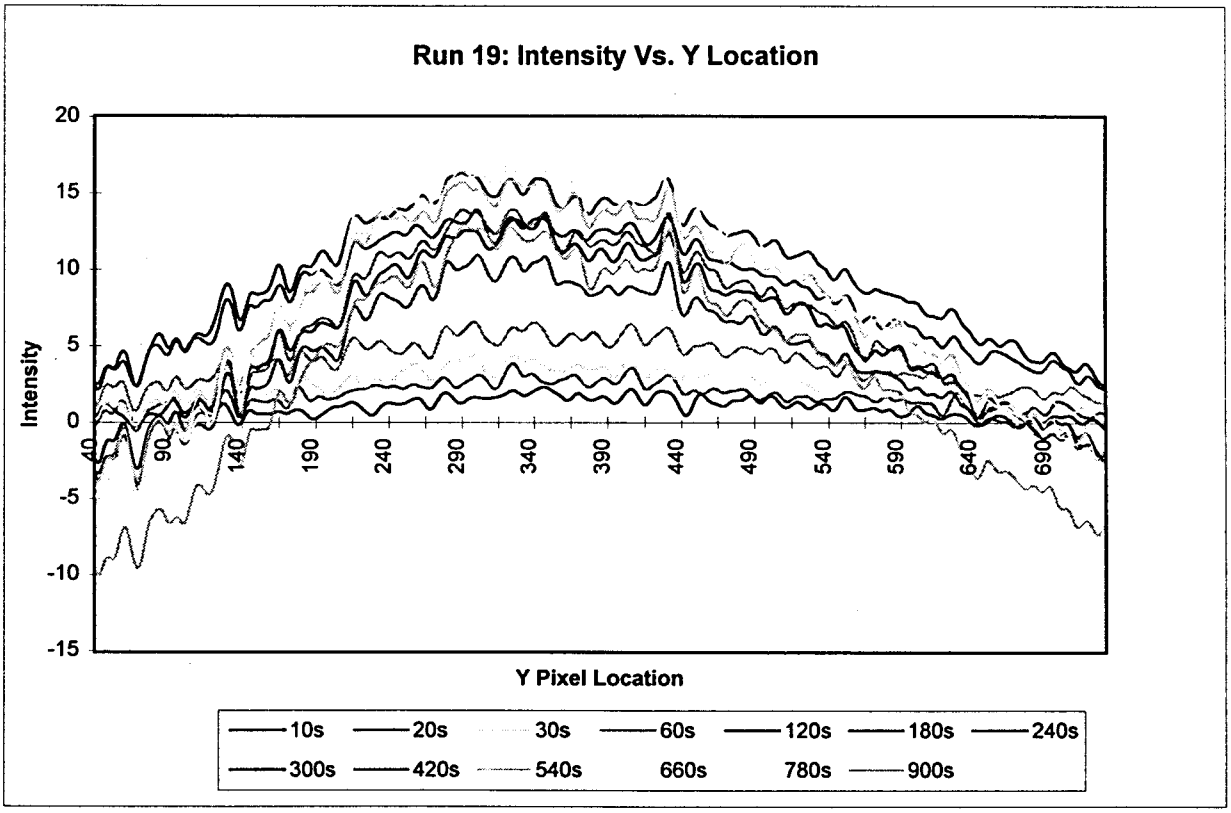
Run 19: Intensity Vs. Y Location
Intensity
Y Pixel Location
10s
20s
30s
60s
120s
180s
240s
300s
420s
540s
660s
780s
900s

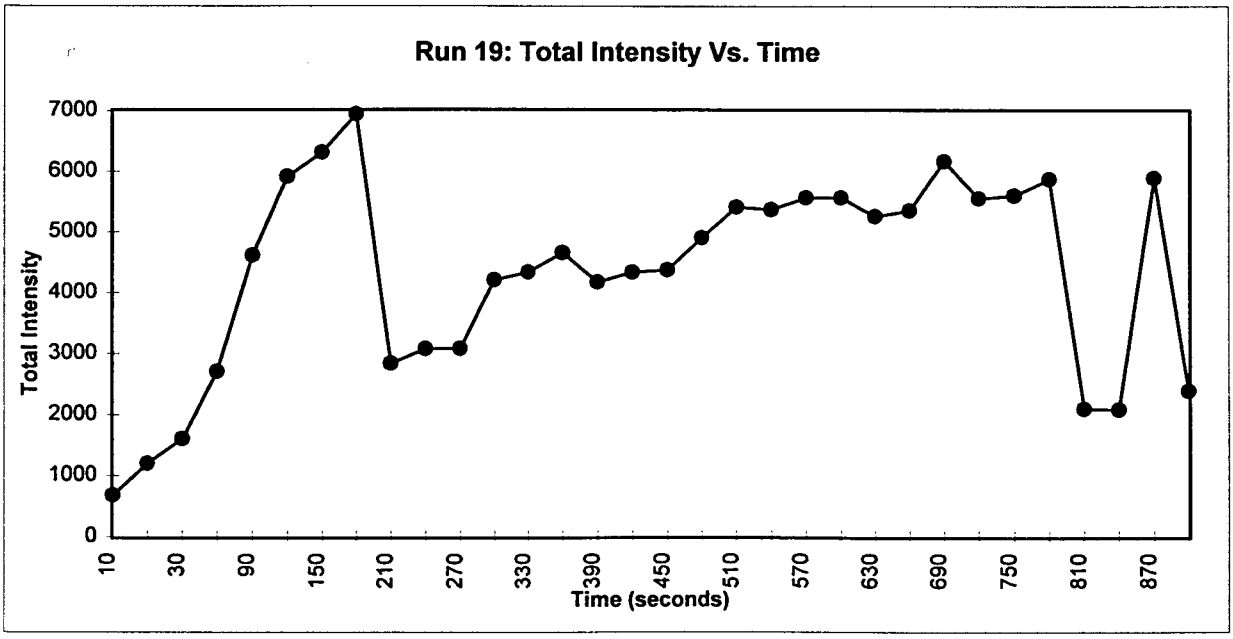
Run 19: Total Intensity Vs. Time
Total Intensity
Time (seconds)

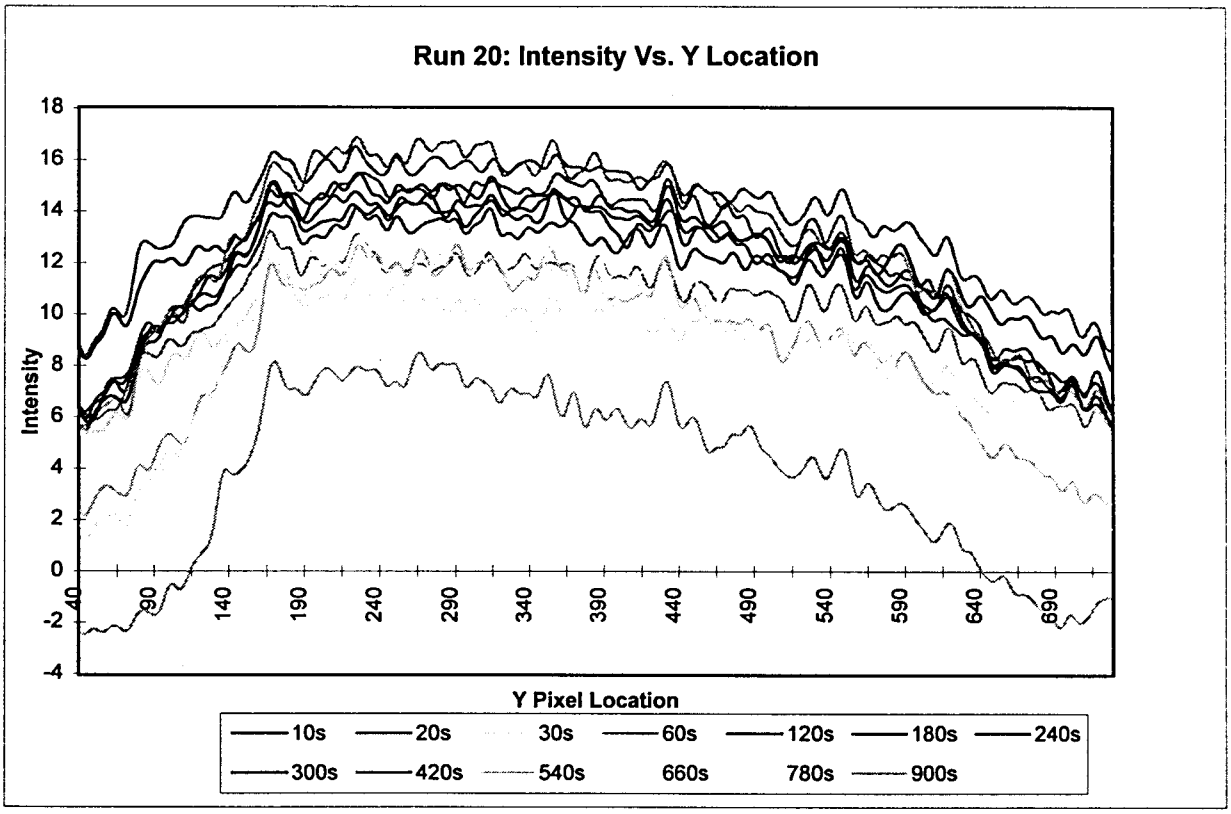
Run 20: Intensity Vs. Y Location
Intensity
Y Pixel Location
10s
20s
30s
60s
120s
180s
240s
300s
420s
540s
660s
780s
900s

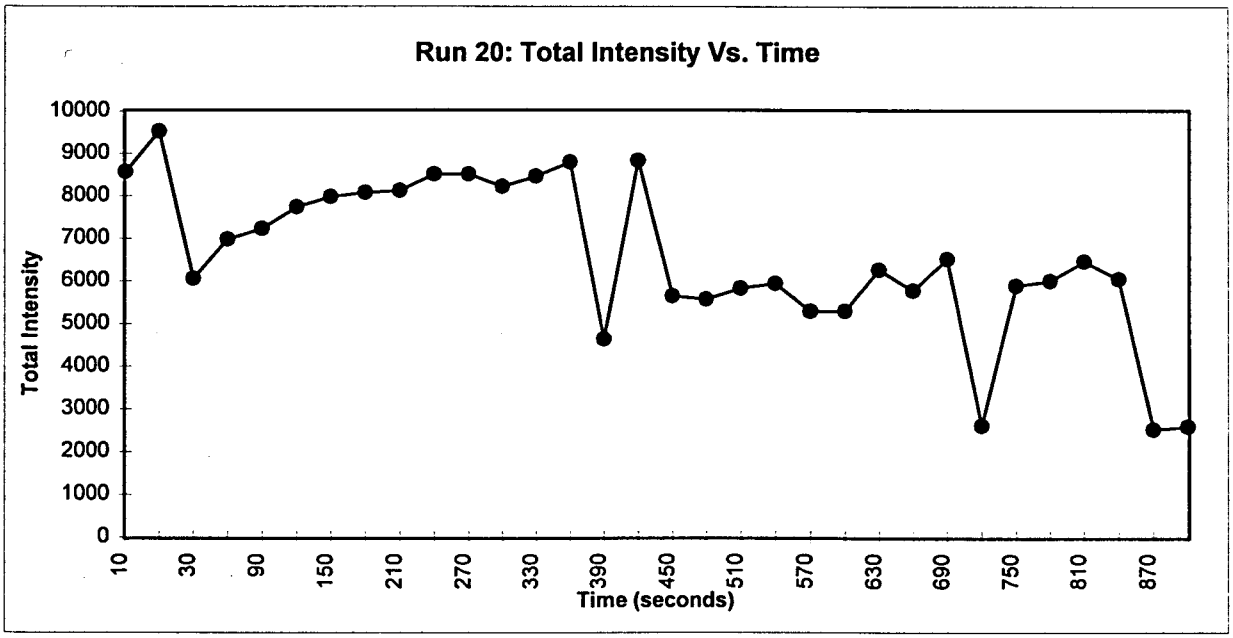
Run 20: Total Intensity Vs. Time
Total Intensity
Time (seconds)

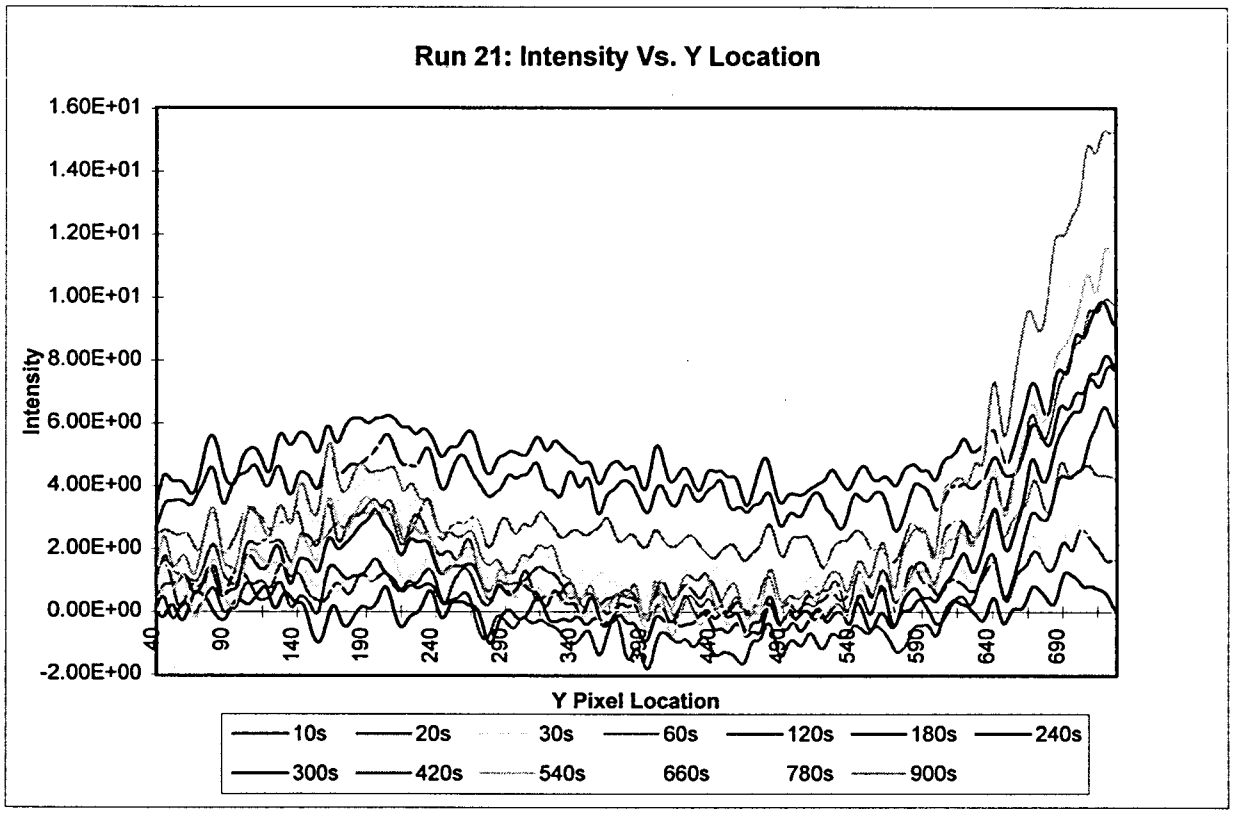
Run 21: Intensity Vs. Y Location
1.60E+01
1.40E+01
1.20E+01
1.00E+01
8.00E+00
6.00E+00
4.00E+00
2.00E+00
0.00E+00
-2.00E+00
Intensity
40
90
140
190
240
290
340
390
440
490
540
590
640
690
Y Pixel Location
10s
20s
30s
60s
120s
180s
240s
300s
420s
540s
660s
780s
900s

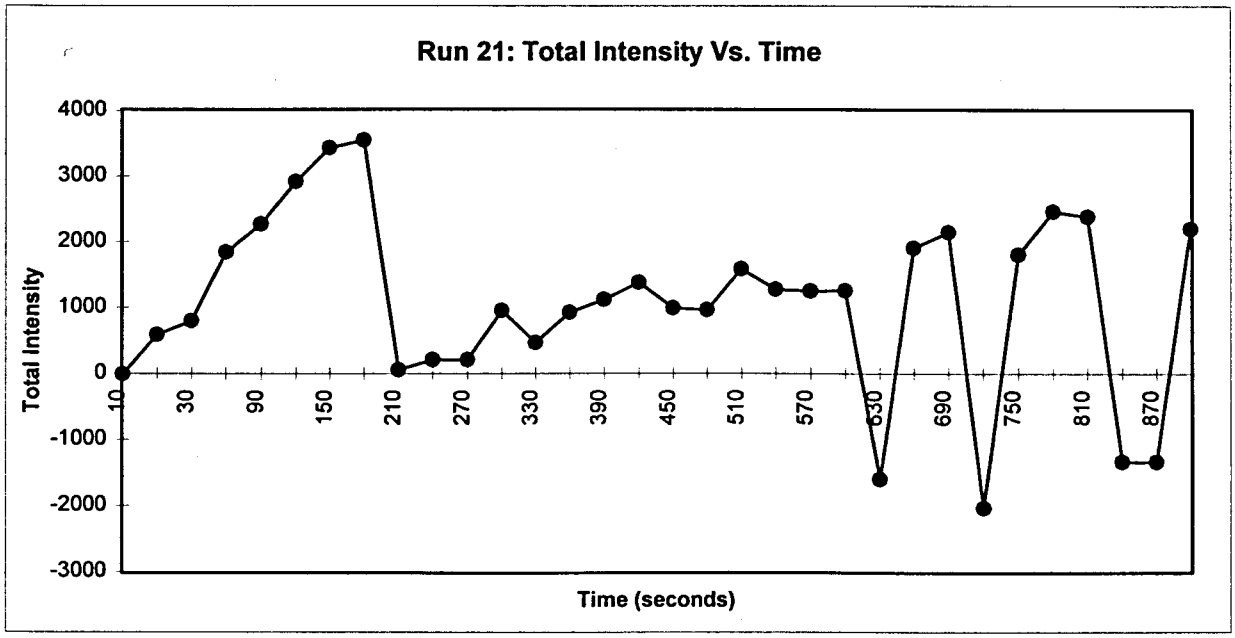
Run 21: Total Intensity Vs. Time
4000
3000
2000
1000
0
-1000
-2000
-3000
Total Intensity
10
30
90
150
210
270
330
390
450
510
570
630
690
750
810
870
Time (seconds)

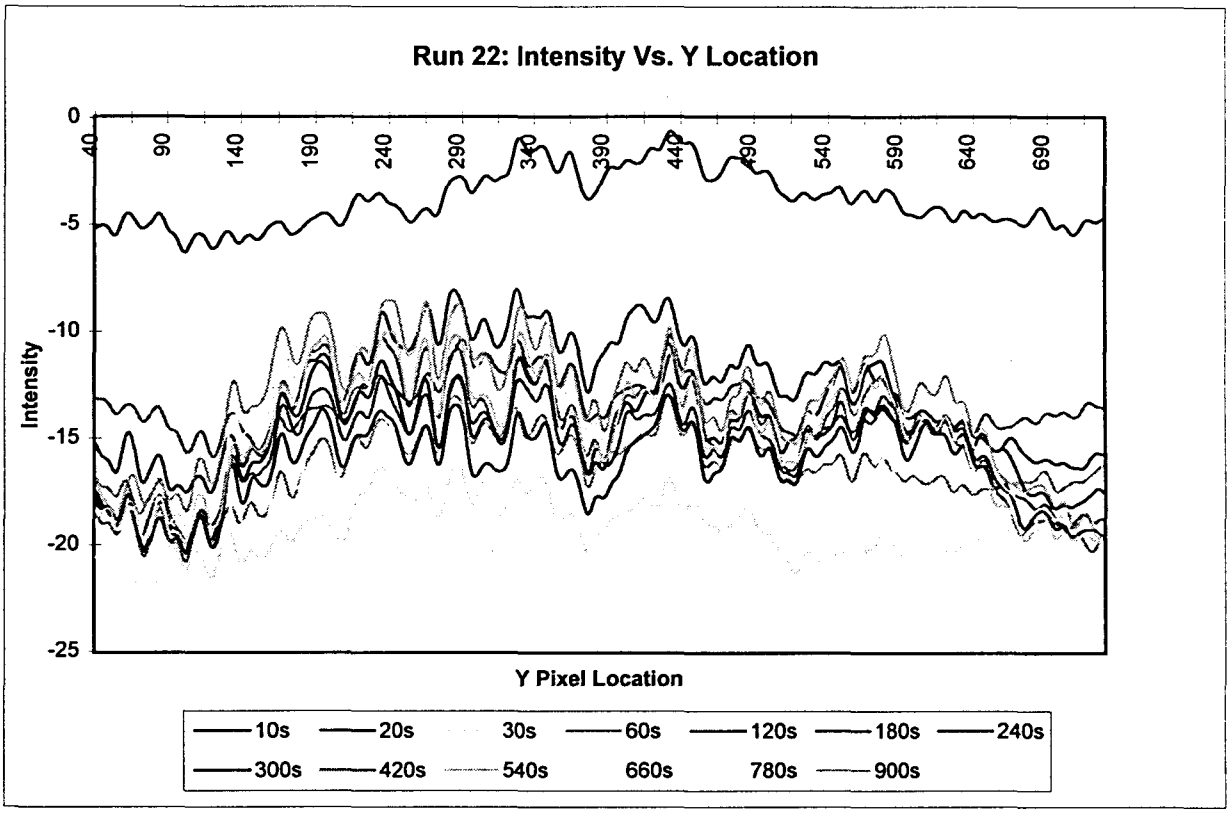
Run 22: Intensity Vs. Y Location
Intensity
0
-5
-10
-15
-20
-25
40
90
140
190
240
290
340
390
440
490
540
590
640
690
Y Pixel Location
10s
20s
30s
60s
120s
180s
240s
300s
420s
540s
660s
780s
900s

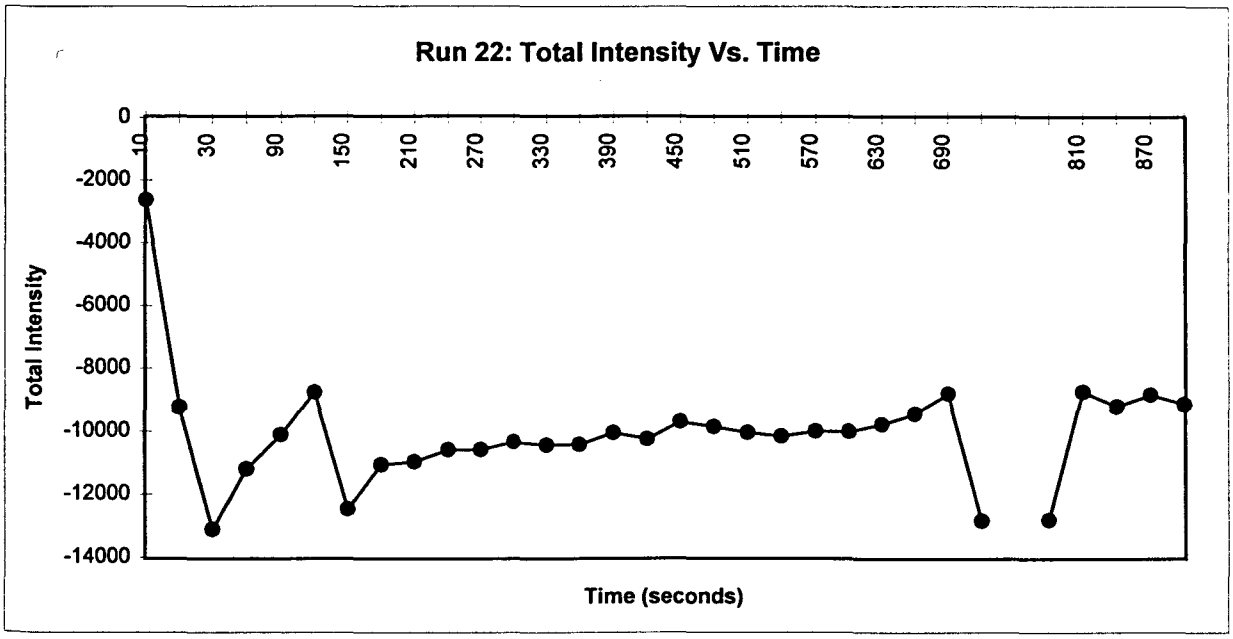
Run 22: Total Intensity Vs. Time
Total Intensity
0
-2000
-4000
-6000
-8000
-10000
-12000
-14000
10
30
90
150
210
270
330
390
450
510
570
630
690
810
870
Time (seconds)

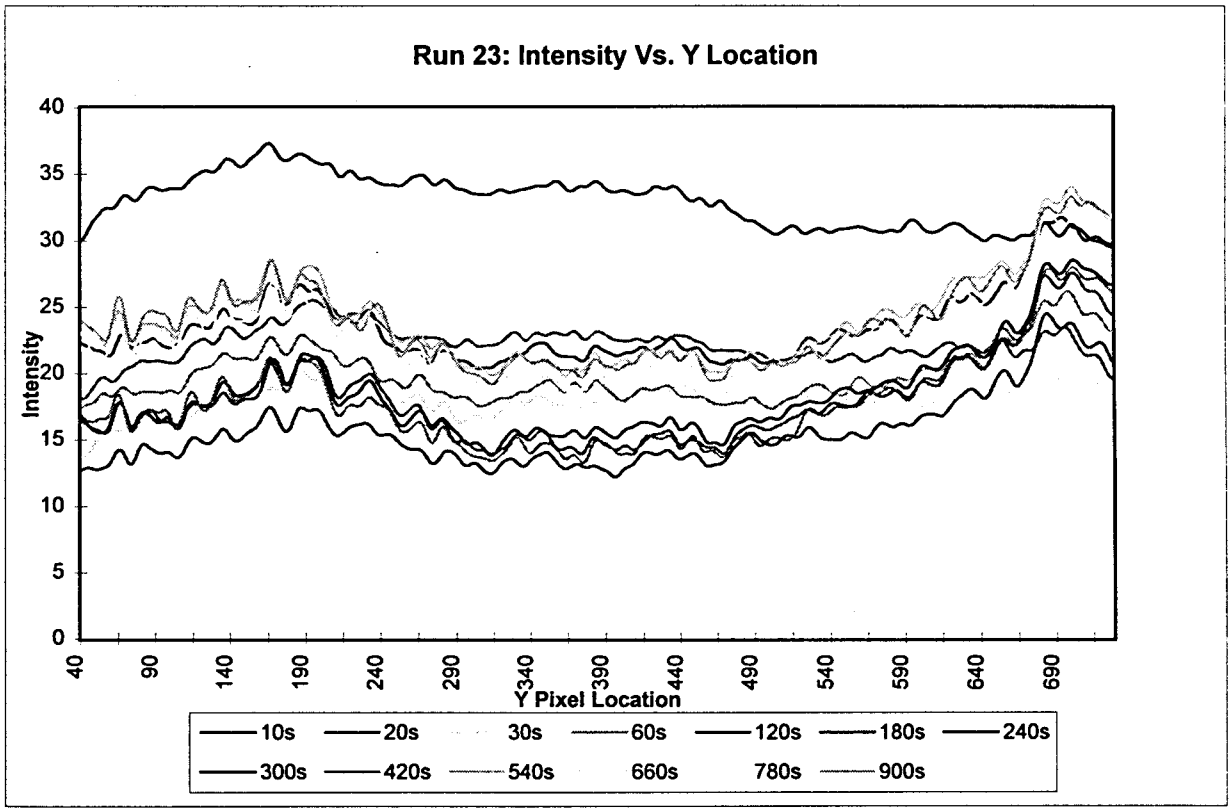
Run 23: Intensity Vs. Y Location
Intensity
Y Pixel Location
10s
20s
30s
60s
120s
180s
240s
300s
420s
540s
660s
780s
900s

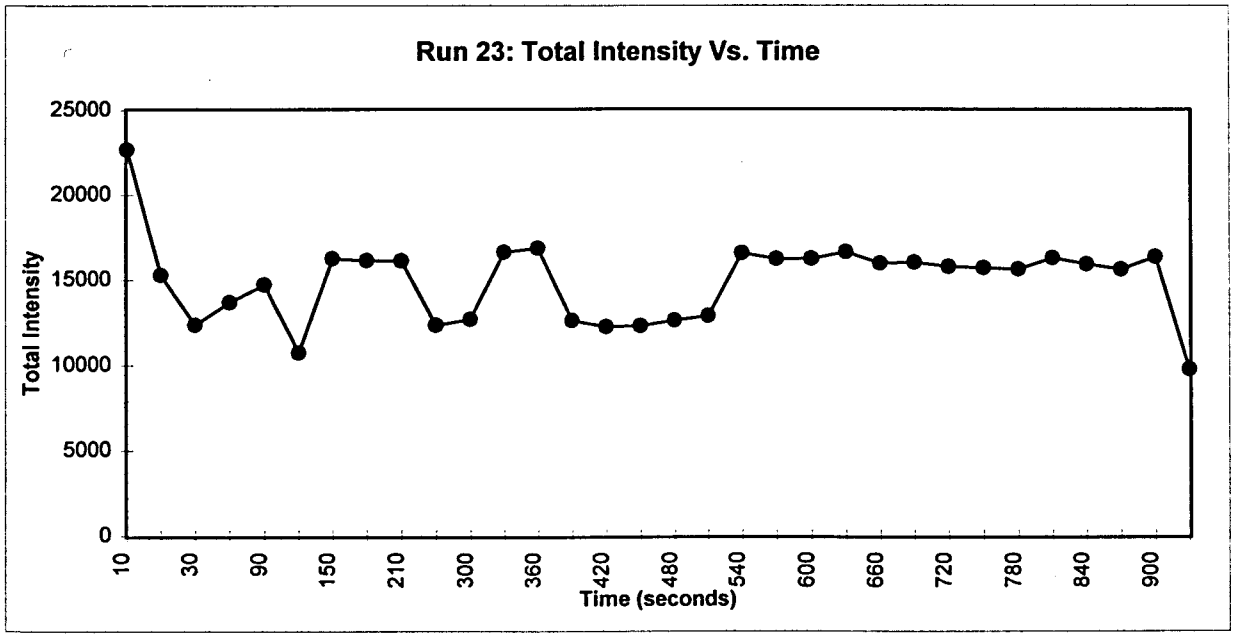
Run 23: Total Intensity Vs. Time
Total Intensity
Time (seconds)

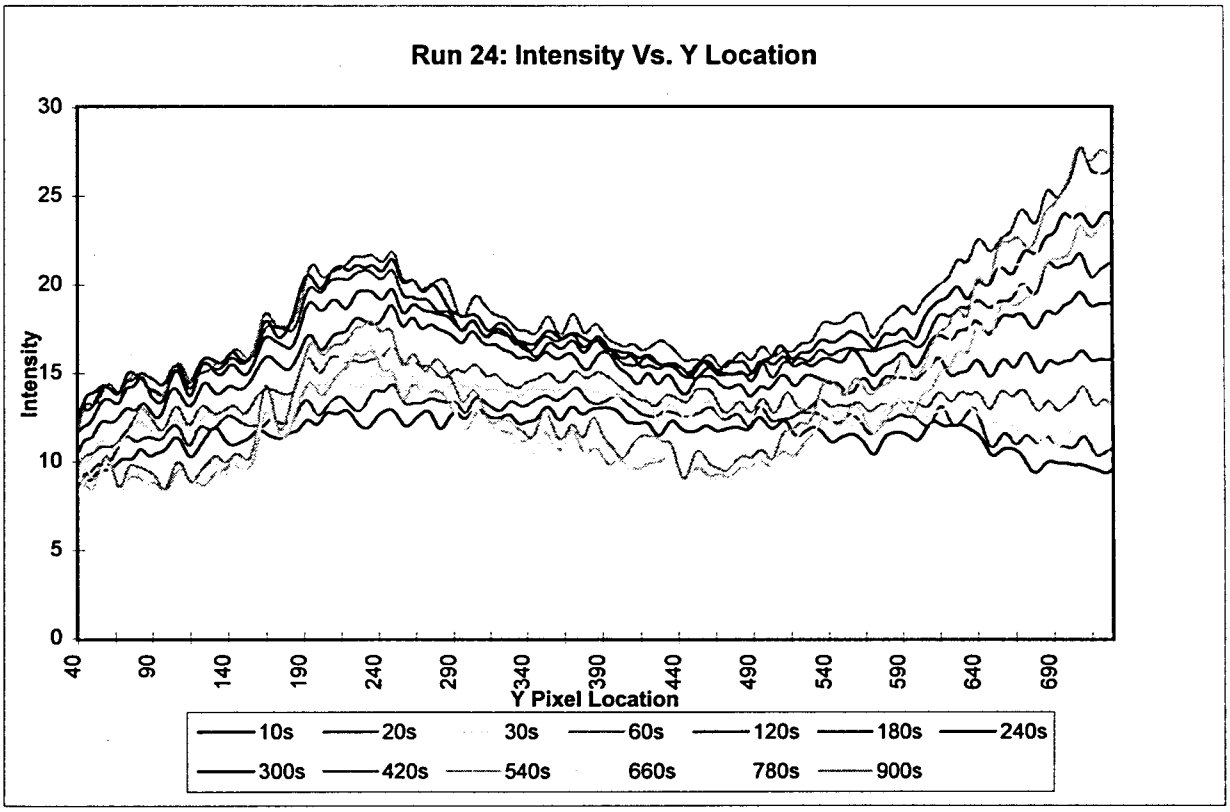
Run 24: Intensity Vs. Y Location
Intensity
30
25
20
15
10
5
0
40
90
140
190
240
290
340
390
440
490
540
590
640
690
Y Pixel Location
10s
20s
30s
60s
120s
180s
240s
300s
420s
540s
660s
780s
900s

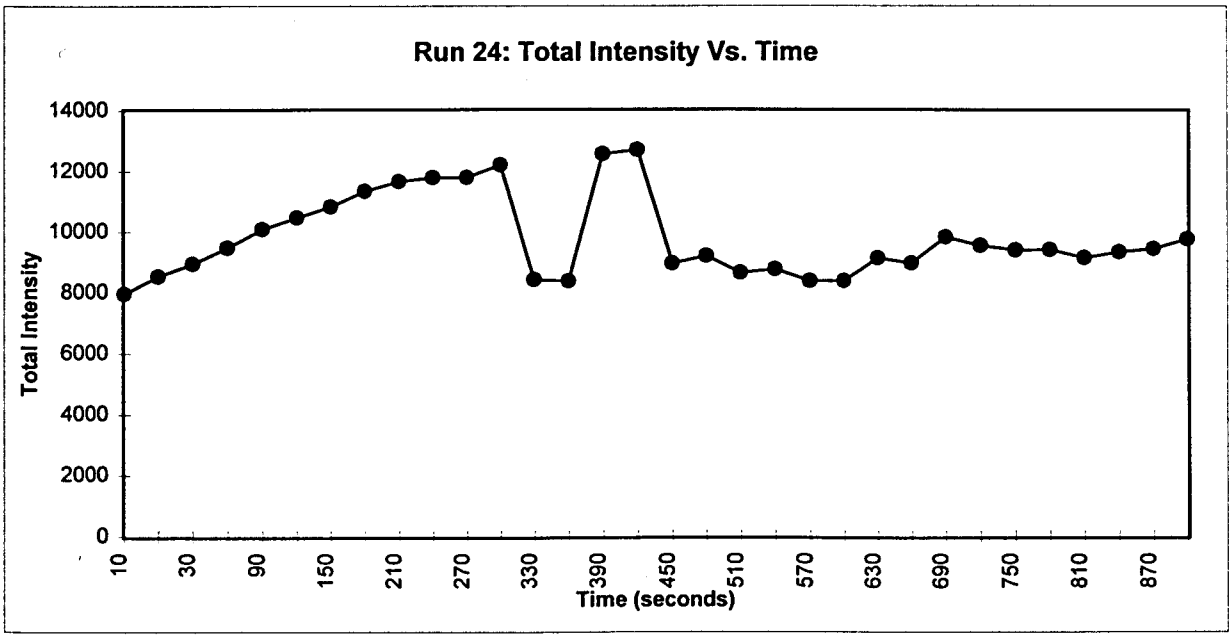
Run 24: Total Intensity Vs. Time
Total Intensity
14000
12000
10000
8000
6000
4000
2000
0
10
30
90
150
210
270
330
390
450
510
570
630
690
750
810
870
Time (seconds)

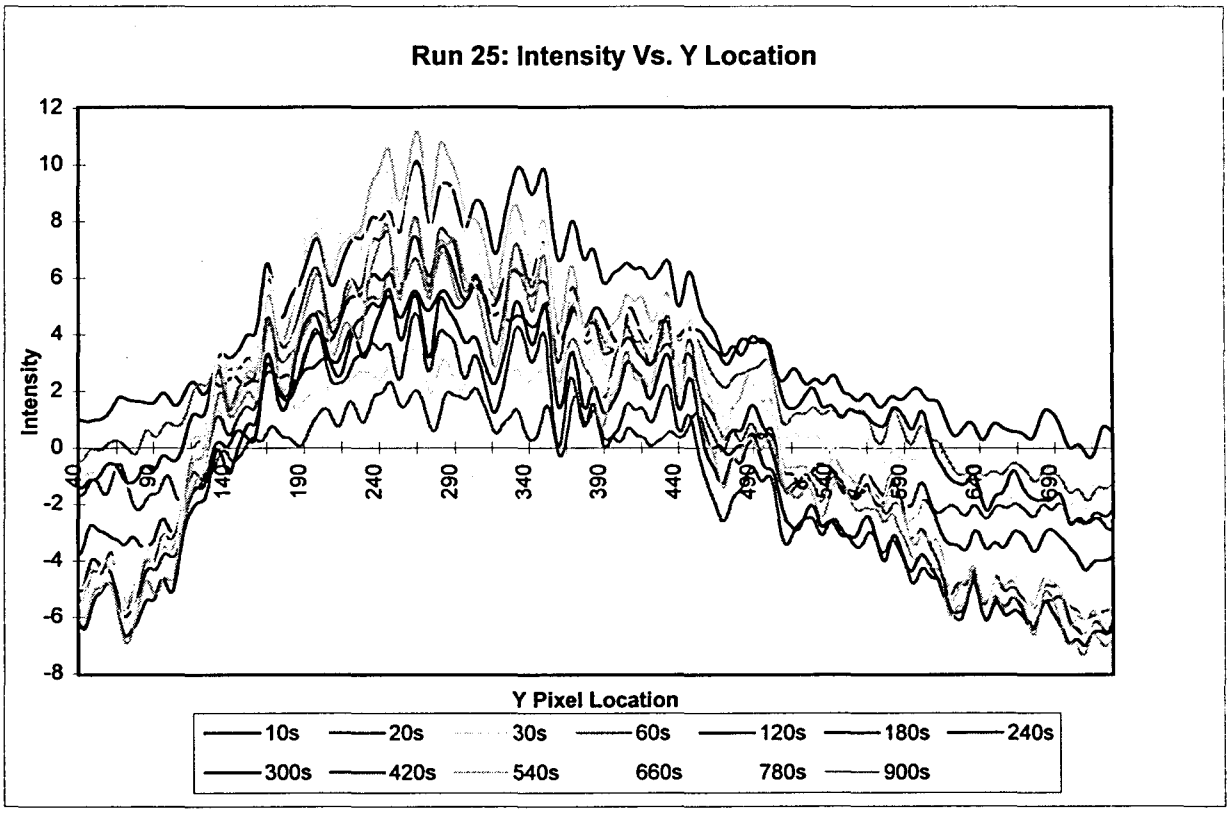
Run 25: Intensity Vs. Y Location
Intensity
Y Pixel Location
10s
20s
30s
60s
120s
180s
240s
300s
420s
540s
660s
780s
900s

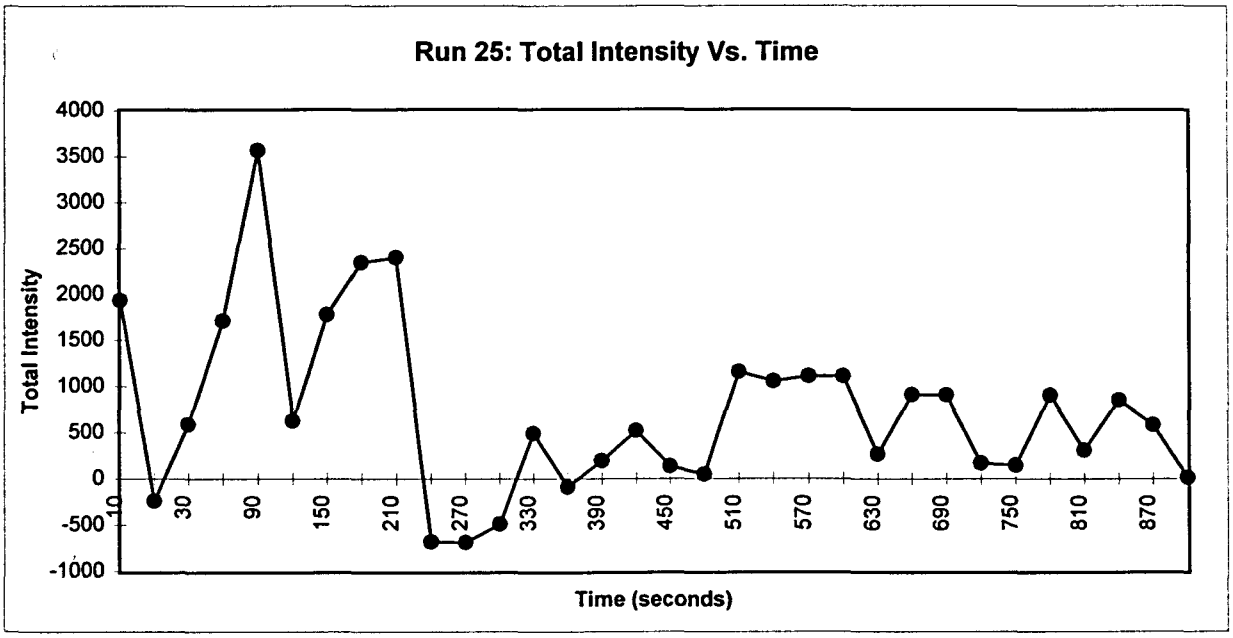
Run 25: Total Intensity Vs. Time
Total Intensity
Time (seconds)

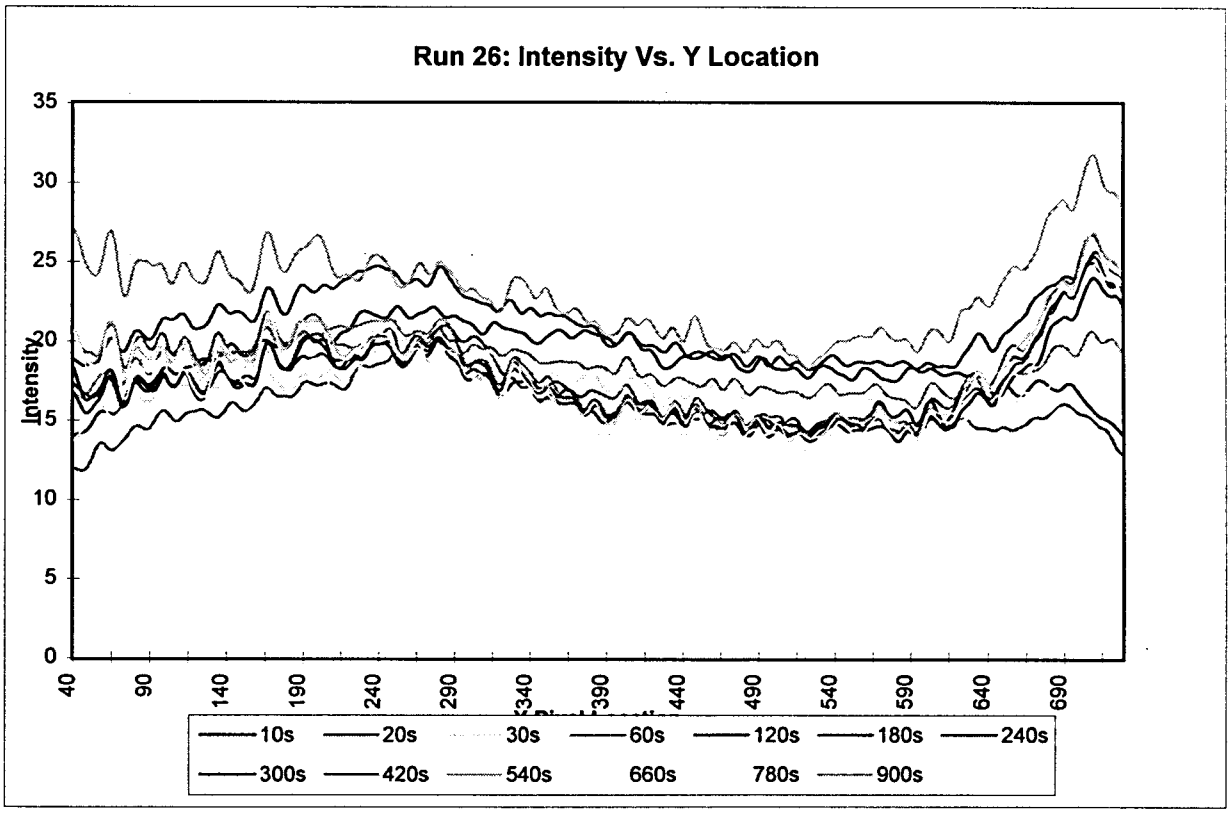
Run 26: Intensity Vs. Y Location
Intensity
35
30
25
20
15
10
5
0
40
90
140
190
240
290
340
390
440
490
540
590
640
690
10s
20s
30s
60s
120s
180s
240s
300s
420s
540s
660s
780s
900s

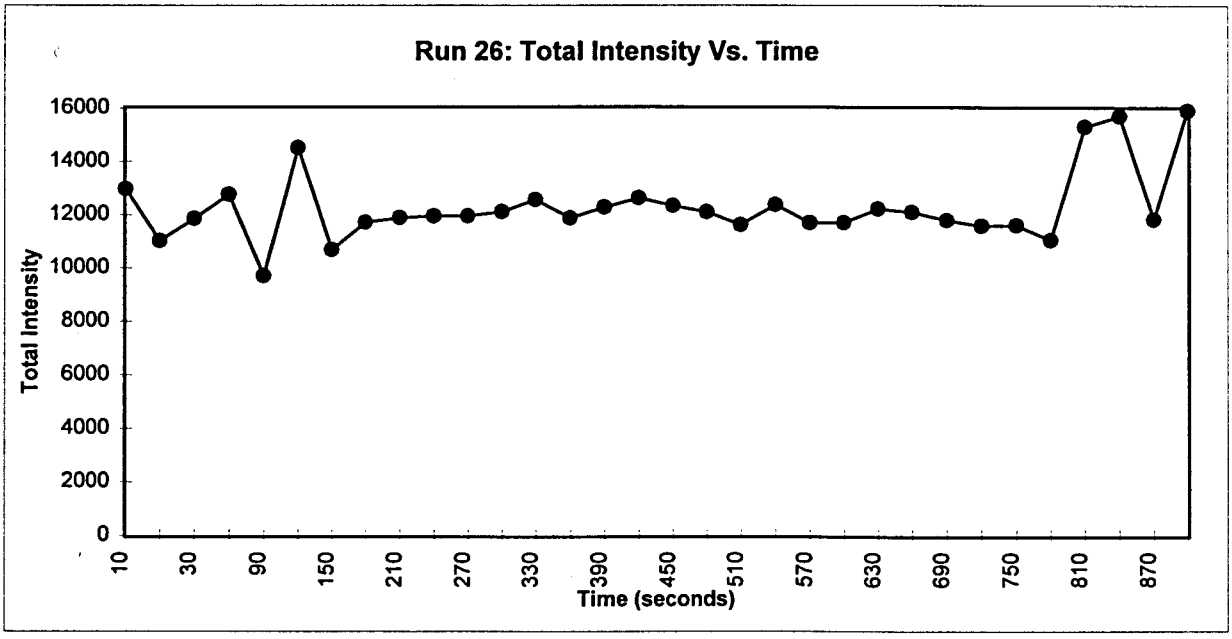
Run 26: Total Intensity Vs. Time
Total Intensity
16000
14000
12000
10000
8000
6000
4000
2000
0
10
30
90
150
210
270
330
390
450
510
570
630
690
750
810
870
Time (seconds)

APPENDIX C: BOUNDARY LAYER PROFILES

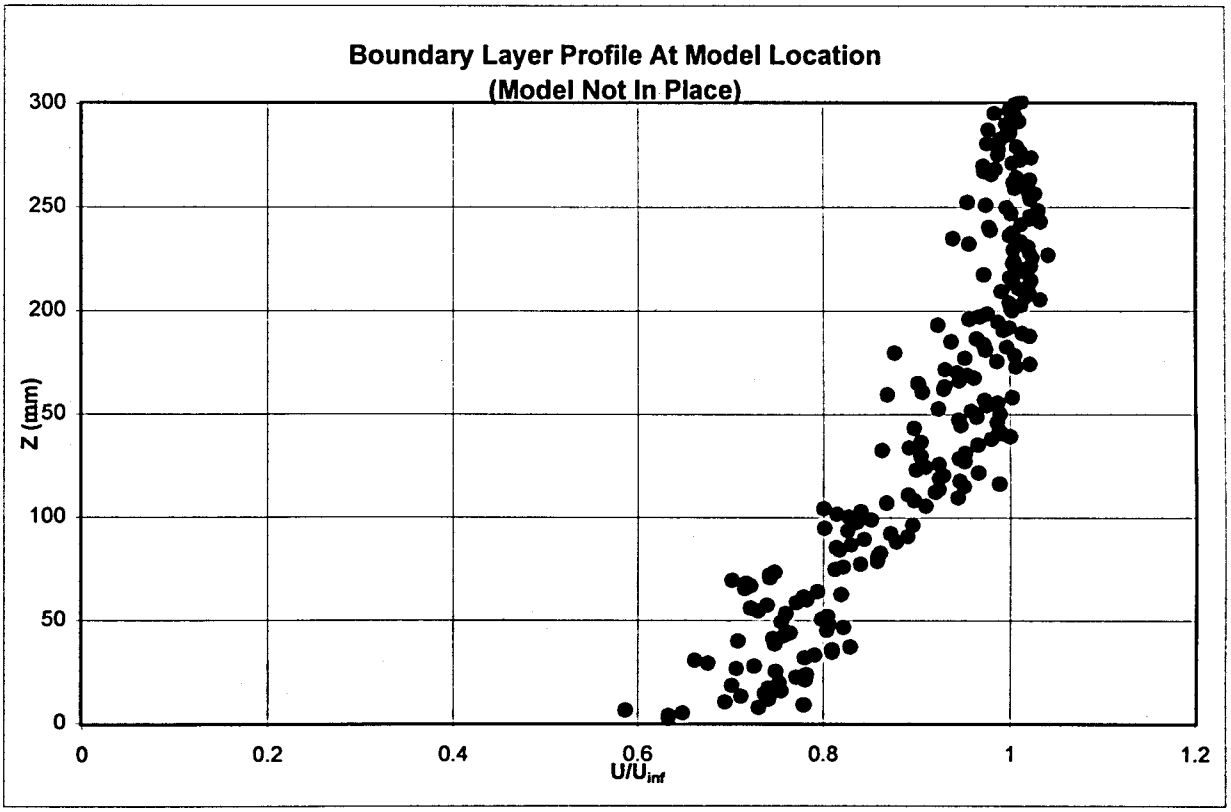
Boundary Layer Profile At Model Location
(Model Not In Place)
300
250
200
150
100
50
0
Z (mm)
0
0.2
0.4
0.6
0.8
1
1.2
U/U_inf

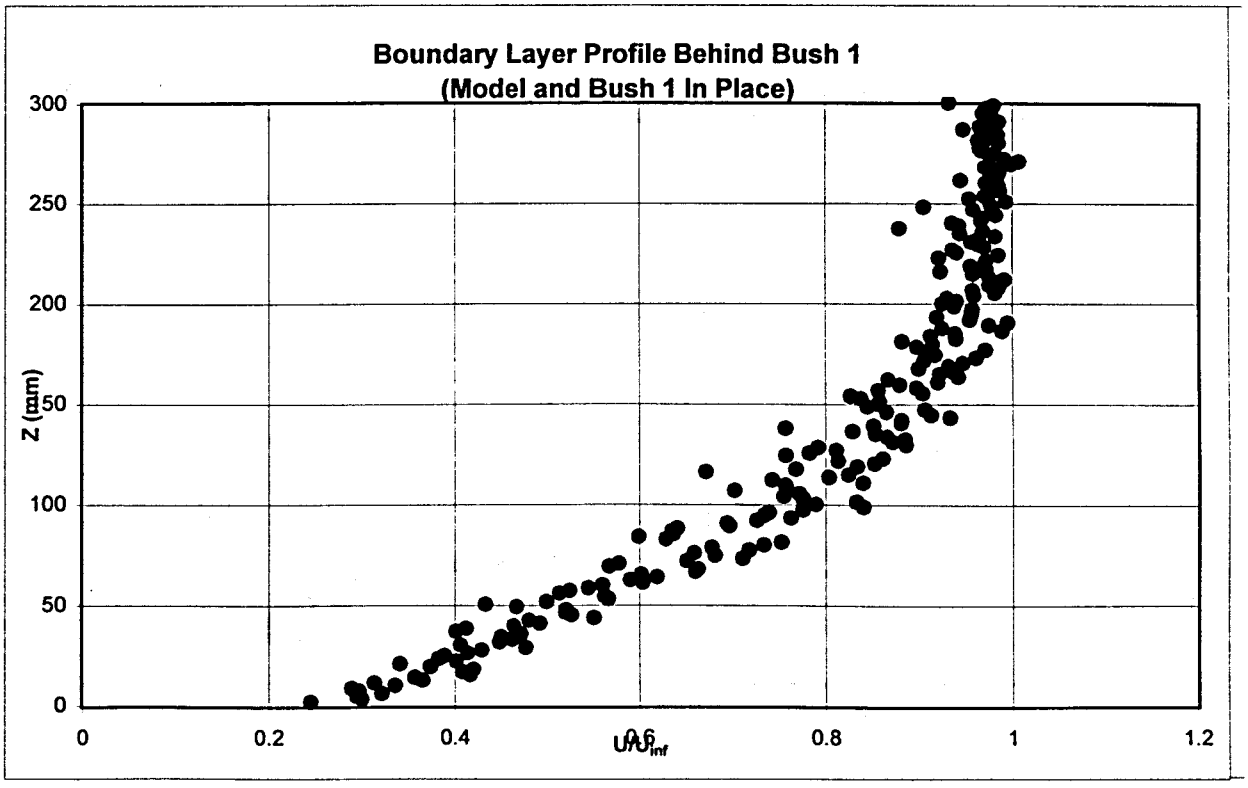
Boundary Layer Profile Behind Bush 1
(Model and Bush 1 In Place)
300
250
200
150
100
50
0
Z (mm)
0
0.2
0.4
0.6
0.8
1
1.2
U/U_inf

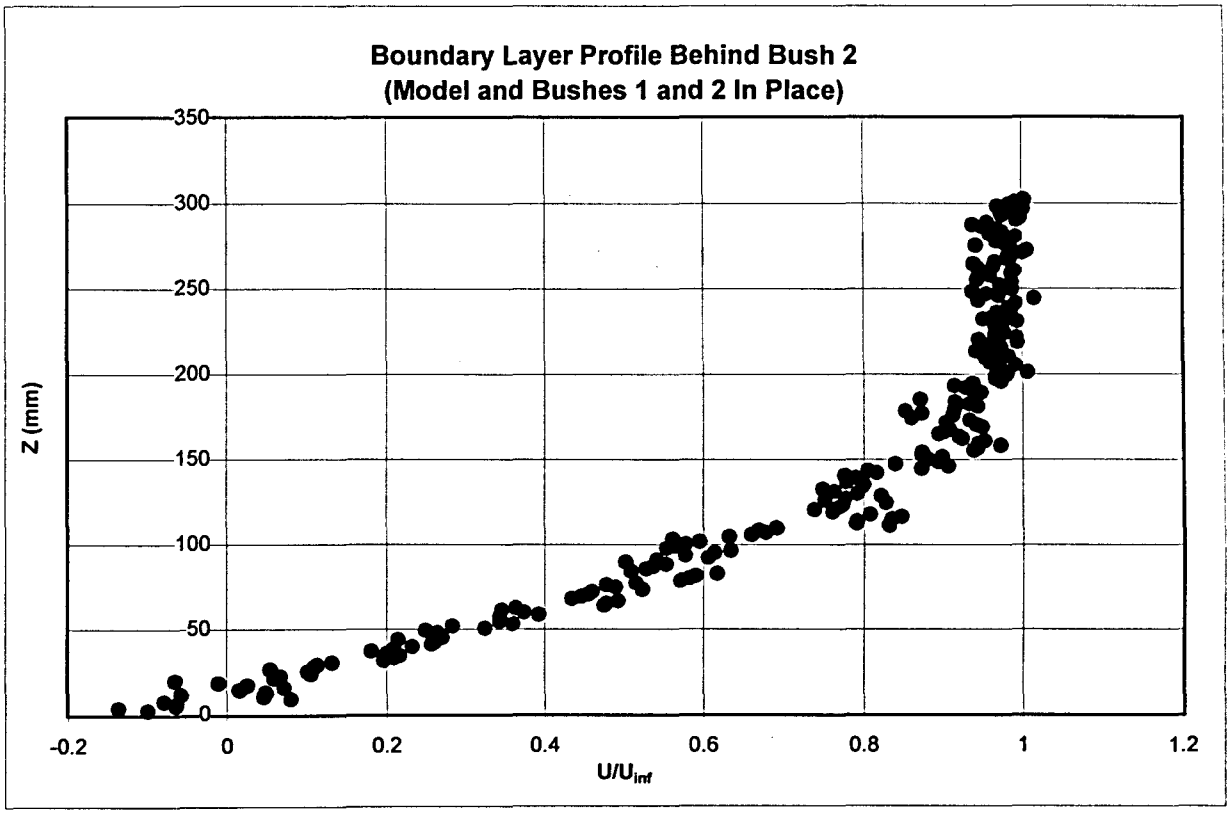
Boundary Layer Profile Behind Bush 2
(Model and Bushes 1 and 2 In Place)
Z (mm)
350
300
250
200
150
100
50
0
-0.2
0
0.2
0.4
0.6
0.8
1
1.2
U/U_inf

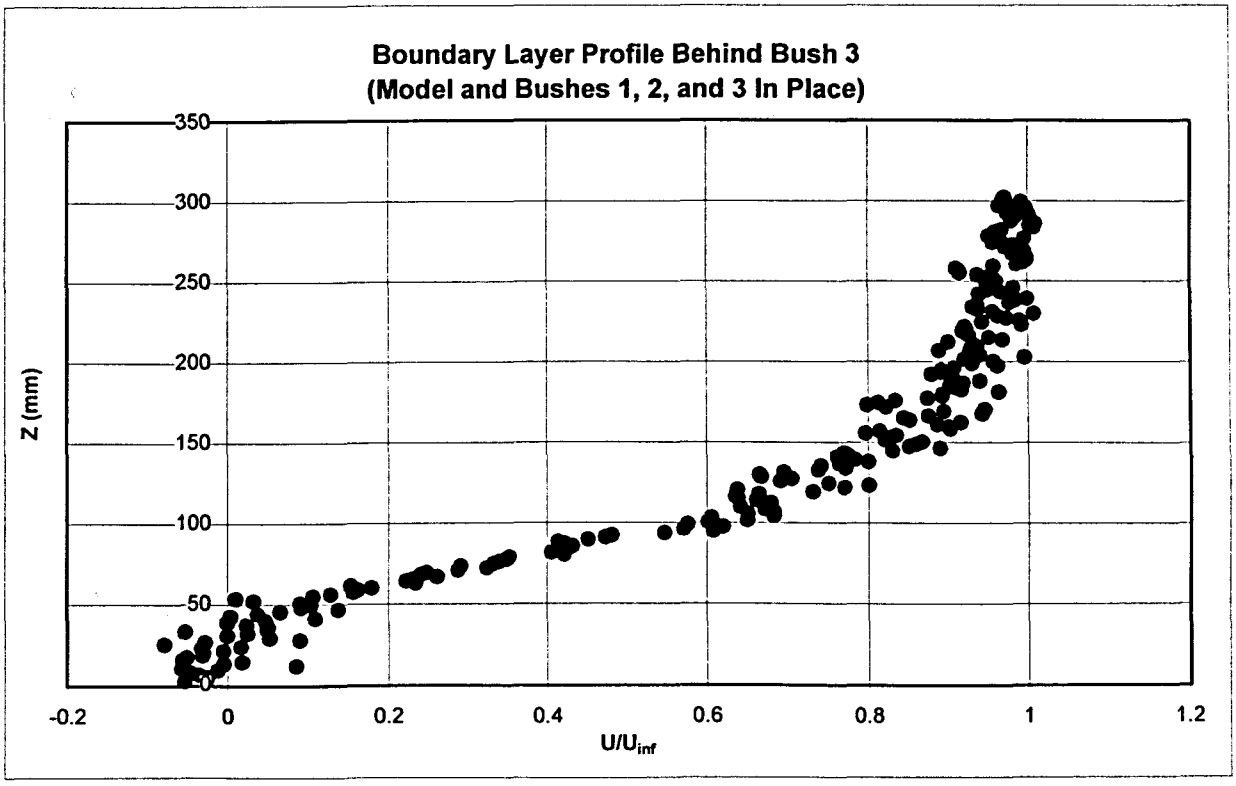
Boundary Layer Profile Behind Bush 3
(Model and Bushes 1, 2, and 3 In Place)
Z (mm)
350
300
250
200
150
100
50
0
-0.2
0
0.2
0.4
0.6
0.8
1
1.2
U/U_inf

APPENDIX D: DESIGN OF ROUGHNESS ELEMENTS

The design of spires and roughness elements used is based on the procedure of Ref 8. The goal is to produce a set of roughness elements for a skin friction coefficient value of 0.0032, and a boundary layer thickness at x = 6H of 20 cm. The roughness blocks will also have a spacing of 15 cm.

1. Spires of height H are designed to produce the desired boundary layer thickness δ at x = 6H.
2. Assume, for example, that δ = 20 cm at 6 spire heights downwind of the spires.
3. The design is based on a power law profile with exponent of α, i.e.,

$$\frac{u}{u_{ref}} = \left(\frac{z}{z_{ref}}\right)^{\alpha}$$

4. The value of α depends on the desired value of friction coefficient, i.e.,

$$C_f = 0.136\left(\frac{\alpha}{1+\alpha}\right)^2$$

5. Definitions:

$$\beta = \frac{\delta}{H_0}\frac{\alpha}{1+\alpha}, \text{ where } H_0 = \text{test section height}$$

$$H = 1.39\frac{\delta}{1+\frac{\alpha}{2}}, \text{ where H is spire height}$$

$$\psi = \beta\left\{\left(\frac{2}{1+2\alpha}\right)+\beta-\frac{1.13\alpha}{(1+\alpha)\left(1+\frac{\alpha}{2}\right)}\right\}\frac{1}{(1-\beta)^2}$$

$$\frac{b}{H} = 0.5H_0\psi\left(\frac{1+\frac{\alpha}{2}}{(1+\psi)\delta}\right), \text{ where b is spire width}$$

6. Spire spacing is H/2

7. Pressure drop factor F:

$$F = \left\{1+\frac{\delta}{H_0}\left(\frac{\alpha(3+2\alpha)}{1+\alpha\left(1-\frac{\delta}{H_0}\right)}\right)\right\}^{-1}$$

8. Increase of δ downwind of 6 spire heights:

$$\Delta\delta = 0.068\alpha\left(\frac{1+2\alpha}{1+\alpha}\right)\Delta x F$$

9. Block roughness height k

$$k = \delta\exp\left(\frac{2}{3}\ln\left(\frac{D}{\delta}\right)-0.1161\sqrt{\frac{2}{C_f}+2.05}\right),$$

where D is the block roughness spacing

10. Calculations:

C_f is obtained through:

$$C_f = \frac{\tau}{\frac{1}{2}\rho u_\infty^2} = \frac{\rho u_*^2}{\frac{1}{2}\rho u_\infty^2} = 2\left(\frac{u_*}{u_\infty}\right)^2$$

where $\frac{u_*}{u_\infty} = 0.06$, resulting in $C_f = .0072$. The rest of the variables calculate as follows:

H_o	=	107 cm
β	=	0.043
H	=	24.19 cm
ψ	=	0.050
b	=	3.553 cm
F	=	0.861
D	=	15 cm
k	=	2.37 cm

So the final design consists roughness spires 24.19 cm tall by 3.553 cm wide, spaced 12.09 cm apart, with 2.37 cm roughness cubes spaced 15 cm apart. This is planned to produce a boundary layer thickness of 20 cm at the test section.

APPENDIX E: FORTRAN COMPUTER CODE FOR DIGITAL PHOTOGRAPHIC ANALYSIS

```
*     Fortran code to convert ASCII photograph files into intensity data
*     By S. Magnus Therneilus, Iowa State University

      implicit none
      real*8 temp(640000), z(800, 800), new(800), smoothed(1000)
      real*8 num, col, row, max, data(1000), fc, ft, dt
      real*8 tmp, avg(1000), row_start, row_end, rows, orig(1000)
      integer x, y, col_int, row_int, num_int, i, j
      integer r_s_int, r_e_int, k, num_smo, n
      integer col_start, col_end, cnt, nn, counter
      character*2 ch1
      character*42 ch2
      character*50 file1, file2, file3, file4, file5, file6, file7
      character*50 file0
      character*50 file11, file22, file33, file44, file55, file66
      character*50 file77
        file0 = '../data/1m0zz710/image01.pgm'
        file1 = '../data/1m0zz710/image16.pgm'
        file11 = '../data/1m0zz710/image16_smoothened.dat'
        file2 = '../data/1m0zz710/image16.pgm'
        file22 = '../data/1m0zz710/image16_smoothened.dat'
        file3 = '../data/1m0zz710/image16.pgm'
        file33 = '../data/1m0zz710/image16_smoothened.dat'
        file4 = '../data/1m0zz710/image16.pgm'
        file44 = '../data/1m0zz710/image16_smoothened.dat'
        file5 = '../data/1m0zz710/image16.pgm'
        file55 = '../data/1m0zz710/image16_smoothened.dat'
        file6 = '../data/1m0zz710/image16.pgm'
        file66 = '../data/1m0zz710/image16_smoothened.dat'
        file7 = '../data/1m0zz710/image16.pgm'
        file77 = '../data/1m0zz710/image16_smoothened.dat'
      open (unit = 9, file = file0, status ='unknown')
      open (unit = 10, file = file1, status ='unknown')
      open (unit = 12, file = file2, status ='unknown')
      open (unit = 14, file = file3, status 'unknown')
      open (unit = 16, file = file4, status ='unknown')
      open (unit = 18, file = file5, status 'unknown')
      open (unit = 20, file = file6, status ='unknown')
      open (unit = 22, file = file7, status ='unknown')
      open (unit = 11, file = file11, status ='unknown')
      open (unit = 13, file = file22, status ='unknown')
```

```
      open (unit = 15, file = file33, status ='unknown')
      open (unit = 17, file = file44, status ='unknown')
      open (unit = 19, file = file55, status ='unknown')
      open (unit = 21, file = file66, status ='unknown')
      open (unit = 23, file = file77, status ='unknown')
      counter = 1
      nn = 9
5     write (*, *), 'File being processed (max 8):', counter
      read (nn, 10) ch1
10    format (A2)
      read (nn, 20) ch2
20    format (A42)
      read (nn, *) col, row
      read (nn, *) max
*
* Read the data
*
      num = col * row - 3
      num_int = int(num)
      col_int = int(col)
      row_int = int(row)
      do y = 1, 1
        read (nn, *, end = 30) (temp(x), x = 1, num_int)
      end do
      i = 1
      do y = 1, row_int
        do x = 1, col_int
          z(x, y) = temp(i)
          i = i + 1
        end do
      end do
*
* OK, everything has been read in now. There are so many columns
* and so many rows. Now it is necessary to go in and look at the
* rows & columns that are of interest.
*
      col_start = 57
      col_end = col_start + 661
    row_start = 256.0
    r_s_int = int(row_start)
    row_end = row_start + 22.0
```

```
      r_e_int = int(row_end)
*
* Next step is to look at removing the sides of the picture
*
      rows = row_end - row_start + 1.0
        k = 0
        do i = 1, col_int
          tmp = 0.0
          do j = r_s_int, r_e_int
            tmp = tmp + z(i, j)
          end do
          avg(i) = tmp / rows
*
* Subtract the original data from all the curves.
*
          if (cnt .eq. 0) then
            orig(i) = avg(i)
          else
            avg(i) = avg(i) - orig(i)
          end if
        end do
        go to 40
30      write (*, *)
40      write (*, *)
        num_smo = 6
        n = 6
        fc = 10.0
        ft = 12.0
        dt = 0.01
        if (cnt .eq. 1) then
          call smooth(avg, num_smo, col_int, n,
     &                fc, ft, dt)
          do i = col_start, col_end
            smoothed(i) = avg(i)
            write (nn + 1, *) i, smoothed(i)
          end do
        end if
        if (cnt .eq. 0) then
          nn = nn + 1
        else
          nn = nn + 2
```

```
        end if
        cnt = 1
        counter = counter + 1
        if (counter .ne. 9) then
          go to 5
        end if
*
* Close all the files
*
        do i = 9, 23
          close (i)
        end do
        write (*, *), 'Done'
        end
*************************************************************************
***
        subroutine smooth(data, num_smo, col_int, n, fc, ft, dt)
          implicit none
          real*8 data(1000), fc, ft, dt, pi, wt, wc
          real*8 sum, wht(1000), wht0, w, pp, h, f, s
          real*8 summ, t
          integer num_smo, n, j, kk, kkk, il, col_int
          integer k, ij, in
*
* FILTER CONSTRUCTION PROGRAM
*
* Definitions:
*  dt  -  sampling interval (s)
*  fc  -  cutoff frequency (Hz)
*  ft  -  terminal frequency (Hz)
*  wht -  weighting factors, n <> 0
*  wht0 -  weighting factor, n = 0
*
          pi = 4.0 * atan(1.0)
          wt = 2.0 * pi * ft
          wc = 2.0 * pi * fc
          sum = 0.0
          do 65 j = 1, n
            s = dreal(j)
            t = s * dt
            wht(j) =(pi/(2.0*t))*((sin(wt*t)+(wc*t)))/(pi*pi-(wt-wc)**2*t**2)
```

```
65          sum = sum + 2.0 * wht(j)
          sum = sum + fc + ft
          do 8 j = 1, n
8           wht(j) = wht(j) / sum
          wht0 = (ft + fc) / sum
          call smonly(data, wht, wht0, num_smo, col_int, n)
*
* FILTER ANALYSIS PROGRAM
*
* Definitions:
*  w  -  Frequency (rad/s)
*  f  -  Frequenzy (Hz)
*  h  -  Amplitude Ratio
*
* WIGHT OUTPUT
*
          kk = 0
c         write (3, 10) kk, wht0
10        format (1h, 5x, 1hn, 9x, 6hweight, /, 6x, i1, 5x, f12.8)
          do 12 k = 1, n
            kkk = 1 * k
c           write (3, 15) kkk, wht(k)
c 15        format (1h, 4x, i2, 5x, f12.8)
12        continue
*
* FILTER ANALYSIS
*
c         write (3, 16)
c 16      format (1h1, 9x, 1hw, 23x, 1hf, 23x, 1hh)
          w = 0.01
          do 40 ij = 1, 40
            summ = 0.0
            do 30 in = 1, n
              pp = dreal(in)
30            summ = summ + wht(in) * cos(pp * w)
            h = wht0 + 2.0 * summ
            f = w / (2.0 * pi * dt)
c           write (3, 50) w, f, h
c 50        format (1h, f20.8, 5x, f20.8, 5x, f20.8)
            w = w + 0.025
40        continue
```

```
      return
      end
*****************************************************************
***
*
* FILTER EMPLOYMENT PROGRAM
*
      subroutine smonly(data, wht, wht0, num_smo,
     &                  col_int, n)
        implicit none
        real*8 data(1000), psum, wht0, wht(1000)
        integer n, i1, i2, num_smo, ick, i, j, k1,
     &       k2, col_int
        i1 = n + 1
        i2 = col_int - n
*
* FOR THIS EXAMPLE, DATA ARE SMOTHENED 10 TIMES
*
        do 99 ick = 1, num_smo
          do 100 i = i1, i2
            psum = 0.0
              do 101 j = 1, n
                k1 = i + j
                k2 = i - j
                psum = psum + wht(j) * (data(k1) + data(k2))
101           continue
              data(i) = psum + wht0 * data(i)
100       continue
99      continue
      return
      end
```

APPENDIX F: PHOTOGRAPHIC RESULTS

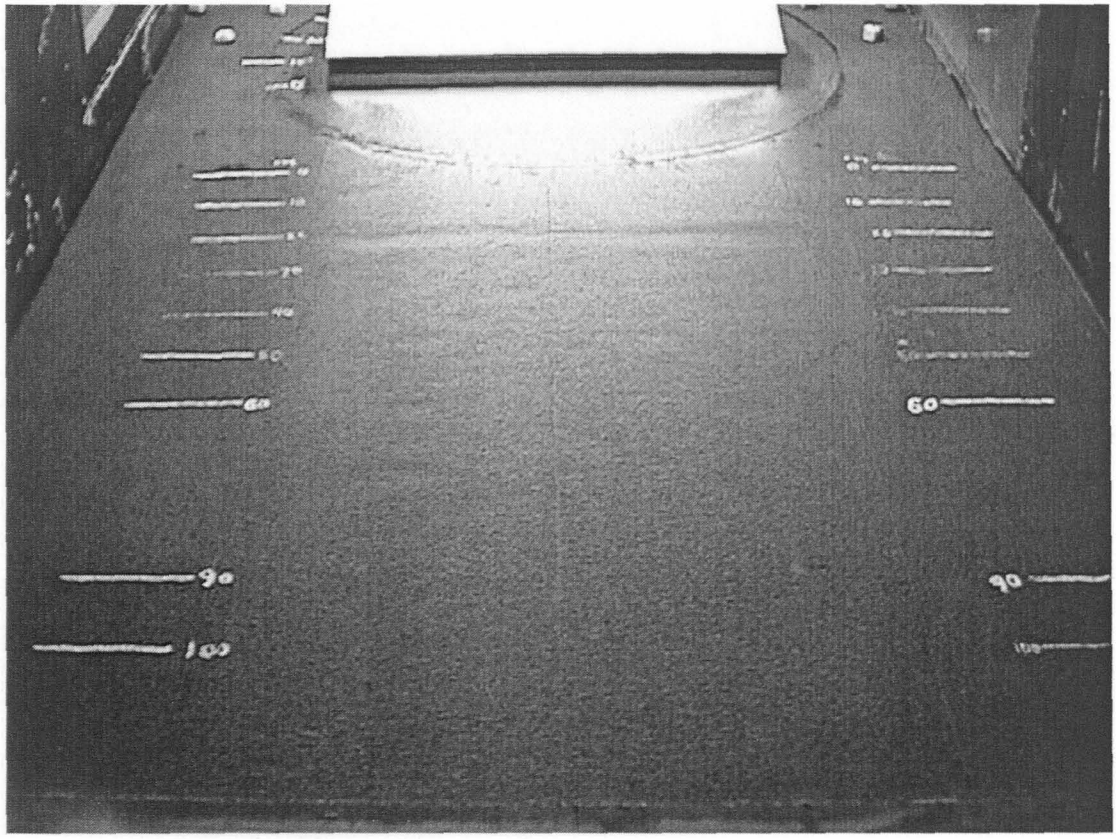

Run 1

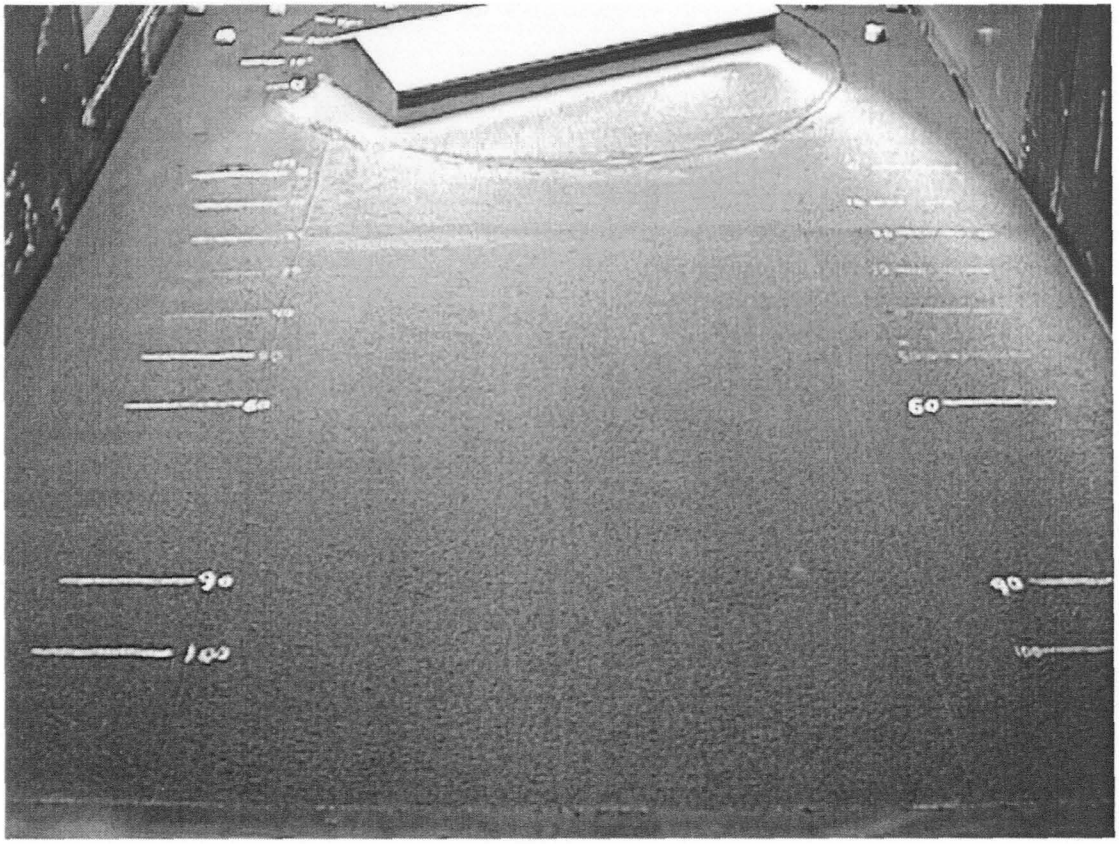

Run 2

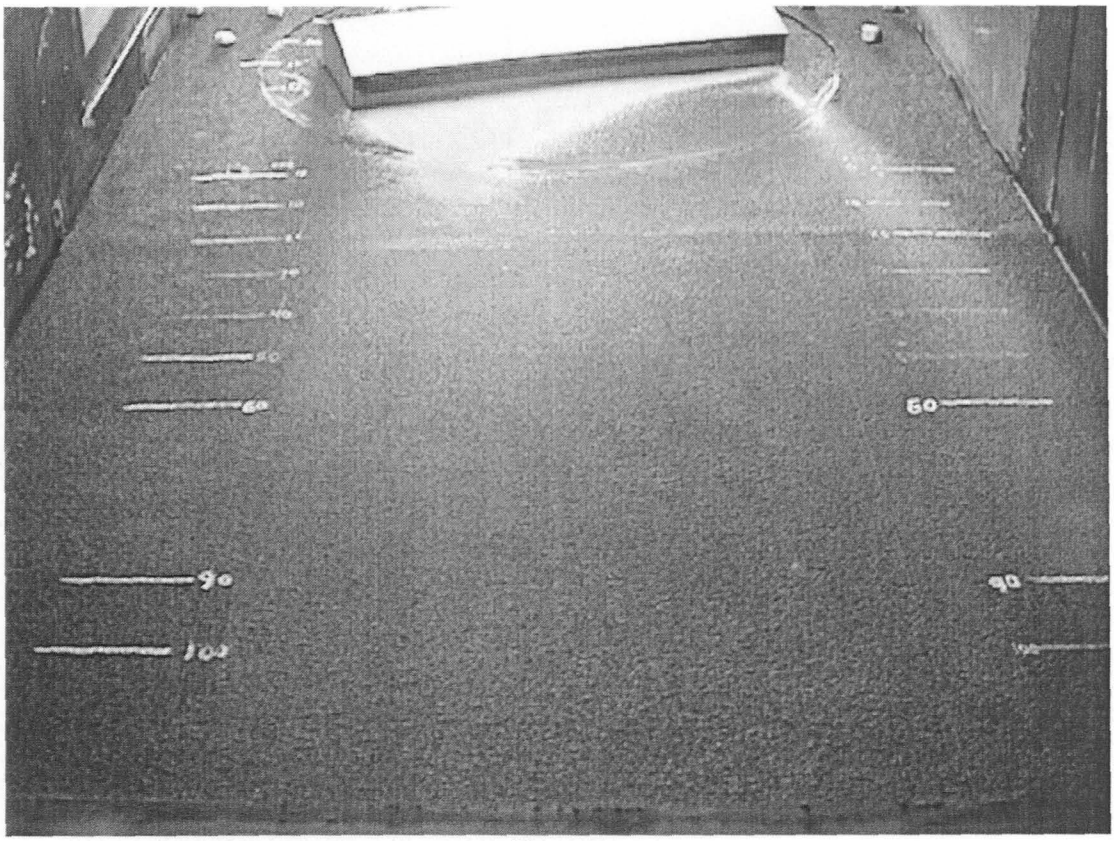

Run 3

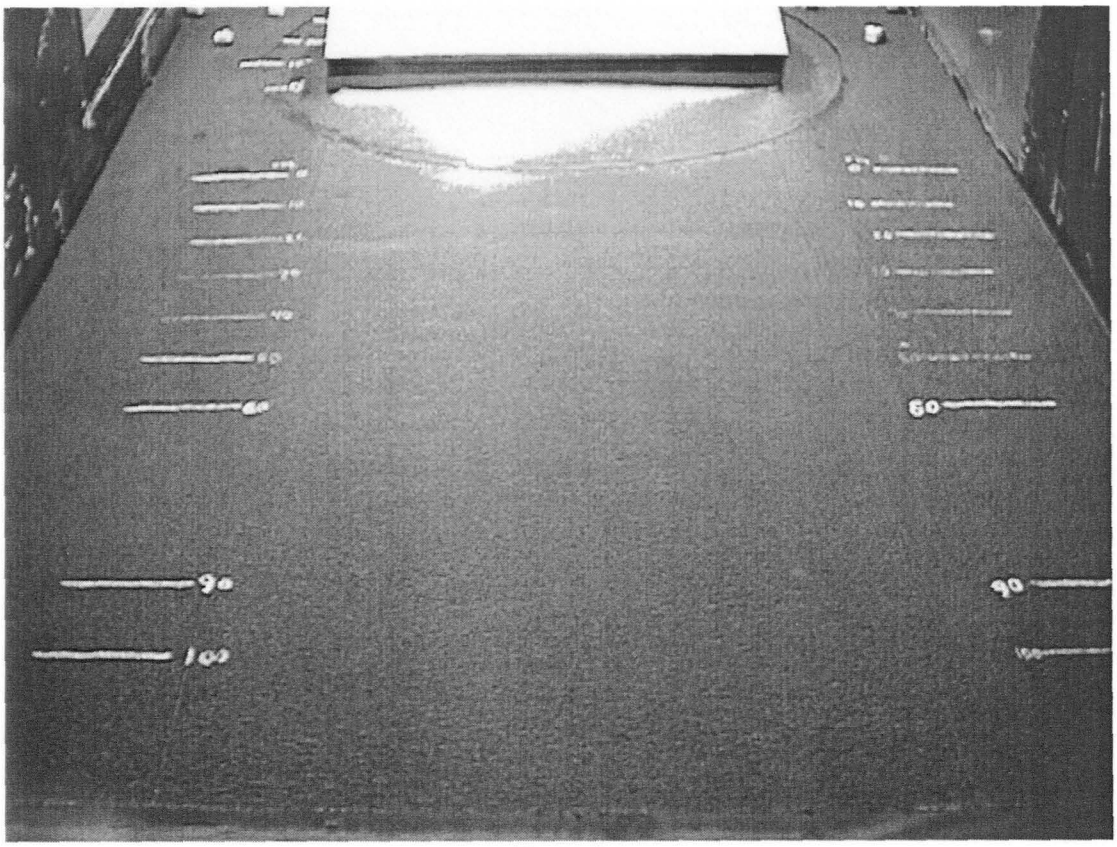

Run 4

Run 5

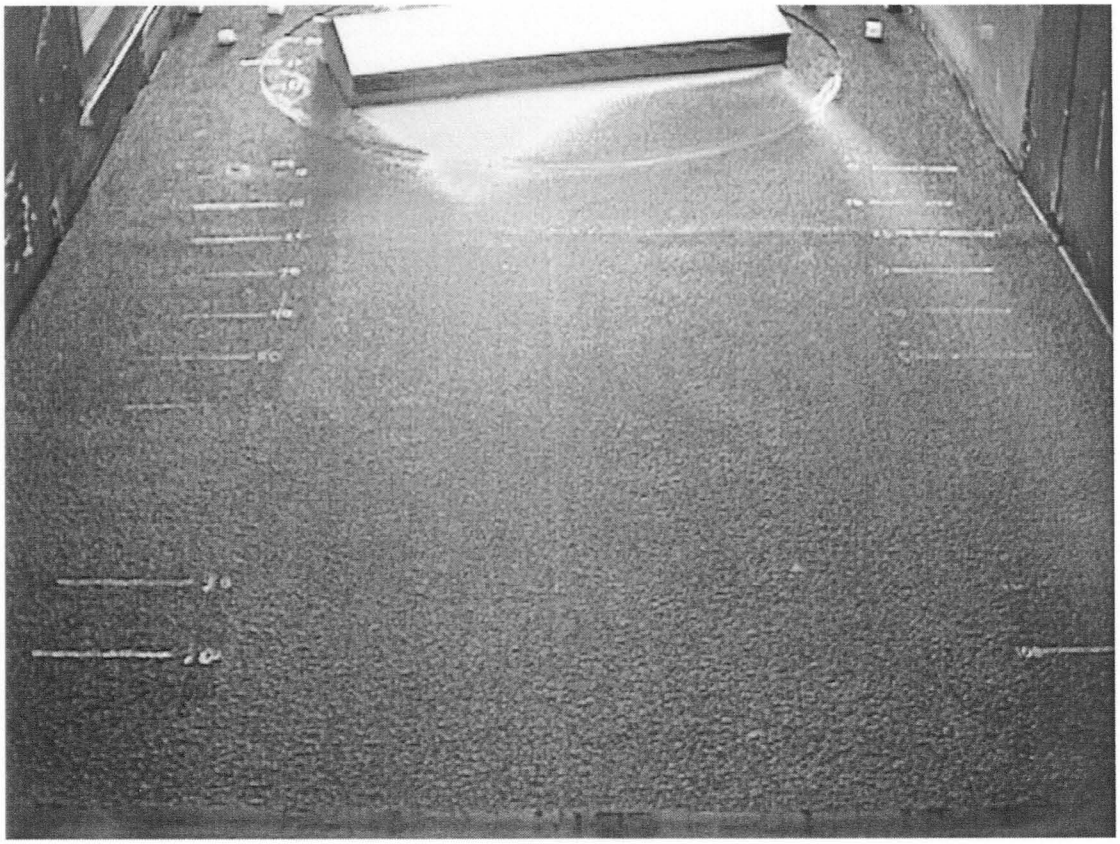

Run 6

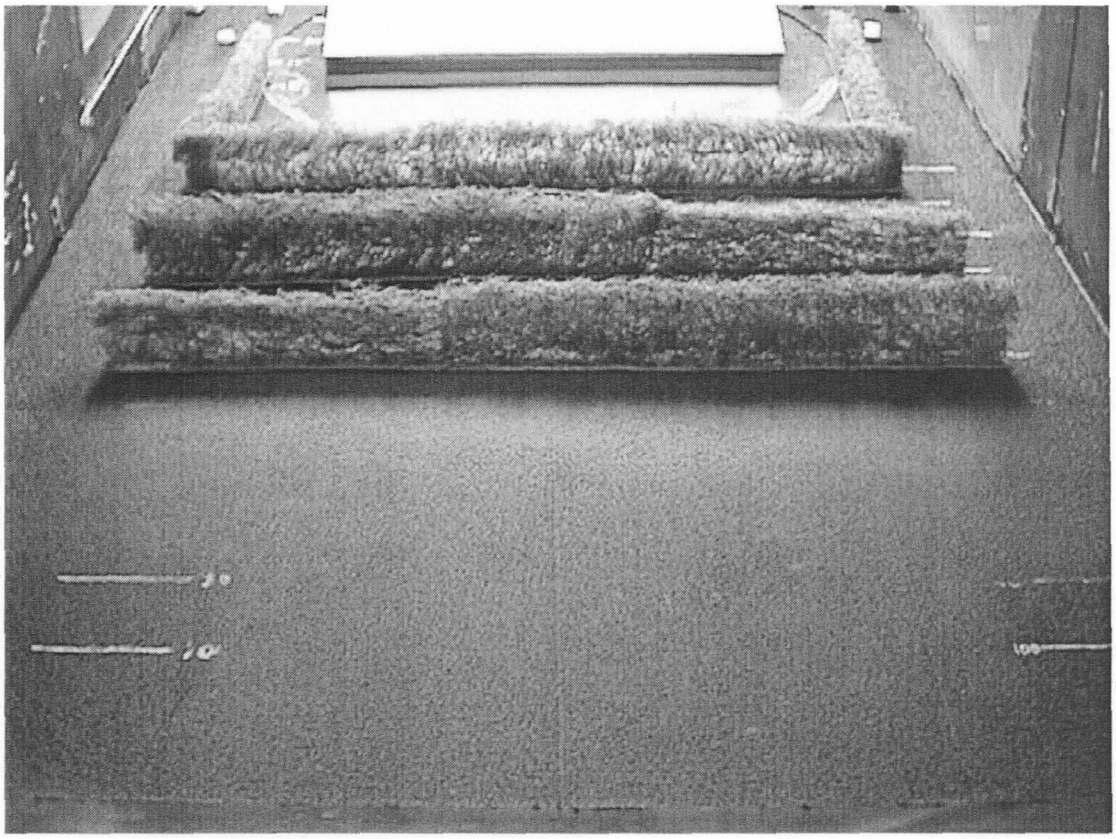

Run 7

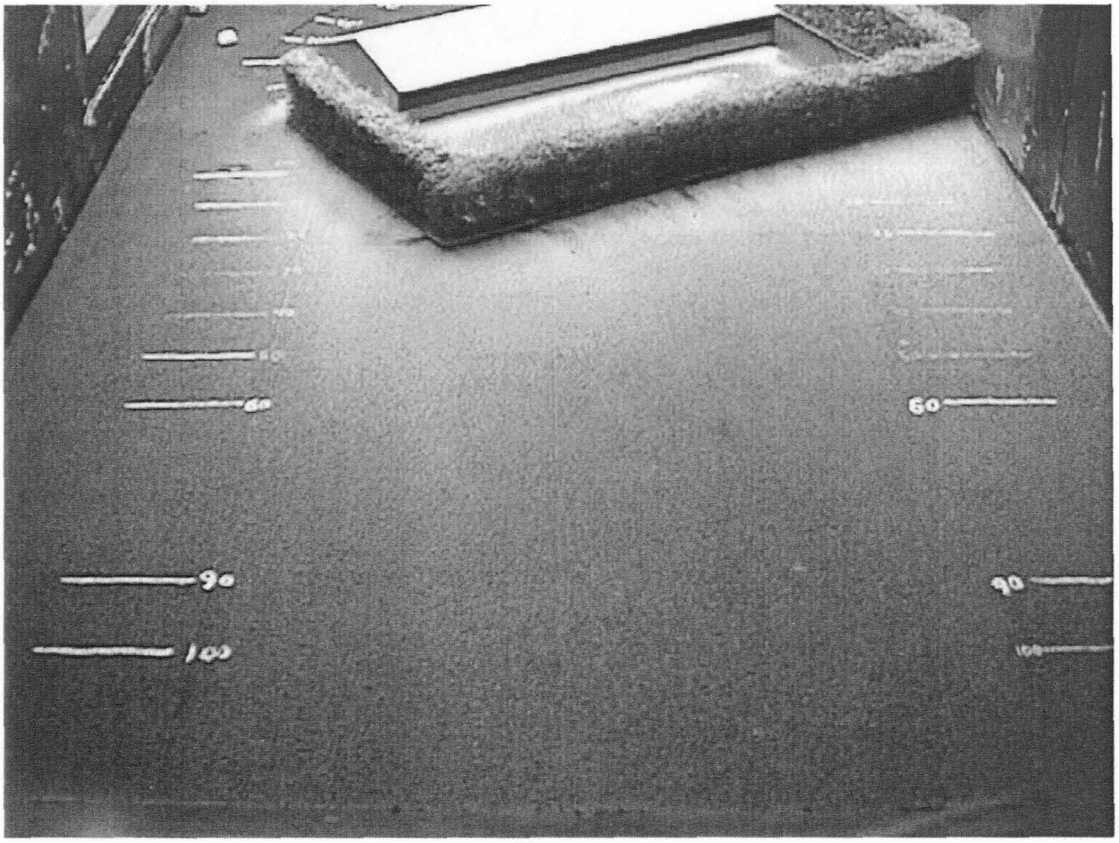

Run 8

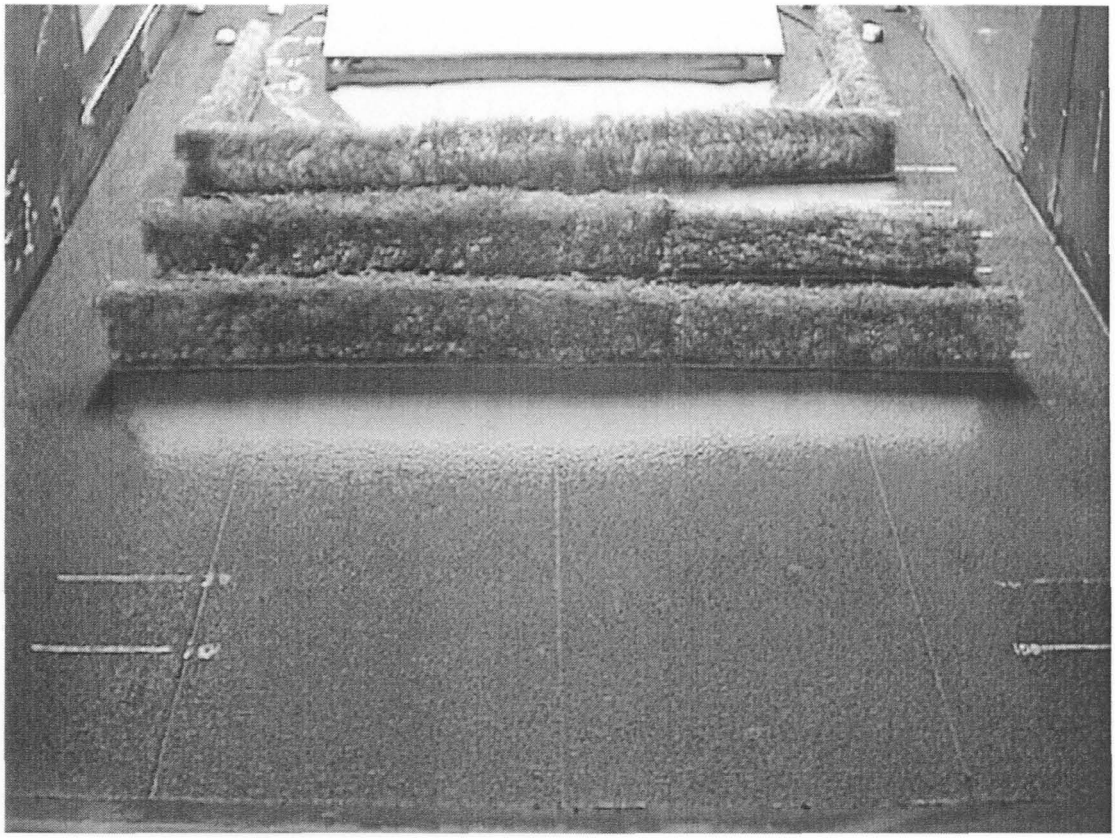

Run 9

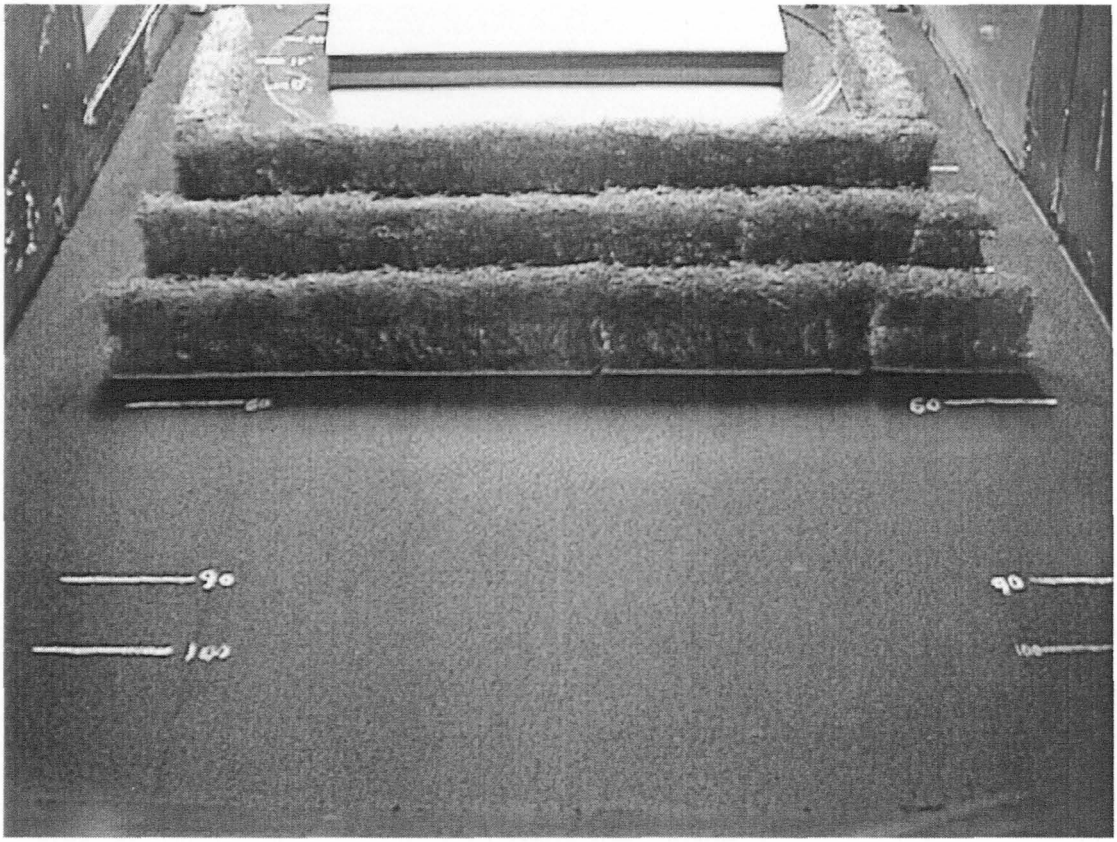

Run 10

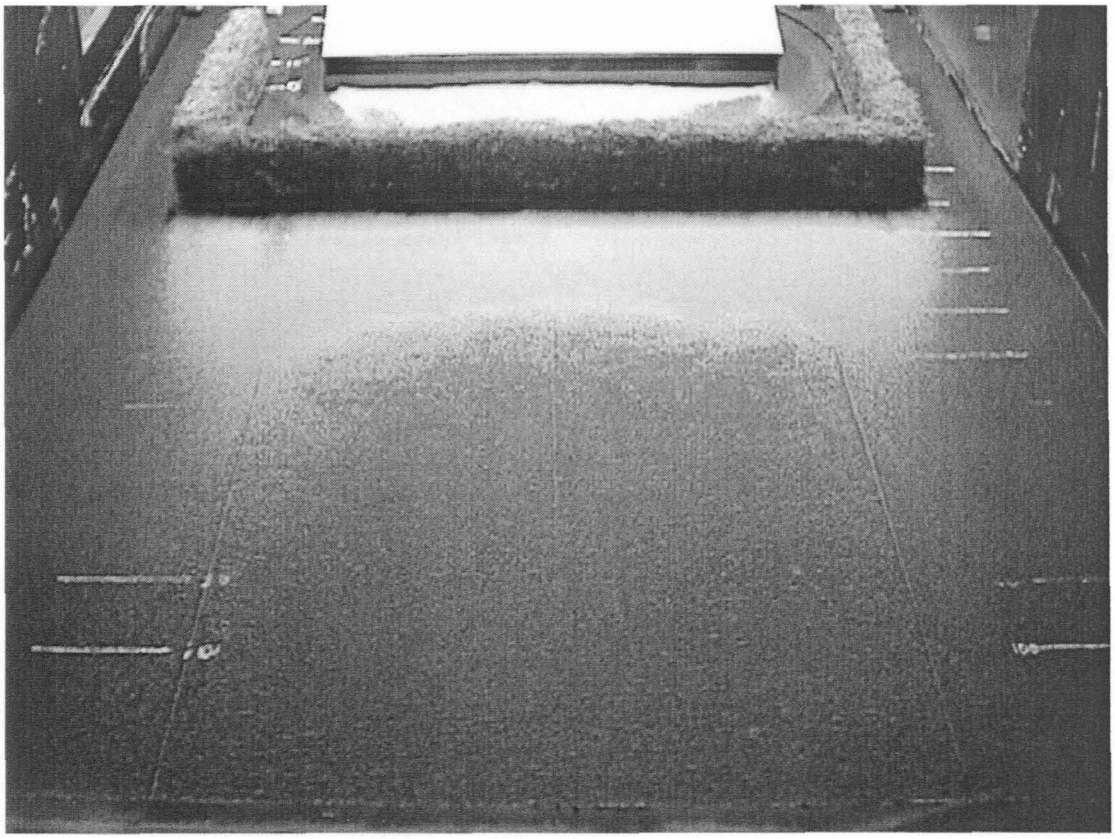

Run 11

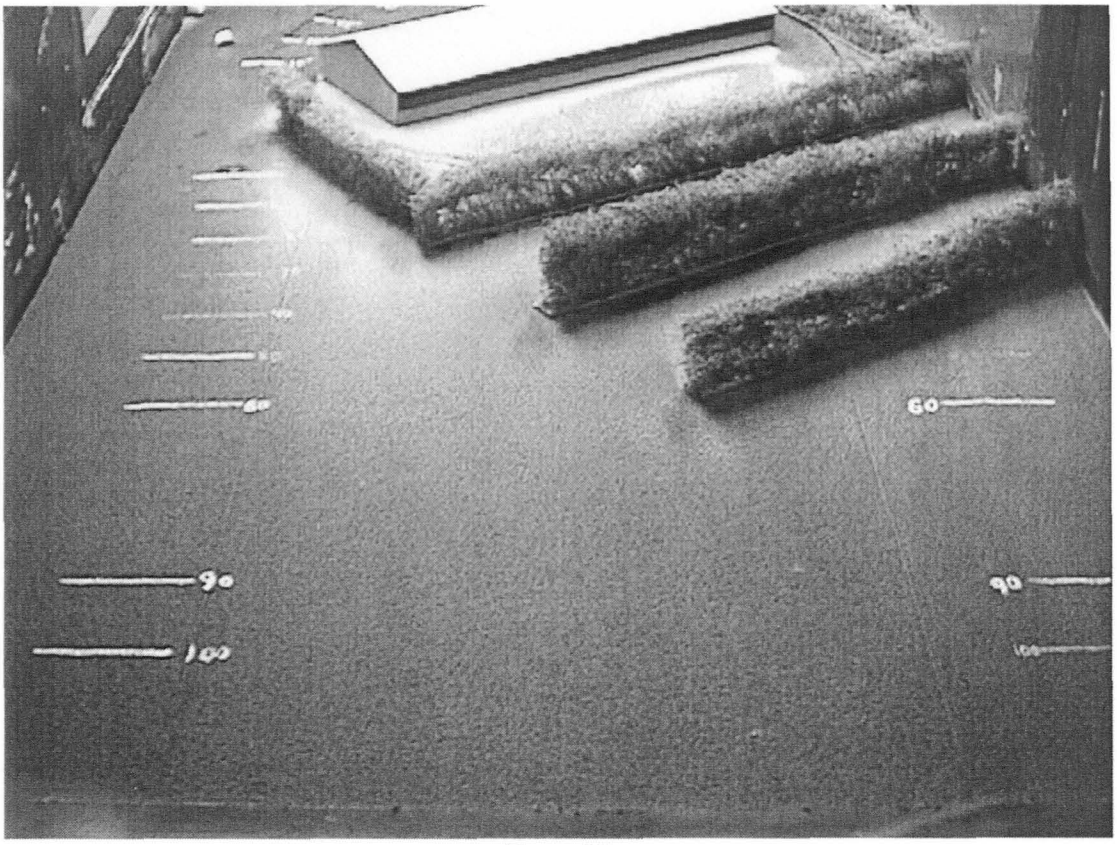

Run 12

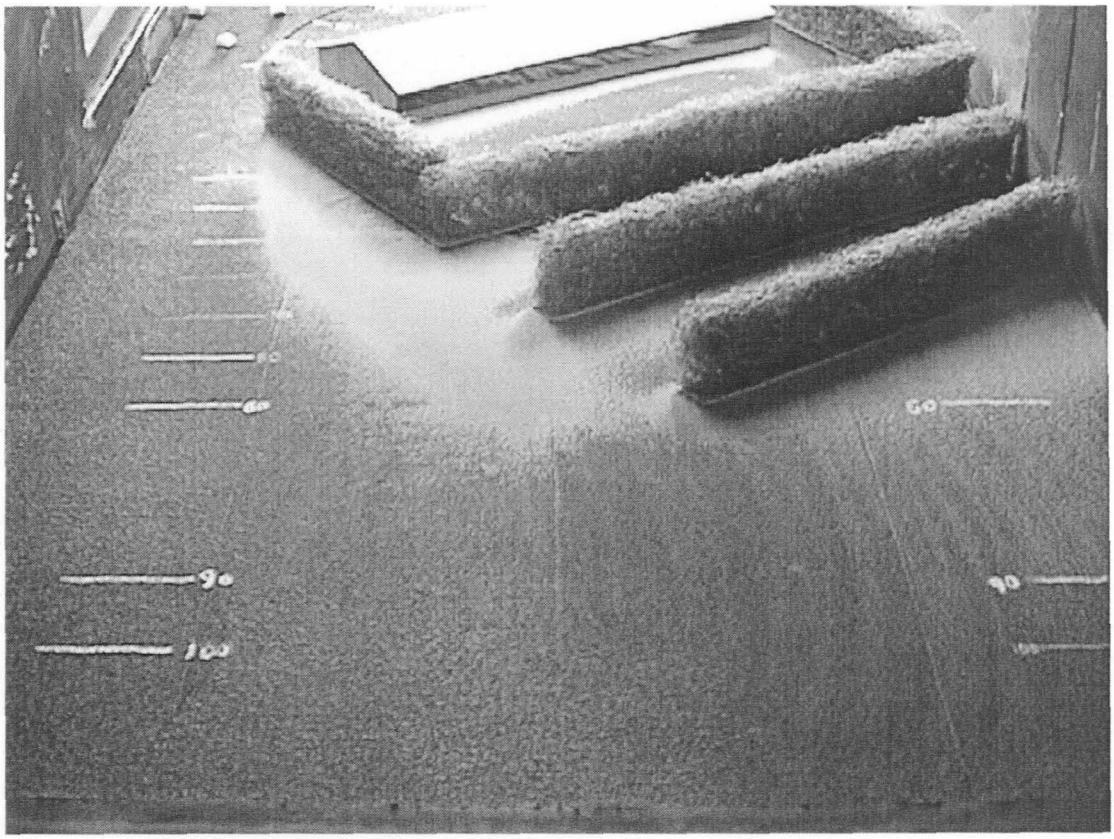

Run 13

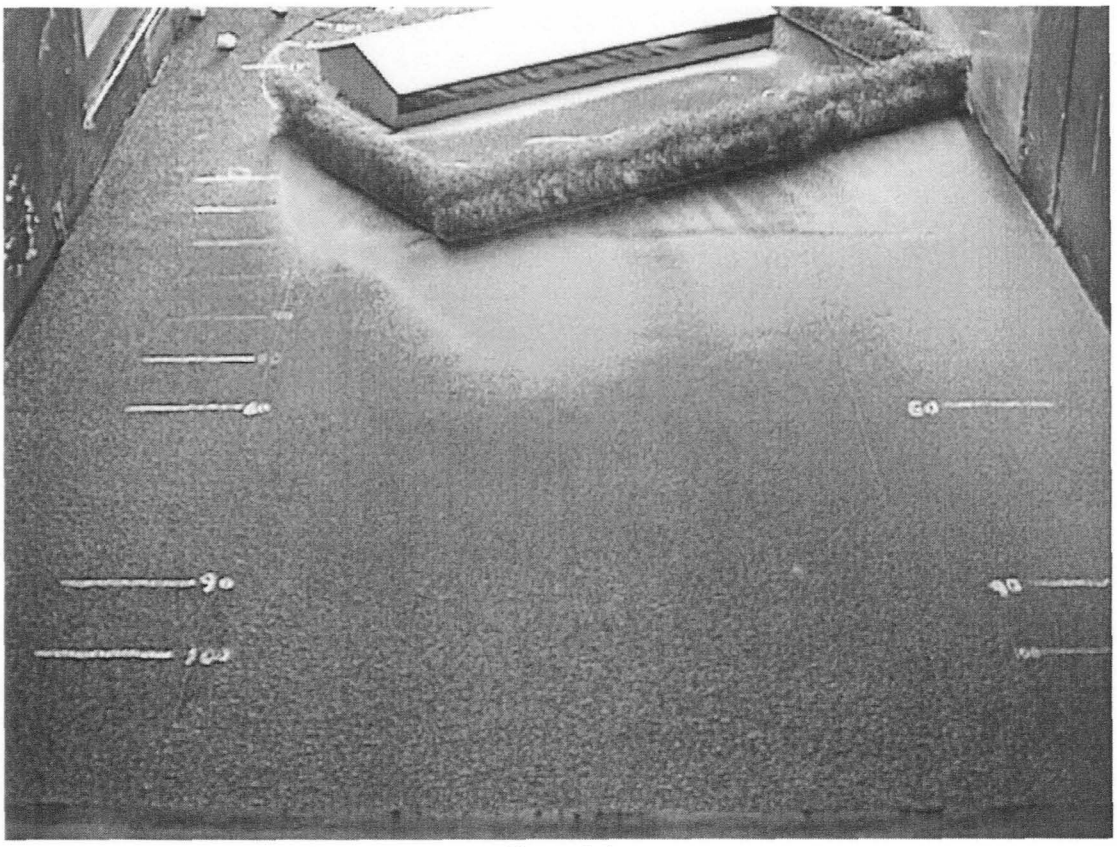

Run 14

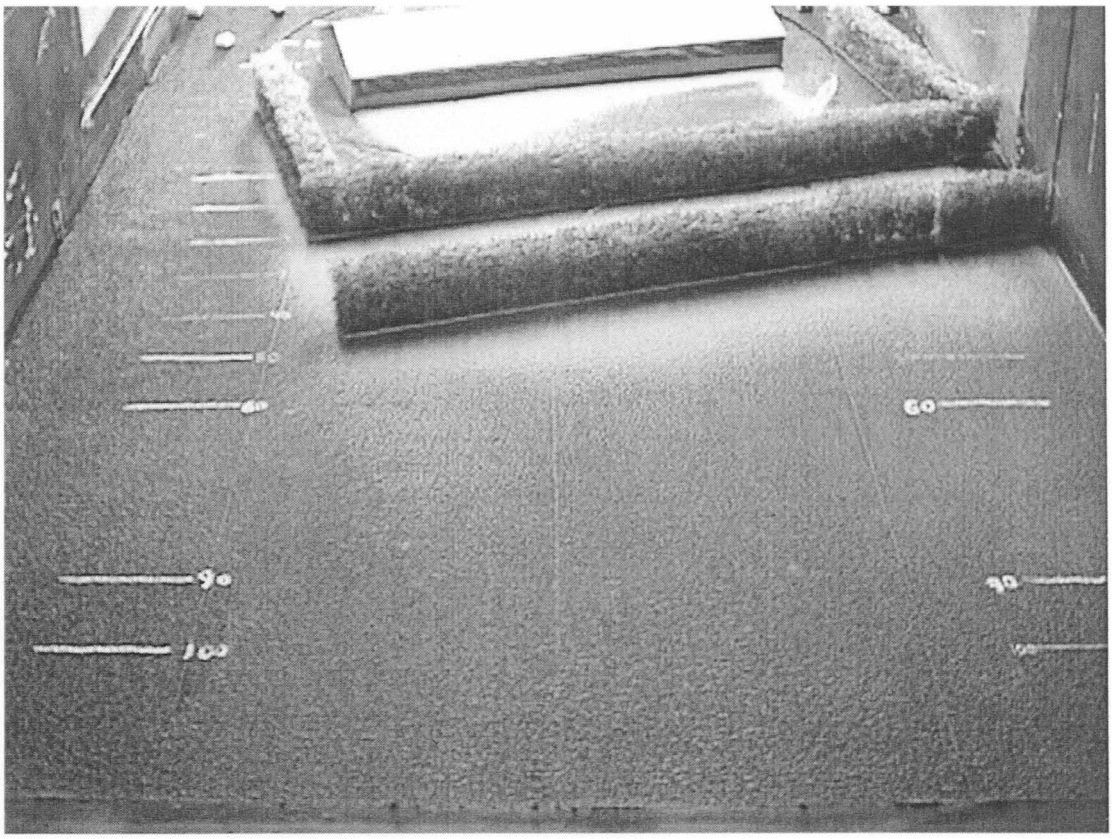

Run 15

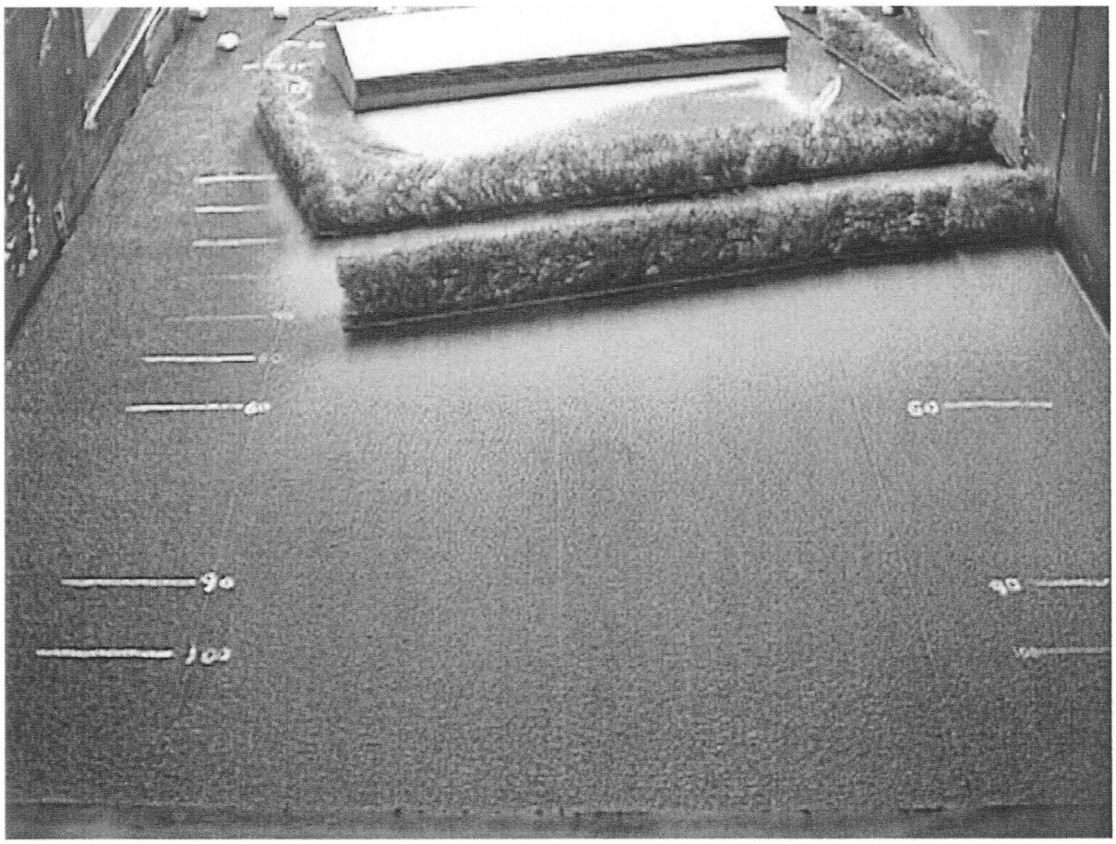

Run 16

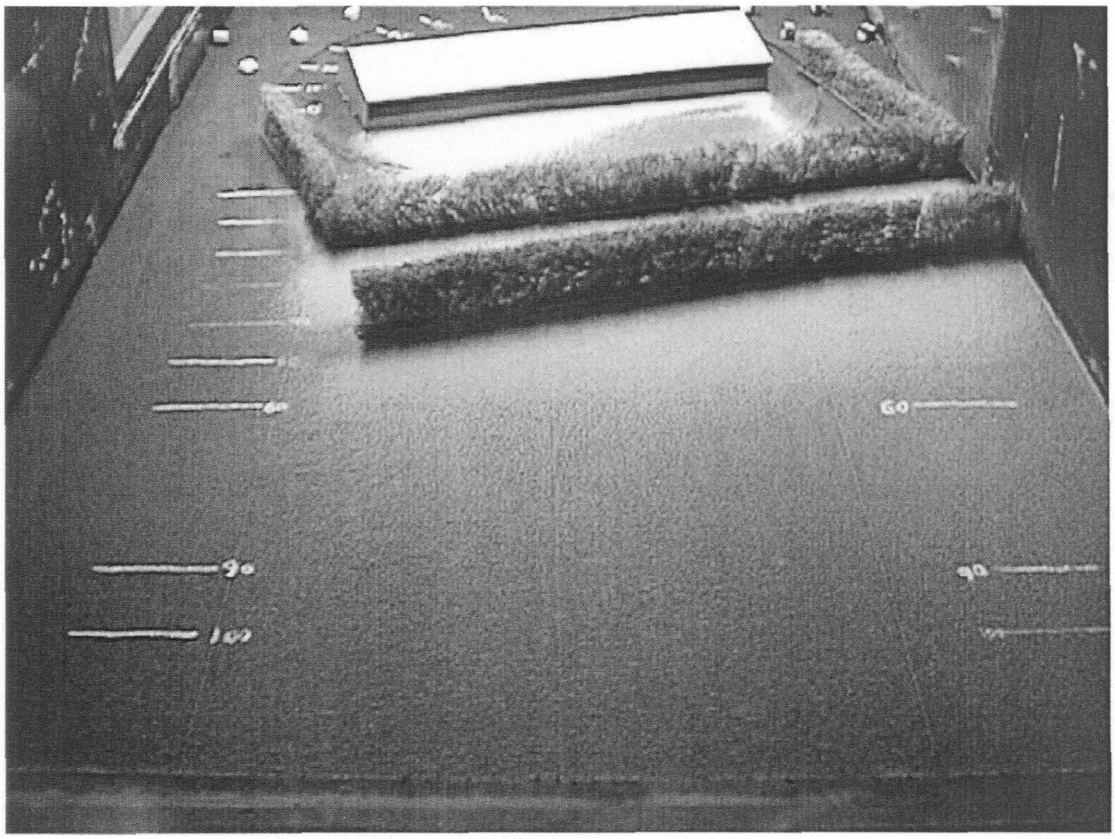

Run 17

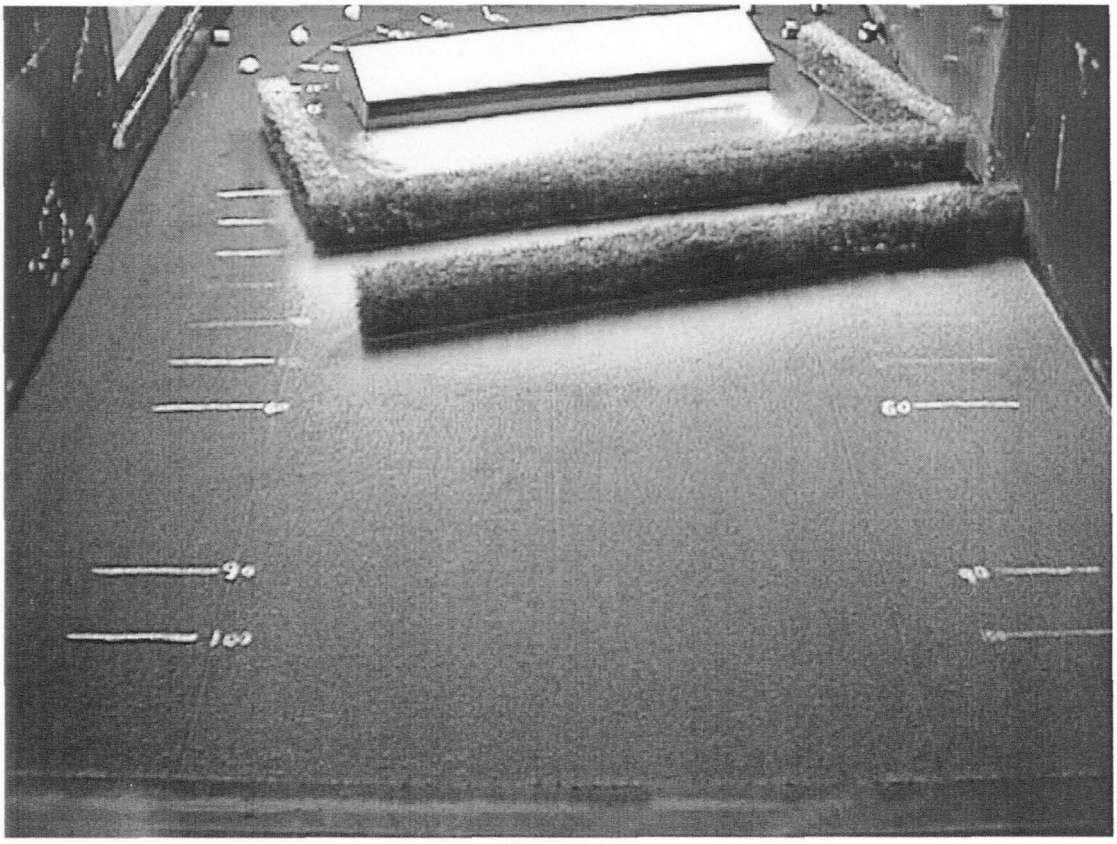

Run 18

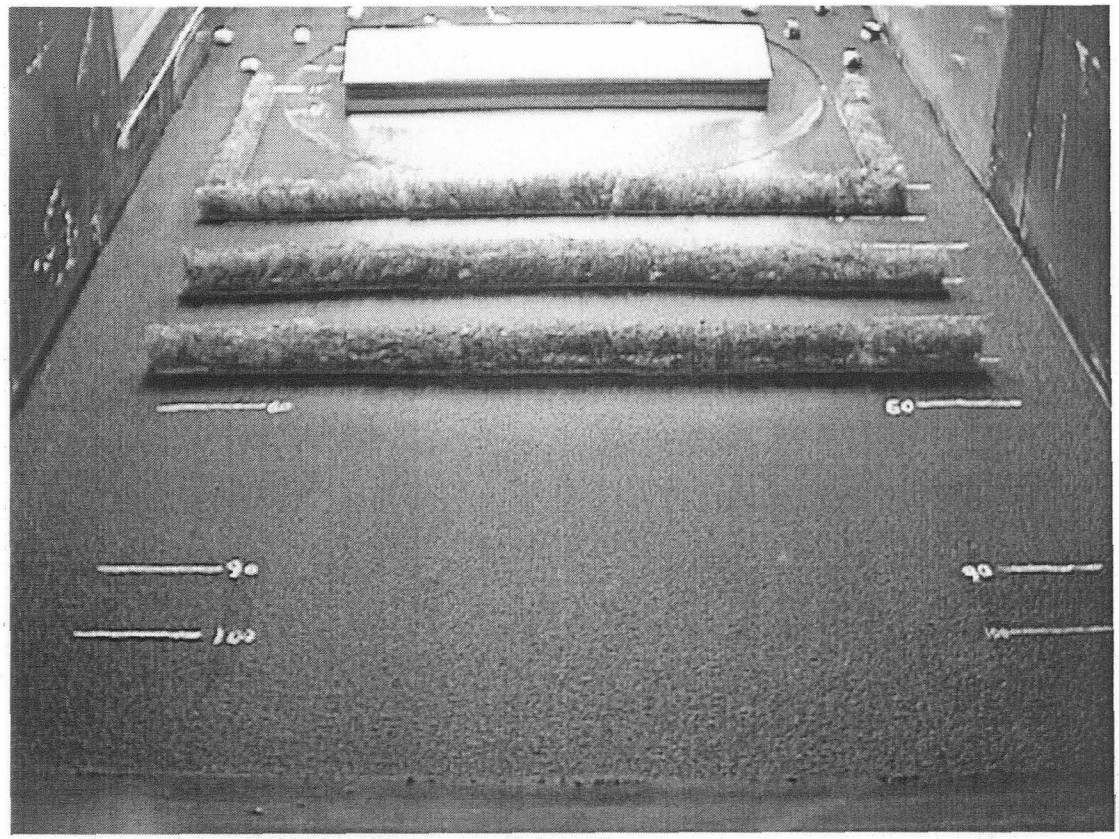

Run 19

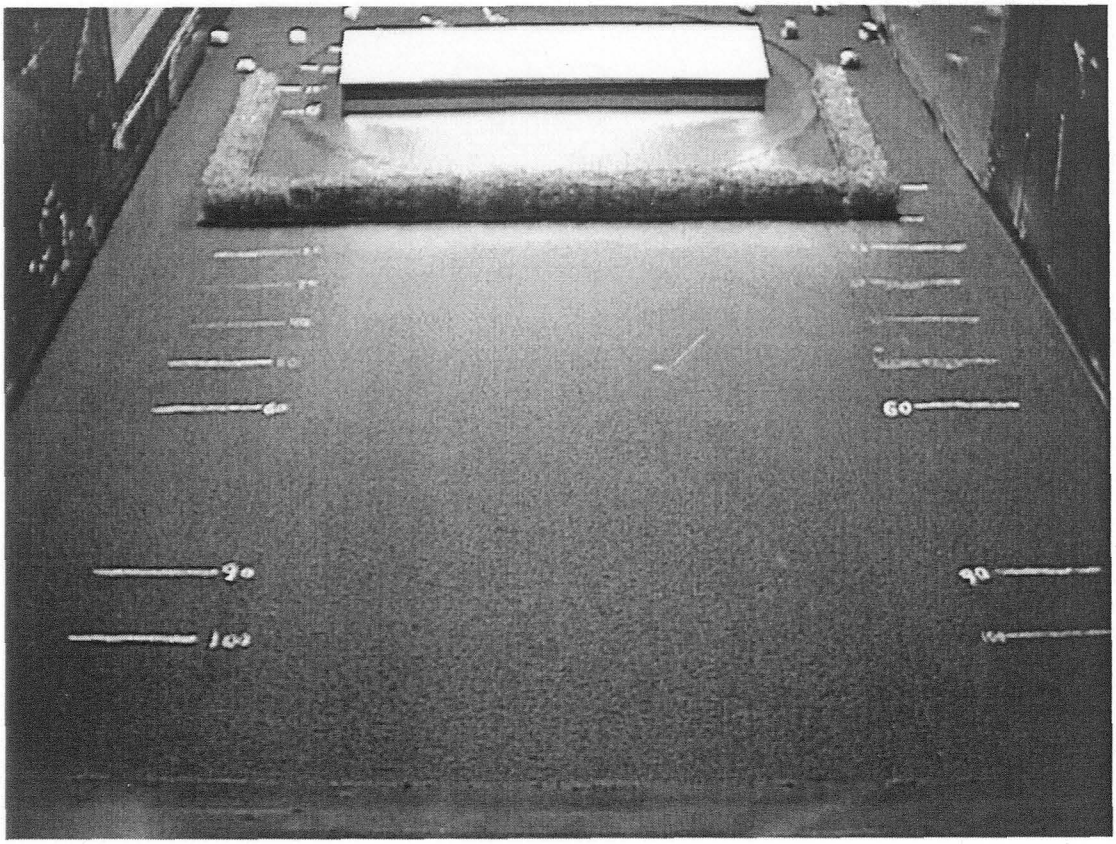

Run 20

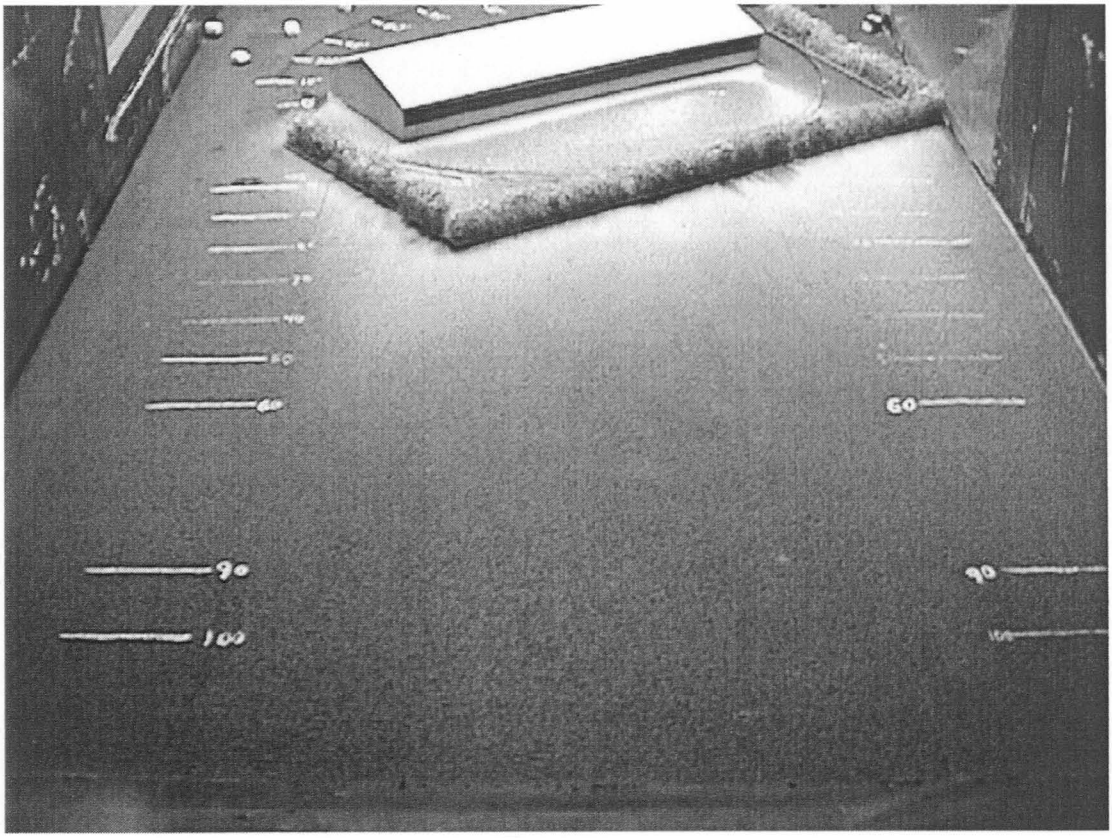

Run 21

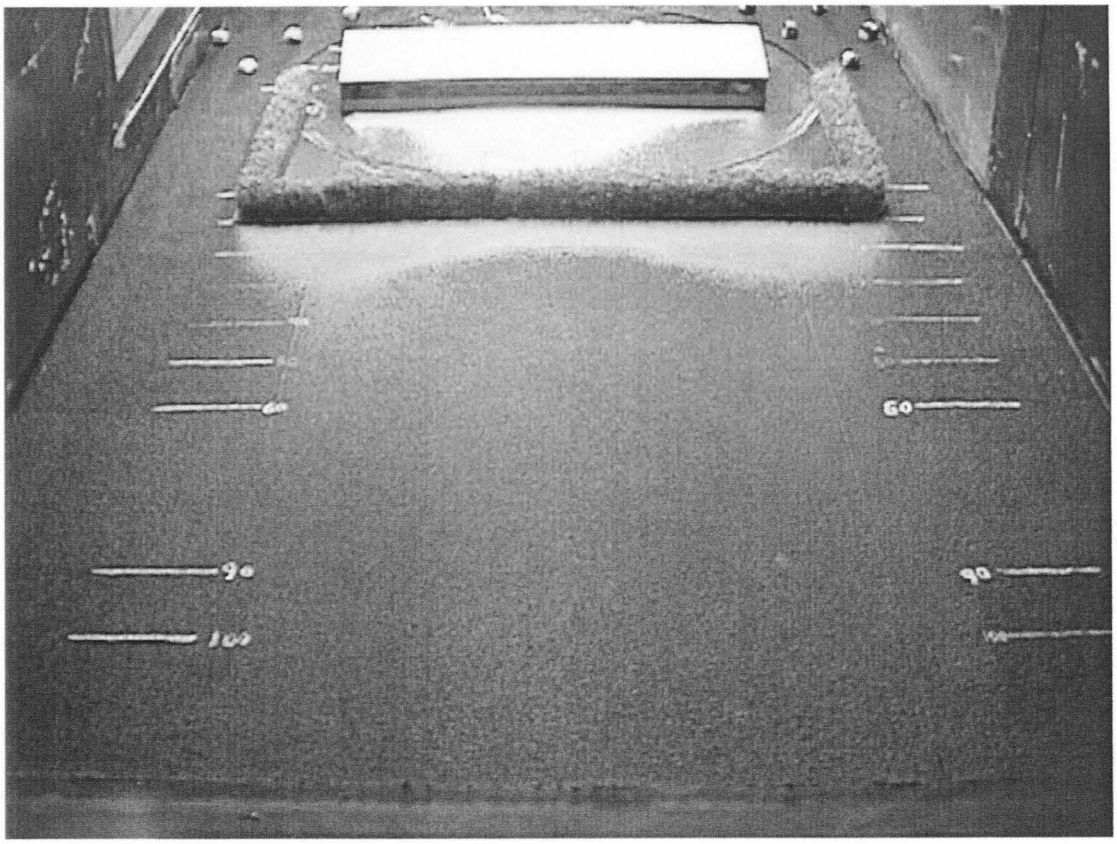

Run 22

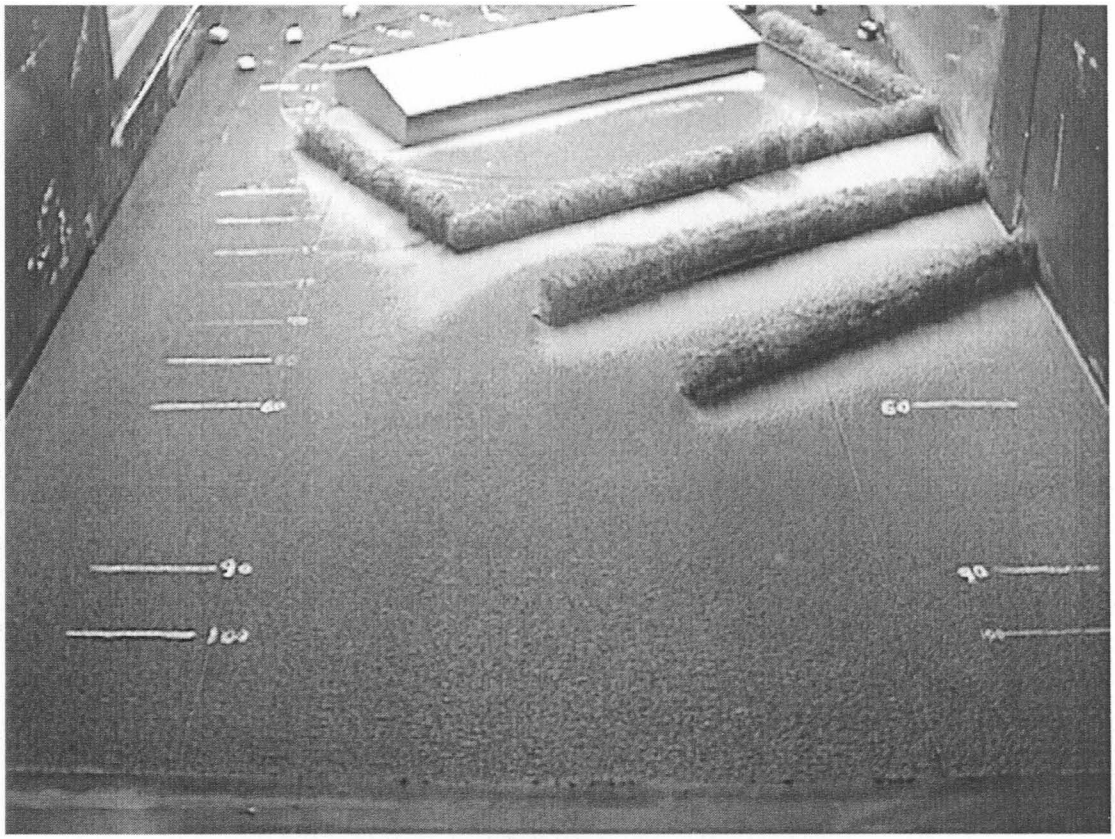

Run 23

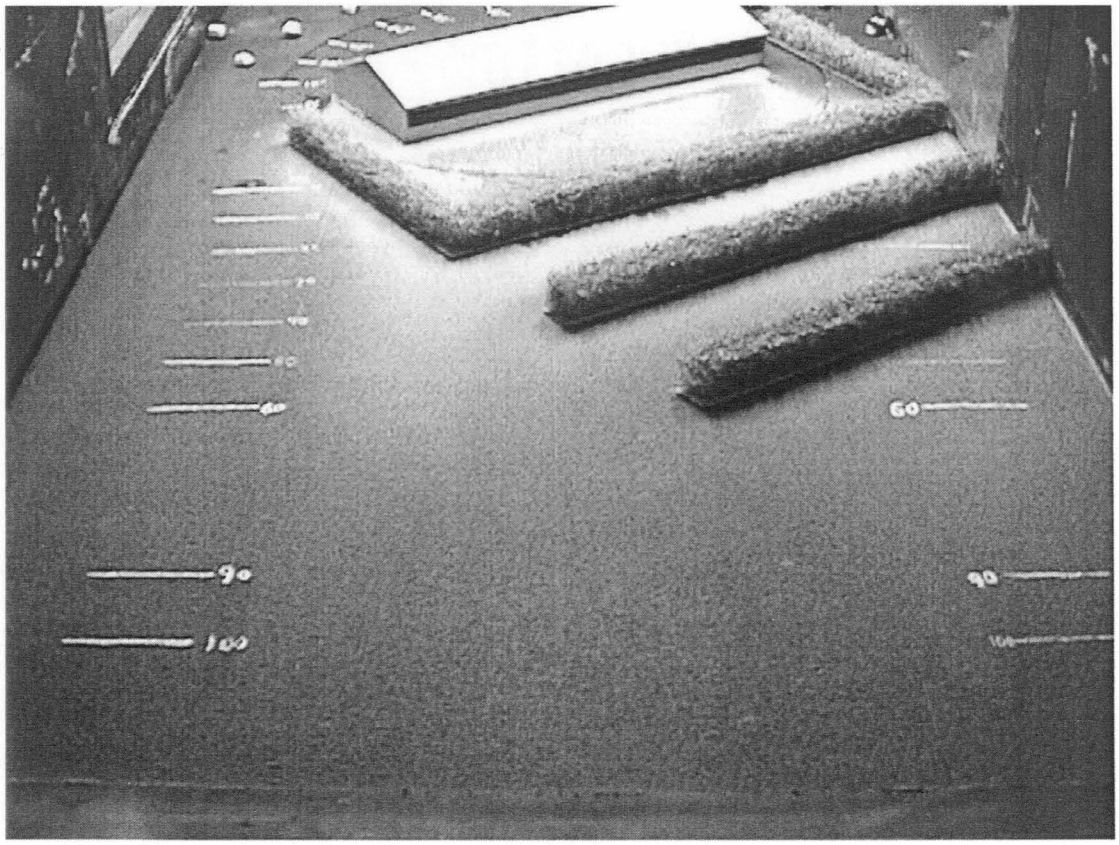

Run 24

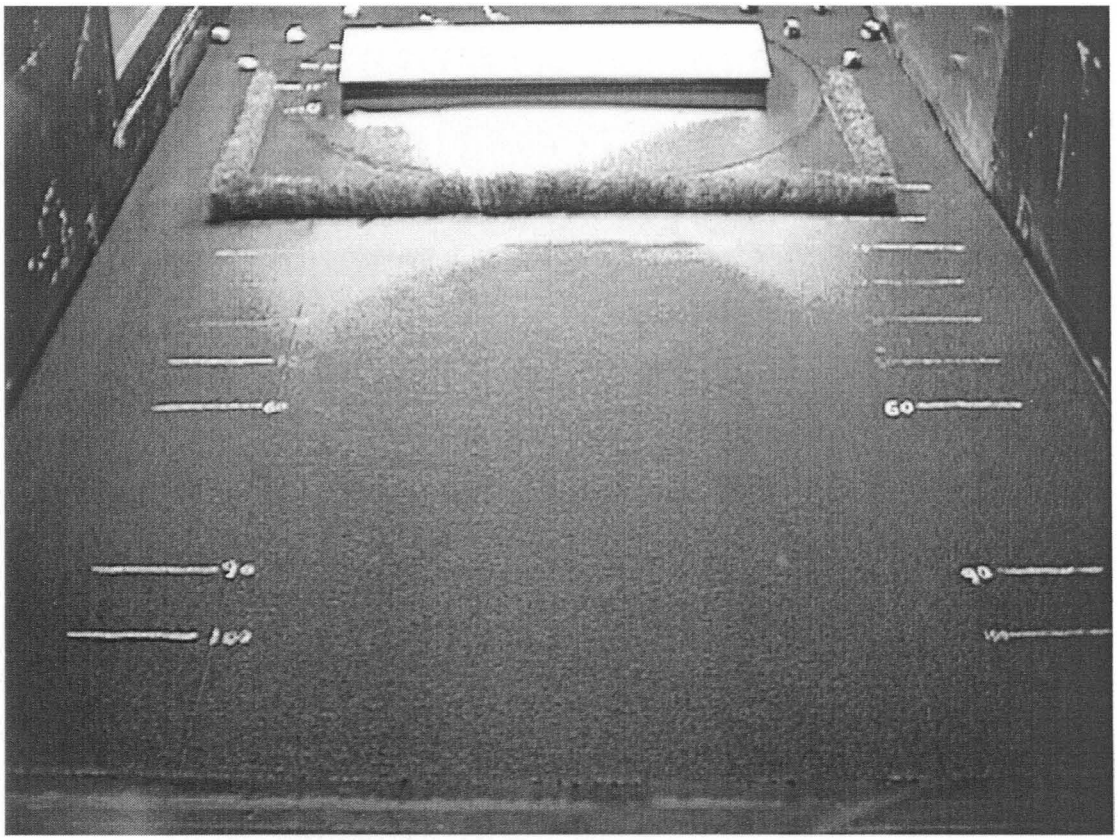

Run 25

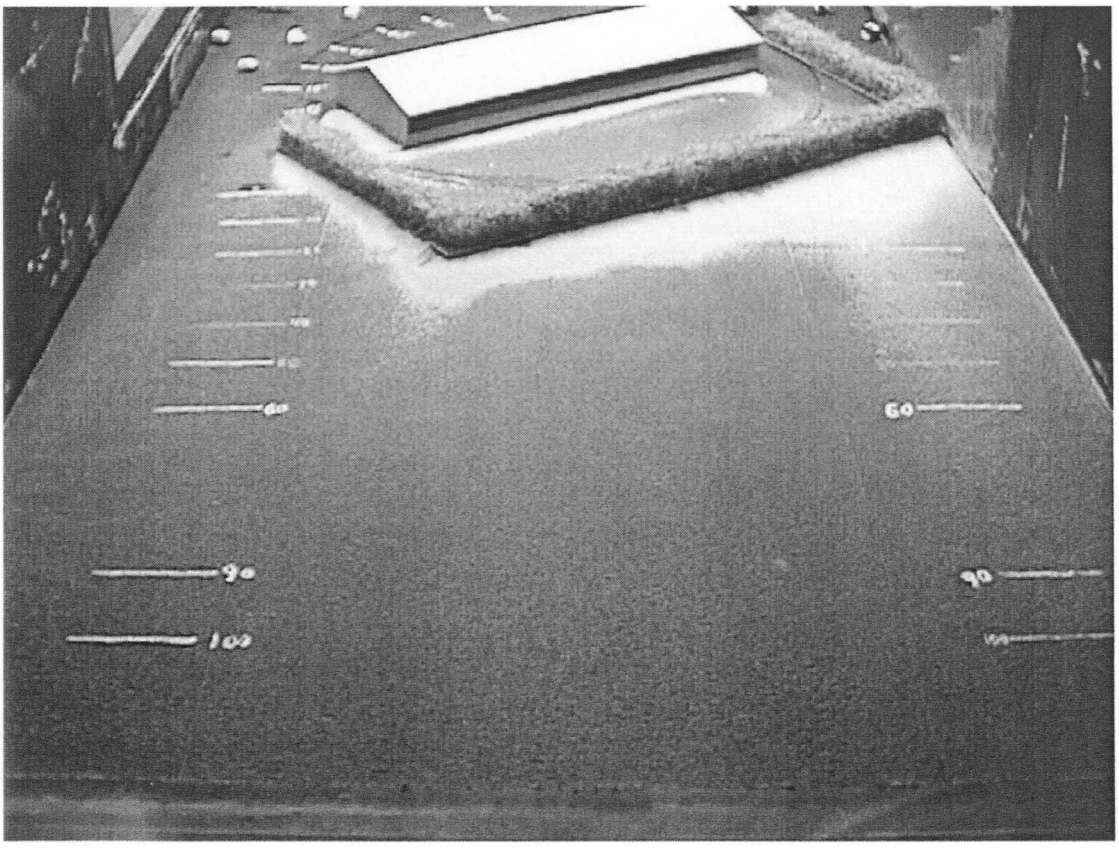

Run 26

REFERENCES

1. J.D. Iversen, Small-Scale Modeling of Snow Drift Phenomena, Wind Tunnel Modeling for Civil Engineering Applications, T. Reinhold, ed., Cambridge University Press, Cambridge, England, 1982, pp. 522-545.
2. Rae, William H. Jr. and Pope, Alan, Low Speed Wind Tunnel Testing, second edition, John Wiley and Sons, New York, New York, 1984.
3. Holman, J. P., Experimental Methods for Engineers, McGraw Hill, Inc., New York, 1994.
4. Bain, D.C., Baker, P.J., and Rowat, M.J., Wind Tunnels: An Aid to Engineering Structure Design, The British Hydromechanics Research Association, Cranfield, Bedford, England, 1971.
5. Cermak, J.E., Wind Tunnel Testing of Structures, JEMD, ASCE Vol. 103, 1977.
6. Cermak, J.E., Wind Tunnel Design for Physical Modeling of the Atmospheric Boundary Layer, Proceedings ASCE Vol. 107, 1981.
7. Cermak, J.E., Micrometerological Wind Tunnel Facility, Description and Characteristics, CER Vol 63, 1963.

8. Irwin, H.P.A.H., The Design of Spires for Wind Simulation, Journal of Wind Engineering and Industrial Aerodynamics, Vol. 7, 1981, pp. 361-366.

9. Snedecor, George W., and Cochran, William G., Statistical Methods, 8th edition, Iowa State University Press, Ames, Iowa, 1989.

10. Rawlings, John 0., Applied Regression Analysis: A Research Tool, Wadsworth and Brooks, Pacific Grove, CA, 1988.

11. Vardeman, Stephen B., Statistics for Engineering Problem Solving, PWC Publishing Company, Boston, 1994.

12. Iversen, J.D., and Jensen, V., Wind Transportation of Dust from Coal Piles, Skibsteknisk Laboratorium, Lyngby, Denmark, SL 81054, Oct. 1981.

13. Iversen, J.D., Particulate Entrainment by Wind, Department of Aerospace Engineering, Project 16999 ISU-ERI-Ames-85010, July 1984.

14. Plate, Erich J., Aerodynamic Characteristics of Atmospheric Boundary Layers, USAEC Division of Technical Information Extension, USA, May 1971.

15. Schlichting, Hermann, Boundary-Layer Theory, McGraw-Hill, Inc., New York, 1987.

16. Xuan, Jie, and Robins, Alan, The Effects of Turbulence and Complex Terrain on Dust Emissions and Depositions from Coal Stockpiles, Atmospheric Environment Vol. 28, No. 11, pp. 1951-1960, 1994.

17. Friedlander, S.K., Turner, J.R., and Hering, S.V., A New Method for Estimating Dry Deposition Velocities for Atmospheric Aerosols, J. Aerosol Sci., Vol. 17, No. 3, pp. 240-244, 1986.

18. Ziskind, G., Fichman, M., and Gutfinger, C., Resuspension of Particulates from Surfaces to Turbulent Flows - Review and Analysis, J. Aerosol Sci., Vol. 26, No. 4, pp. 613-644, 1995.

19. Moghadam, Mahmoud Mobara, Particle Deposition Due to Point or Line Source Diffusion, a Dissertation, Iowa State University Press, Ames, Iowa, 1984.

20. Wang, Hao, and Takle, Eugene S., On Shelter Efficiency of Shelterbelts in Oblique Wind, Agricultural and Forest Meteorology, Vol. 81, 1996, pp. 95-117.

21. Wang, Hao, and Takle, Eugene S., A Numerical Simulation of Boundary Layer Flows Near Shelterbelts, Boundary-Layer Meteorology, Vol. 75, 1995, pp. 141-173.

ACKNOWLEDGMENTS

I would like to thank the following people for their participation and aid in this research. The Iowa Corn Promotion Board, the Iowa Pork Producers Association, and the Iowa Soybean Board for providing direction and funding to the project. S. Magnus Thernelius for pioneering a new method of acquiring particle deposition data, and for quite possible performing more than half of the work himself. Dr. James Iversen, Dr. Bruce Munson, and Dr. William James for helping me understand the concepts involved, and for providing guidance. Dr. Bundy for introducing me to a brave new frontier of aerospace engineering. Dr. Philip Iversen and Jave Pascual for providing statistical inputs, and analyzing the results. William Jensen for helping operate the hardware and make improvements where needed. And finally, Jennifer Rossi for providing support and motivation to me throughout my graduate studies.